The Effects of the Portage Diversion on Adjacent Agricultural Land

by

Jerrold Rentz

A Thesis submitted to the Faculty of Graduate Studies of

The University of Manitoba

in partial fulfilment of the requirements of the degree of

MASTER OF SCIENCE

Department of Biosystems Engineering

University of Manitoba

Winnipeg

Abstract

Increasing soil salinity levels is an ongoing plight for agricultural producers around the world, and the area around the Portage Diversion is no exception. This study was carried out around the Portage Diversion northwest of Portage la Prairie, Manitoba, where 14 agricultural fields were evaluated for soil salinity using the electromagnetic induction technique. Of those fields, eight were combined into five groundwater monitoring areas, and one was selected for a groundwater modelling evaluation.

The analysis of the electromagnetic survey apparent conductivity (EC_a) data revealed areas of weakly to moderately conductive soils adjacent to the Portage Diversion. The calibration of the survey results was conducted by collecting 542 soil samples from 65 sampling locations. The samples were analyzed for basic soil salinity parameters and were further used to calculate the following parameters: pore-water salinity, volumetric water content, and porosity. Additional analysis was conducted using these parameters and their correlations to EC_a. The analysis yielded strong correlations of EC_a with saturated-paste or pore water conductivity, with Pearson r^2 correlation coefficients exceeding 0.75 for the DualEM 1S V-H mode and 0.86 for the V-V mode. These correlations are explained by moisture conditions being near field capacity. The study showed that in clay-rich soil, volumetric water content did not affect EC_a below 10%, indicating a threshold. These results suggest that EC_a can be used in clay-rich soils to parametrize sulphate-dominated salinity. It also shows that at high field capacity, salinity can be estimated relatively accurately from saturated paste conductivity without considering soil moisture content.

Groundwater modelling analysis showed that various processes affect soil salinity within the modelled area, including seepage from the Portage Diversion, evapotranspiration, and excessive snowmelt/recharge. The maximum lateral extent of influence that the Portage Diversion has on adjacent lands was modelled using the largest flood on record and was 112 m within the alluvial soils and 240 m along the surficial sands. It was also determined through chemical analysis on that the dominant salt ion within the groundwater is gypsum.

Acknowledgements

I would like to acknowledge and thank many people for their support in this project. First and foremost, I would like to thank my excellent Fiancé Kristin Barbour for supporting me throughout this journey, my son Grayson for motivating me to finish this project and all my family members for their support. I would also like to express my sincerest thanks to my advisory committee, Dr. Sri Ranjan thank you for your guidance and support throughout these last few years; Dr. Ferguson for his support and contribution to all of the data analysis that has gone into the project; and finally, Dr. Holländer for all that you taught me about groundwater and modelling, and of course your unwavering patience throughout all of the modelling difficulties. Without all of the help I'm not sure I would've been able to reach this point. So, to you all, Thank You. I would also like to thank all of the members of my former and current Faculty who provided encouragement throughout the project, Dr's Chow, Chakhmouradian, Reguir, and of course Mr. Jeff Young, Mrs. Karen Ferreira, Mr. Emeka Ndulue, and Dr. Mante.

This project would not have been made possible without the support of my current employer Manitoba Infrastructure – Water Infrastructure. Thank you for providing me the funding and support to undertake this project while working. There are many people that I must thank for their support, guidance, etc. Firstly, Messrs. Ron Richardson and Doug McMahon for initiating the project and allowing me to undertake this journey; Mrs. Anne-Marie Hamilton for her support and guidance throughout the project; Mr. Evan Graham for his GIS support in the early stages of the project; Mr. Peter Johnson for all of his HEC-RAS support; Ms. Heather Ganske and Ms. Natasha Woelcke for their support, encouragement, and friendship. Finally, Mr. Chris Propp, and Mrs. Angela McLean for stepping into supervisory roles after Ron's retirement to oversee the project. External to Manitoba Infrastructure, I would like to thank Mr. Bob Eilers for all of his guidance early on in the project, as well as all of the agricultural producers who were involved in the project.

Dedication

To Kristin, Grayson, and my family

Table of Contents

The Effects of the Portage Diversion on Adjacent Agricultural Land 1

Abstract i

Acknowledgements ii

Dedication iii

Table of Contents iv

List of Tables vii

List of Figures viii

List of Abbreviations xiii

1 Introduction 1

1.1 Overview 1

1.2 Scope of work 4

1.3 Objective 4

1.3.1 Research question – What are the effects of salinity and water content on apparent conductivity in an alluvial setting in the Canadian prairies? 4

1.3.2 Research question – What is the impact of a drainage canal on piezometric levels and soil salinity in adjacent agricultural lands? 4

1.4 Thesis outline 5

2 Literature review 5

2.1 Effects of salinity and water content on apparent conductivity in an alluvial setting in the Canadian prairies 5

2.1.1 The Portage la Prairie alluvial fan 5

2.1.2 Soil types within the study area 8

2.1.3 Salinization processes 9

2.1.4 Socio-economic and seepage impacts of irrigation canals and ditches 12

2.1.5 Geophysical techniques in agriculture 14

2.1.6 Laboratory techniques to analyze soil conductivity 18

2.2 The impact of a drainage canal on piezometric levels and soil salinity in adjacent agricultural lands 19

2.2.1 Model types 19

2.2.2 Modelling with data scarcity 20

3 Effects of salinity and water content on apparent conductivity in an alluvial setting in the Canadian prairies 22

3.1 Contribution of authors 22

3.2 Introductory statement 22

3.3 Abstract 22

3.4 Introduction 23

3.5 Study area 27
3.5.1 Geology and geohydrology 27
3.5.2 Soils 28
3.5.3 Sulphate salinity in groundwater and soil-water 30

3.6 Materials and methods 32
3.6.1 Instrumentation 32
3.6.2 Electromagnetic survey 33
3.6.3 Correction of data for departure from LIN 33
3.6.4 Soil sampling 34
3.6.5 Laboratory analysis 35
3.6.6 Depth weighting 37
3.6.7 Linear regressions 37

3.7 Results 38
3.7.1 Distributions of paste extract and soil moisture parameter values 38
3.7.2 Regression results for EC_e and EC_w 41
3.7.3 Regression results for other parameters 45
3.7.4 Regression results for combined parameters 46
3.7.5 Dependence of results on porosity and clay content 49

3.8 Application of results 51
3.8.1 Conversion of apparent conductivity results to salinity 51
3.8.2 Electromagnetic induction survey results of individual fields 53

3.9 Discussion 60
3.9.1 Review of apparent conductivity prediction results 60
3.9.2 Comparison of EC_a-EC_e and EC_a-water content correlations obtained in other studies 62
3.9.3 Comparison of physical relationships with other studies 64
3.9.4 Effects of sulphates on apparent conductivity 66
3.9.5 Effects of clay on apparent conductivity 67
3.9.6 Additional electromagnetic induction surveys results 68
3.9.7 Effects of microtopography on salinity 69

3.10 Conclusions 71
3.10.1 Field surveys 71
3.10.2 Statistical analysis 72

4 Hydrogeological investigation of soil salinity adjacent to a flood protection infrastructure 74

4.1 Contribution by authors 74

4.2 Introductory statement 74

4.3 Abstract 74

4.4 Introduction 75

4.5 Study area 77
4.5.1 Location and site description 77
4.5.2 Climate and precipitation 77
4.5.3 Regional geology and geohydrology 78
4.5.4 Overburden 79
4.5.5 Soil salinity 80

4.5.6 Drainage canal 80
4.6 Methodology 81
4.6.1 Field program and data collection 81
4.6.2 Assessment of the hydraulic conductivity of the aquifers 82
4.6.3 Water Sampling, chemistry, and hydrogeochemical modelling 83
4.6.4 Precipitation and evapotranspiration 83
4.6.5 Determination of flood levels 84
4.6.6 Snowpack measurements 84
4.7 Numerical modelling 85
4.7.1 Model design 85
4.7.2 Initial model parameterization 87
4.7.3 Model calibration 89
4.7.4 Sensitivity analysis 91
4.8 Results 92
4.8.1 Calibration results 92
4.8.2 Sensitivity analysis 93
4.8.3 Effect of the 2017 and 2011 flood events 95
4.8.4 Groundwater chemistry 97
4.9 Discussion 100
4.9.1 Uncertainties in the model performance 100
4.9.2 Source of sulphate 100
4.9.3 Soil salinization influences and the effect of the Portage Diversion 101
4.9.4 Model applications within the region 103
4.10 Conclusions 103
5 Overall conclusions 104
6 Practical extension of this work 106
7 References 107
Appendix A – Apparent conductivity overview maps 120
Appendix B – Additional soil salinity maps 127

List of Tables

Table 2.1 Summary of soil types in the study areas (Michalyna and Smith 1972)..... 9
Table 3.1 Correlations between ECa and weighted predictors for V-H measurements..... 42
Table 3.2 Correlations between ECa and weighted predictors for V-V measurements..... 43
Table 3.3 Percentage of sub-area with different levels of salinity. 52
Table 3.4 General information on surveyed fields stratigraphy from: Michalyna and Smith (1972). 54
Table 3.5 Summary of Chemical Analysis from the surveyed fields with ECe values >4 $dS.m^{-1}$. 56
Table 3.6 Summary of relationships determined between ECa, ECe, ECw and volumetric water content. 61
Table 4.1 Summary of agricultural soil types within the study area, where hydraulic conductivity was analyzed throughout the soil profile (Michalyna and Smith 1972). 80
Table 4.2 Daily amounts of recharge added to simulate snowmelt in cm. 91
Table 4.3 Calibrated material parameters within the monitored layer and statistical analysis of the model fit as a whole. Statistical fitting is defined as: Acceptable (A) and Not Acceptable (NA) for RMSE and MAE, and Good (G) and Excellent (E) for NSE. 93
Table 4.4. Range of model sensitivities from SPs #1-4 where "N/A" indicates insensitive..... 93
Table 4.5 Statistical analysis of SP #4 sensitivities. 95
Table 4.6 Saturation indices of analyzed groundwater samples at 25°C. 99

List of Figures

Figure 1.1 Geographical map of southern Manitoba showing the location of the Portage Diversion. 1
Figure 1.2 An example cross-section from the Portage Diversion at STA. 15+200 (Hatch Ltd. 2015). 2
Figure 1.3 Select Portage Diversion flood events by volume of water (Hydata 2020) 3
Figure 2.1 The evolution of the Assiniboine River other the past 7030 years (Rannie et al. 1989) SOURCE: Republished with permission of Canadian Science Publishing, from: Holocene evolution of the Assiniboine River paleochannels and Portage la Prairie alluvial fan, Rannie, W. F., Thorleifson, L. H., and Teller, J. T., volume 26, issue 9, ©1989. Permission conveyed through Copyright Clearance Center, Inc. 6
Figure 2.2 Surficial geology map of the study region (Adapted from: Gilliland 1965). 7
Figure 2.3 Geologic cross-section of the study region from A:A' which is denoted in Figure 2.2 (Adapted from: Gilliland 1965). 8
Figure 2.4 Soils map of the study region (adapted from: Michalyna and Smith 1972). 10
Figure 2.5 Irrigation suitability of the soils within the study region, where irrigation classes 1 and 2 are most suitable for irrigation and classes 3 and 4 are least to unsuitable for irrigation (Michalyna and Smith 1972). 11
Figure 2.6 Transmitter and receiver orientations for both the Geonics EM-38 and DualEM 1S (Abdu et al. 2007). 16
Figure 2.7 A. The relative sensitivity of the EM38 and DualEM; and B. The cumulative response to depth of the EM38 and DualEM orientations (Abdu et al. 2007). 17
Figure 3.1 Photograph from an area of high salinity showing a surface soil sample speckled with fine-grained crystals that are interpreted to be gypsum**.** 29
Figure 3.2 Groundwater and soil-water samples from three locations in the study area that exhibit relatively (a) low, (b) intermediate and (c) high levels of salinity. The groundwater samples correspond to freshwater, brackish water, and saline water, respectively, using Hem's classification (Hem, 1985). Each soil sample is from a location that is close to the corresponding groundwater monitoring well and has similar soil: for MW17-09, the soil sample is 200 m from the monitoring well; for MW13, it is 5 m; and for MW17-03, it is 45 m. Groundwater sampling

was done using procedures outlined in ASTM D4448-01 (ASTM, 2013), and samples were analyzed at a private laboratory. For MW17-09 and MW17-03, the soil-water results are an average of individual results for 8 depths over the upper 120 cm, and for MW17-13, they are for a single sample at approximately 2.1 m depth. 31
Figure 3.3 Depth sensitivity of DualEM-1S when operated at LIN in a layered medium. a Cumulate sensitivity shown for the sensitivity at depths larger than the specified value. Vertical dashed line show the exploration depth above which material contributes 70% of the response. b Relative sensitivity of the V-V and V-H modes. Horizontal lines define the layers used in the present study. Layer 9 corresponds to all depths greater than 1.2 m. c Sensitivity of the V-H and V-V modes to the individual layers. d Adjusted sensitivity values with the total sensitivity of the upper 8 layers adjusted to 100%. 33
Figure 3.4 LIN approximation and correction for DUALEM 1 S instrument. a Departures of instrument ECa reading over a uniform Earth from the true conductivity. Top axis show the corresponding induction number for the V-V mode. Note that the V-V configuration has much larger departures from the true reading than the V-H mode. **b** Correction factor used to multiply observed the observed EC_a to yield the true conductivity. Individual symbols show the correction factors for the data measured in the present study. 35
Figure 3.5 Histograms of properties derived directly by laboratory measurements for the full suite of 65 soil samples at each depth. Each panel also shows a normal distribution fitted to the observed distribution and the mean and standard deviation of the observed values. 39
Figure 3.6 Histograms of properties derived from laboratory measurements for the full suite of 65 soil samples at each depth. Each panel also shows a normal distribution fitted to the observed distribution and the mean and standard deviation of the observed values. 41
Figure 3.7 with single-parameter variables: a weighted ECe, b weighted ECw, c weighted volumetric water content, d weighted porosity, and e weighted relative water saturation. The weighting is matched to V-H or V-V mode respectively. Dashed black line shows least-squares fitted linear trend and annotations show equation of the fitted trend, squared correlation coefficient and number of samples. Dashed red line and red labels for the weighted volumetric water content and porosity results show the fit for a quadratic function. 44
Figure 3.8 Regression of LIN-corrected V-H mode (left column) and LIN-corrected V-V mode (right column) ECa with combined-parameter variables **a** weighted ECw x θ ($\sigma w \cdot \theta$), **b** weighted

ECw x θ2 (σw·θ2) and **c** weighted ECw x [θ-θ0]2 (σw·[θ-θ0]2) with θ0 = 0.08. Weighting is matched to V-H or V-V mode respectively. Short dashed black line shows least-squares fitted linear trend and annotations show equation of the fitted trend, squared correlation coefficient and number of samples. Long dashed grey line in (b) shows the equation determined by Dalton and Van Genuchten (1986) i.e., $\sigma_a = 1.29\sigma w\theta^2+0.25$ dS.m^{-1}. 47
Figure 3.9 Contour plots of the ECa response at sample locations as a function of weighted ECw and weighted porosity values. Upper panel shows V-H response and lower panel shows V-V response. The contour maps were each constructed using a 100x100 point grid produced using natural neighbor interpolation. Dark symbols show the actual data points plotted using a more intense colour scale. 48
Figure 3.10 Porosity-sorted regression of LIN-corrected ECa data with **a** V-H weighted ECw, **b** V-V weighted ECw, **c** V-H weighted ECw x θ2, and **d** V-V weighted ECw x θ2. Left panels show results for 19 lowest porosity-samples for the corresponding mode with the linear trend constrained to pass through the origin and right panels show results for 46 highest-porosity samples with the linear trend including a non-zero intercept. Short dashed black line shows least-squares fitted linear trend and annotations show equation of the fitted trend, squared correlation coefficient and number of samples. Blue dashed lines are 95% confidence levels.... 50
Figure 3.11 Conversion of measured EC_a values into equivalent EC_e maps for one sample sub-area of the study. **a** Measured V-H and V-V EC_a values. **b** V-H and V-V EC_a values corrected for departure from LIN responses. **c** Equivalent EC_e maps for the upper 0.5 m and the upper 1.5 m computed using the linear regression results for the full data set (shown in Figure 3.7. Each map is based on 1630 original data points. Gridded data with a 5 m spacing was produced using kriging and a manually-fitted exponential variogram with a length scale defined by the data of 105 m for the V-H mode and 120 m for the V-V mode. Black crosses show the location of individual data points. Distance axes are shown in UTM14 N coordinates relative to a reference point at the southwest corner of the sub-area. 52
Figure 3.12 Soil salinity survey of Section 29-13-7W showing both V-H and V-V mode. 55
Figure 3.13 Soil salinity survey of Section 16-12-7W showing both V-H and V-V mode. 57
Figure 3.14 Soil salinity survey of Section 5-13-7W showing both V-H and V-V mode. 58
Figure 3.15 Soil salinity survey of Section 32-12-7W showing both V-H and V-V mode. 59

Figure 3.16 Soil salinity survey of Sections 5-12-7W and 4-12-7W showing both V-H and V-V mode. 60
Figure 3.17 A comparison between the soil salinity analysis from the V-H mode to microtopography in Section 29-13-7W. 70
Figure 3.18 A comparison between the soil salinity analysis from the V-H mode to microtopography in Section 5-13-7W. 70
Figure 4.1 Map showing the location of Delta Marsh (hatched) and the general study area. 78
Figure 4.2 Electromagnetic induction survey of the study area illustrating areas of low to high concentrations of salinity. 81
Figure 4.3 Observed piezometric head and precipitation data within the study area. Note: SP #3 displays sharp decreases in the piezometric head due to water sampling events. 82
Figure 4.4 Plan view of the model area showing model discretization. Standpipes are located at varying depths at the defined circles and the canal is within the dashed area. 86
Figure 4.5 A) 3-Dimensional view of the model area, illustrating the model slices and boundary conditions. B) Plan view of the slice at elevation 248.4 m illustrating the distribution of the i) silty clay loam, ii) silty clay, iii) fine sandy loam. 87
Figure 4.6 Eastern boundary condition where A) is the HEC-RAS simulated piezometric elevations, and B) is the assumed decrease in the piezometric head after the operation of the canal showing both linear and non-linear scenarios. 89
Figure 4.7 Model calibration results of the SPs showing observed head vs. predicted head along with water level in the canal. 92
Figure 4.8 Summary of the sensitivity analysis of SP #4 where A) is hydraulic conductivity (m/s) and B) is specific yield (S_y). 94
Figure 4.9 Cross-Section A-A' showing the lateral movement of groundwater from the canal dike through the alluvial soils during both the 2017 and 2011 flood events, where the red star denotes the approximate location of the treed/homestead area. 96
Figure 4.10 Cross-Section B-B' showing the lateral movement of groundwater from the canal dike through the fine sandy loam during both the 2017 and 2011 flood events, where the red star denotes the approximate location of the treed/homestead area. 97
Figure 4.11 Groundwater sampling results for the standpipes within the study area. 98
Figure 4.12 Saturation Indices of SP #1 and SP #3. 99

Figure A.1 Overview of the apparent conductivity results within the study region (exploration depth 0.5 m). 121
Figure A.2 Overview of the apparent conductivity results within the study region (exploration depth 1.5 m). 122
Figure A.3 Apparent conductivity map of Section 29-13-7W. 123
Figure A.4 Apparent conductivity map of Section 16-12-7W. 123
Figure A.5 Apparent conductivity map of Section 5-13-7W. 124
Figure A.6 Apparent conductivity map of Section 32-12-7W. 124
Figure A.7 Apparent conductivity map of Sections 5-12-7W and 4-12-7W. 125
Figure A.8 Apparent conductivity map of Sections 8-12-7W, 9-12-7W, and N4-12-7W. 125
Figure A.9 Apparent conductivity map of Sections 20-12-7W and 21-12-7W. 126
Figure A.10 Apparent conductivity map of Section 29-12-7W. 126
Figure B.1 Overview of the equivalent ECe results within the study region (exploration depth 0.5 m). 128
Figure B.2 Overview of the equivalent ECe results within the study region (exploration depth 1.5 m). 129
Figure B.3 Soil salinity survey of Sections 8-12-7W and 9-12-7W showing both V-H and V-V mode. 130
Figure B.4 Soil salinity survey of Sections 20-12-7W and 21-12-7W showing both V-H and V-V mode. 130
Figure B.5 Soil salinity survey of Section 29-12-7W showing both V-H and V-V mode. 131
Figure B.6 Soil salinity survey of Section 8-13-7W showing both V-H and V-V mode 131

List of Abbreviations

AET	Actual Evapotranspiration
ATV	All-Terrain Vehicle
Da	Deadhorse Silty Clay
Dc	Deadhorse Clay Loam
Df	Dugas Clay
EC	Electrical Conductivity
EC_a	Apparent Conductivity
EC_e	Saturated Paste Extract
EC_w	Pore-Water Salinity
ER	Electrical Resitivity
EMI	Electrical Magnetic Induction
FDM	Finite Difference Model
FEM	Finite Element Model
Ga	Gnadenthal Loam
GIS	Geographic Information Systems
GPR	Ground Penetrating Radar
Hb	Hochfield Fine Sandy Loam
H-H	Horizontal transmitter coil-axis and horizontal receiver coil-axis configuration
K	Hydraulic Conductivity
LIN	Low Induction Number
MAE	Mean Absolute Error
ME	Mean Error
Mo	Morris Clay
Nc	Nuenberg Loam
Ne	Neuhorst Silty Clay Loam
NSE	Nash-Sutcliffe Model Efficiency
Oc	Osborne Clay
θ_v	Volumetric Soil Water Content
θ_g	Gravimetric Soil Water Content

φ	Porosity
Pa	Plum Coulee Clay
PET	Potential Evapotranspiration
ppm	Parts Per Million
ρ_b	Bulk Density
ρ_g	Average Particle Density
ρ_w	Water Density
r^2	Pearson Coefficient of Determination
Ra	Reinland Fine Sandy Loam
Rr	Red River Clay
Rr-Mo	Red River - Morris Osborne Clay
Rrs	Red River Clay (Saline Phase)
RMSE	Root Mean Squared
SAR	Sodium Adsorption Ratio
S	Saturation Percentage
SP	Standpipe
Sr	Water Saturation
SWE	Snow Water Equivalent
TDS	Total Dissolved Solids
V-H	Vertical transmitter coil-axis and horizontal receiver coil-axis configuration
V-V	Vertical transmitter coil-axis and vertical receiver coil axis configuration
Wi	Willowbend Loamy Fine Sand to Clay Loam

1 Introduction

1.1 Overview

The risk of flooding in Manitoba is a critical problem that many face every spring. To help mitigate this risk various pieces of flood protection infrastructure have been constructed by the Province of Manitoba. Some of these structures include the Red River Floodway, the Shellmouth Dam, and the Portage Diversion. The Portage Diversion is a critical component of Manitoba's flood protection infrastructure that protects areas from flooding from Portage la Prairie to Winnipeg, Manitoba. It is located 2 km west of Portage la Prairie, Manitoba (Figure 1.1).

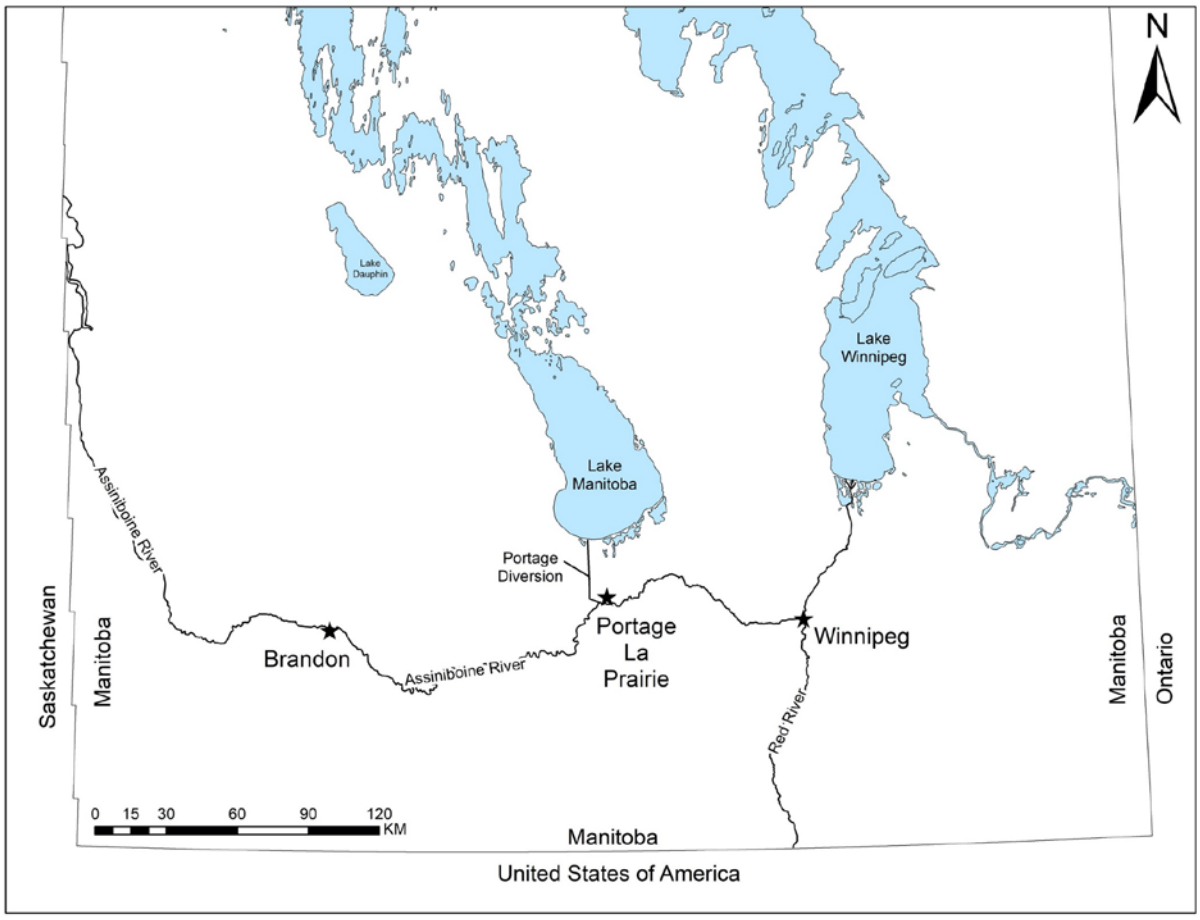

Figure 1.1 Geographical map of southern Manitoba showing the location of the Portage Diversion.

The Portage Diversion was constructed between 1965 and 1970 and is situated on an alluvial fan that generally slopes to the north. It is approximately 29 km in length and consists of an inlet structure, two drop structures to control flow velocity within the diversion, a failsafe location on the west dike, and an outlet structure which is located on the southern shore of Lake Manitoba. The width of the diversion varies along its length but generally ranges from approximately 190 m to 365 m (crest to crest) with the height of the dikes ranging from approximately 2.5 m to 4 m. A sample cross-section is given in Figure 1.2. Within the centre of the diversion is a low flow (pilot) channel that extends up to 3 m in to the subsurface. This channel was designed to aid the flow of water as well as to provide a source of clean water for irrigation. The diversion was designed to convey a maximum flow rate of 708 m^3/s of water. The Portage Diversion has operated 39 times in the past 50 years (Figure 1.3), most notably in both 2011 and 2014 when it operated above its original design capacity.

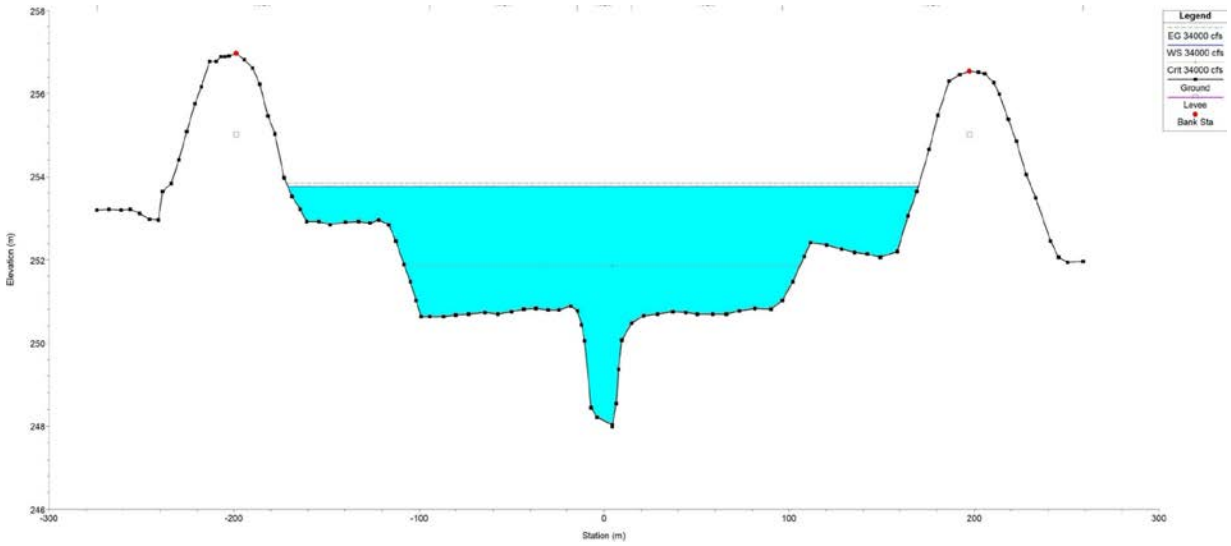

Figure 1.2 An example cross-section from the Portage Diversion at STA. 15+200 (Hatch Ltd. 2015).

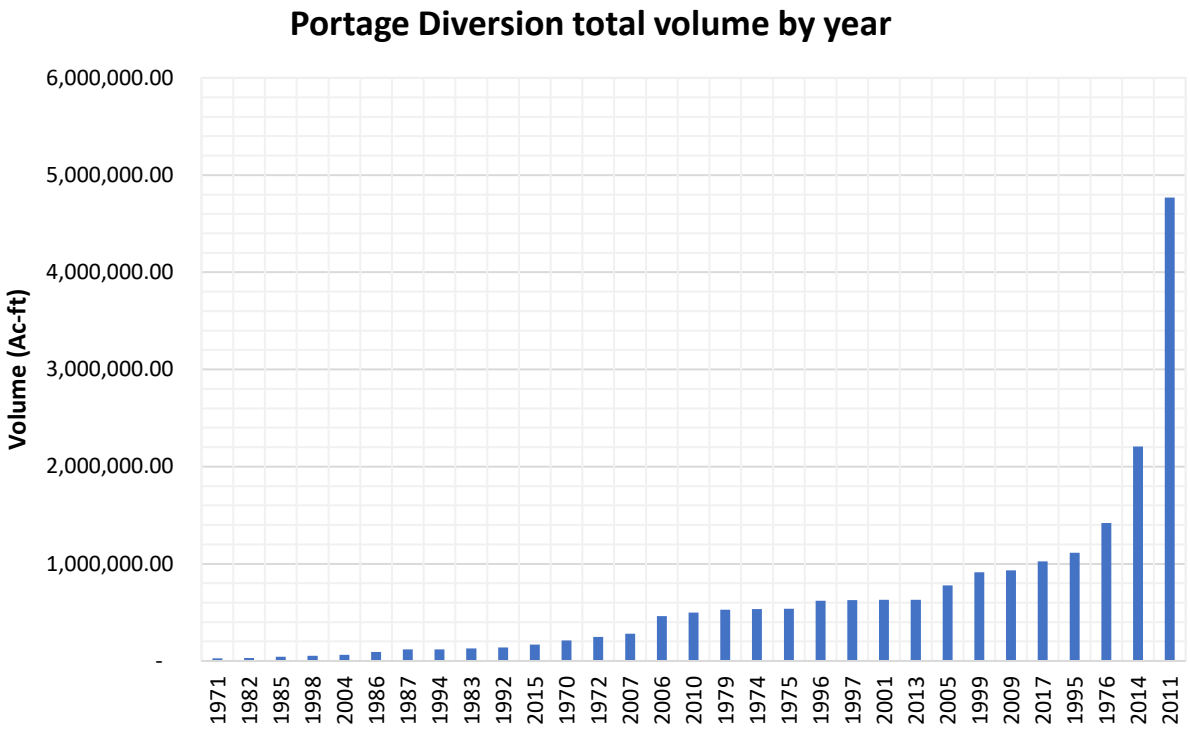

Figure 1.3 Select Portage Diversion flood events by volume of water (Hydata 2020)

Prior to the construction of the Portage Diversion some of the local producers were concerned that its operation could potentially result in increases in soil salinity within fields that did not have existing soil salinity issues (Gilliland 1965). As such, the canal was constructed on a route which passed over less permeable soils (relative to other proposed routes) to limit seepage during operation. It was also intended to be operated only in the spring when the surficial soils would be frozen, limiting seepage. Despite this routing, agricultural producers have reported that soil salinity within the lands near the Diversion has increased.

In other areas of the country and around the world, there have been well-documented cases where irrigation canals and ditches have been a direct or indirect cause of increased soil salinity through various processes (e.g. Joshi and Agnihotri 1984; Chang et al. 1985; Skarie et al. 1986; Hollanders et al. 2005; Araki et al. 2011). Some of these processes include seepage, constant soil saturation, and saline groundwater use due to a lack of available irrigation water within the canal (Araki et al. 2011; Chang et al. 1985; Hollanders et al. 2005; Joshi and Agnihotri 1984). In essence, irritation canals and ditches are similar to the Portage Diversion just at a smaller scale. The general scope of this thesis is to conduct a soil salinity survey on the fields adjacent to the Portage

Diversion, evaluate the effect that the Diversion has had on adjacent agricultural fields, and determine possible sources of salinity if possible.

1.2 Scope of work

The scope of this project is to examine the effect that the Portage Diversion has on groundwater and soil salinity on the adjacent agricultural lands (i.e. <2.5 km from the Dikes). Electromagnetic induction surveys were conducted on 14 fields near the Portage Diversion (shown in Appendix A). Soil samples were taken and analyzed for salinity to generate salinity. Using the soil sample analyses, we further investigated the relationship between apparent conductivity (ECa), saturated paste extract (EC_e), and moisture content. Guided by the data from the electromagnetic induction surveys, a series of monitoring wells were installed as transects around the Portage Diversion to determine its effects on adjacent agricultural lands. Groundwater levels were monitored continuously and water samples taken seasonally to analyze for salinity. Using the collected data, a groundwater model was developed to determine the influence the Portage Diversion had on the local groundwater table elevation and salinity.

1.3 Objective

The main objective of this research is to determine if the Portage Diversion has had an impact on the adjacent agricultural lands and caused an increase in soil salinity.

1.3.1 Research question – What are the effects of salinity and water content on apparent conductivity in an alluvial setting in the Canadian prairies?

- Conduct extensive electromagnetic induction surveys over 14 areas and characterize areas of salinization.
- Investigate the relationship between EC_a, EC_e, soil salinity, and moisture content.

1.3.2 Research question – What is the impact of a drainage canal on piezometric levels and soil salinity in adjacent agricultural lands?

- Conduct a hydrogeological investigation into piezometric levels in the fields near the Portage Diversion.
- Create a 3D groundwater model using FEFlow 7.0 to investigate the Portage Diversion's influence on an adjacent agricultural field.

1.4 Thesis outline

This thesis consists of six chapters, two of which are manuscript chapters. Chapter 1 is an introductory chapter that describes the objectives and research questions of the work. Chapter 2 is a literature review that consists of various topics related to the thesis. Chapters 3 and 4 are modified version of manuscripts. Chapter 3 specifically discusses the relationship between EC_a, EC_e, and moisture content. It also examines the various sites which were analyzed using electromagnetic induction, and includes additional information, that was excluded from the manuscript due to confidentiality restrictions. The additional information includes soil salinity maps and other data pertaining to individual sites. Chapter 4 presents a groundwater monitoring and analysis program, the analyses included in situ aquifer testing and chemical analysis. Chapter 4 also includes groundwater modelling scenario to predict the effect of the Portage Diversion on one agricultural field. Chapter 5 concludes the thesis with the overall outcomes of the project. Chapter 6 presents recommendations for future work and research.

2 Literature review

2.1 Effects of salinity and water content on apparent conductivity in an alluvial setting in the Canadian prairies

2.1.1 The Portage la Prairie alluvial fan

The headwaters for the Assiniboine River are located in eastern Saskatchewan, after which the river meanders its way through Manitoba until it merges with the Red River in Winnipeg, Manitoba. Rannie et al. (1989) examined the form of meanders in the Portage la Prairie and determined that during the Holocene epoch, the path of the river had varied significantly. The rivers path has changed eight times in the last 7000 years, with three paths resulting in the river flowing into Lake Manitoba. These paths were defined as the Willowbend Phase (~ 7000 years ago), Flee Island Phase (7000 – 4500 years ago), and the Blind Phase (~ 4500 years ago). In addition to examining the meanders of the Assiniboine River, Rannie et al. (1989) carbon-dated material recovered from the subsurface within the former meanders to determine the approximate age of each phase. The general direction and ages of the phases are shown Figure 2.1. Due to the migration in paths of the Assiniboine River, a large alluvial fan formed at the base of the Manitoba escarpment with a diameter of 30-45 km (Rannie et al. 1989).

Stratigraphically, the study area is complex and consists of an alluvial fan deposit that ranges in thickness from 1.5 to 7.5 m that overlies glaciolacustrine clay, various offshore silts and clays, deltaic sands, as well as till units and both stratified and undifferentiated drift (Cherry et al. 1971; Fenton 1970; Fenton and Anderson 1971; Gilliland 1965). The surficial geology of the region is illustrated in Figure 2.2; further subsurface detail is given in Figure 2.3. The depth to till within the region varies greatly with the till surface consisting of a series of ridges and valleys with surface elevations ranging from 243 m to 225 m (Gilliland 1965). The underlying drift ranges from 27 to 92 m thick and consists of a lower stratified unit, that consists of interbedded sand, silt, and clay as well as an undifferentiated unit which consists of interbedded till and stratified sediment (Fenton 1970; Fenton and Anderson 1971). The bedrock within the area consists of the gypsum/anhydrite rich Amaranth formation and Devonian carbonates. Depth to bedrock has been reported to range in depth from 36 to 61 m (Gilliland 1965).

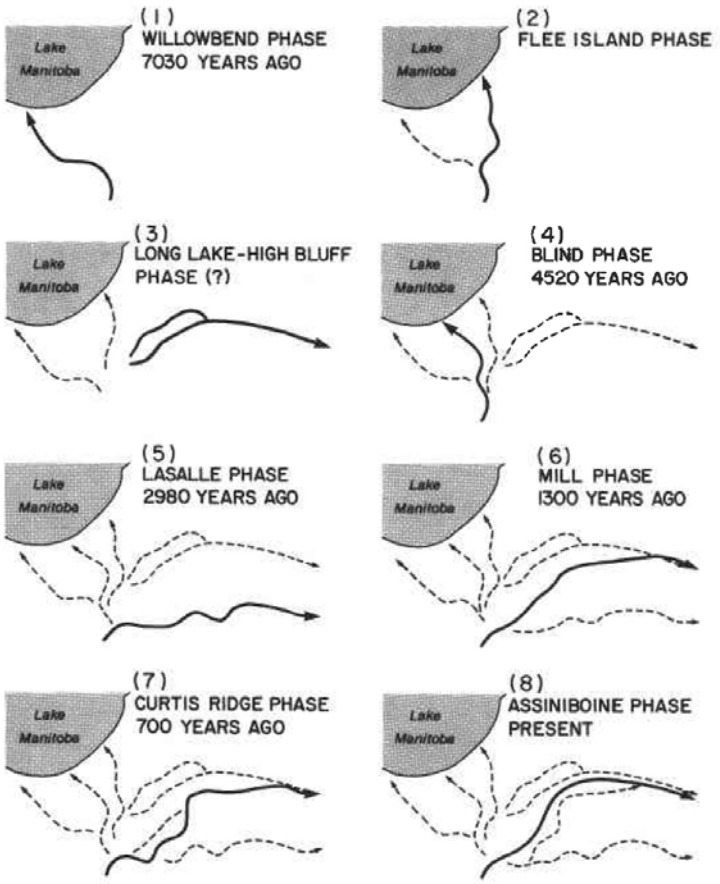

Figure 2.1 The evolution of the Assiniboine River other the past 7030 years (Rannie et al. 1989) SOURCE: Republished with permission of Canadian Science Publishing, from: Holocene evolution of the Assiniboine River paleochannels and Portage la Prairie alluvial fan, Rannie, W. F., Thorleifson, L. H., and Teller, J. T., volume 26, issue 9, ©1989. Permission conveyed through Copyright Clearance Center, Inc.

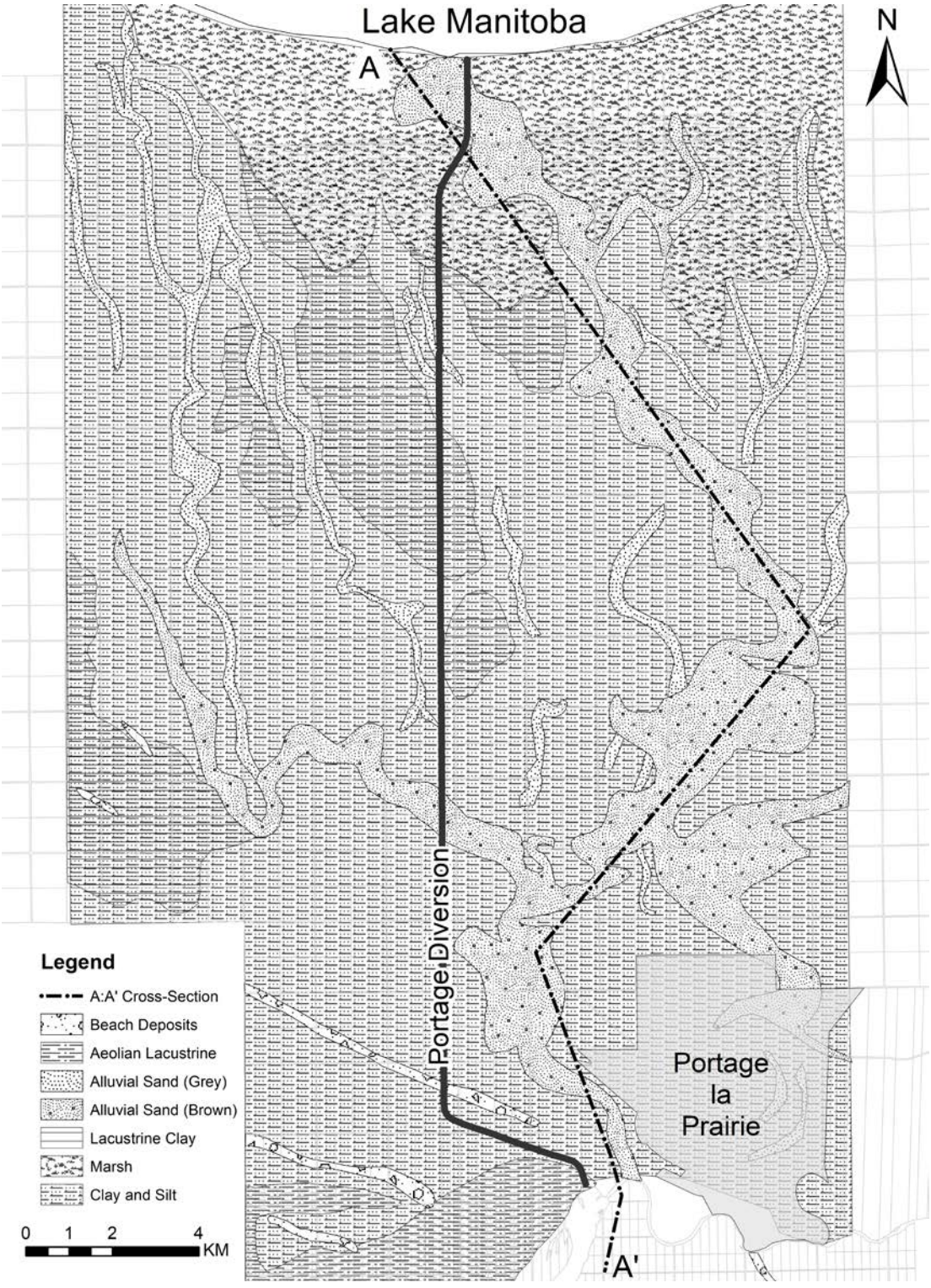

Figure 2.2 Surficial geology map of the study region (Adapted from: Gilliland 1965).

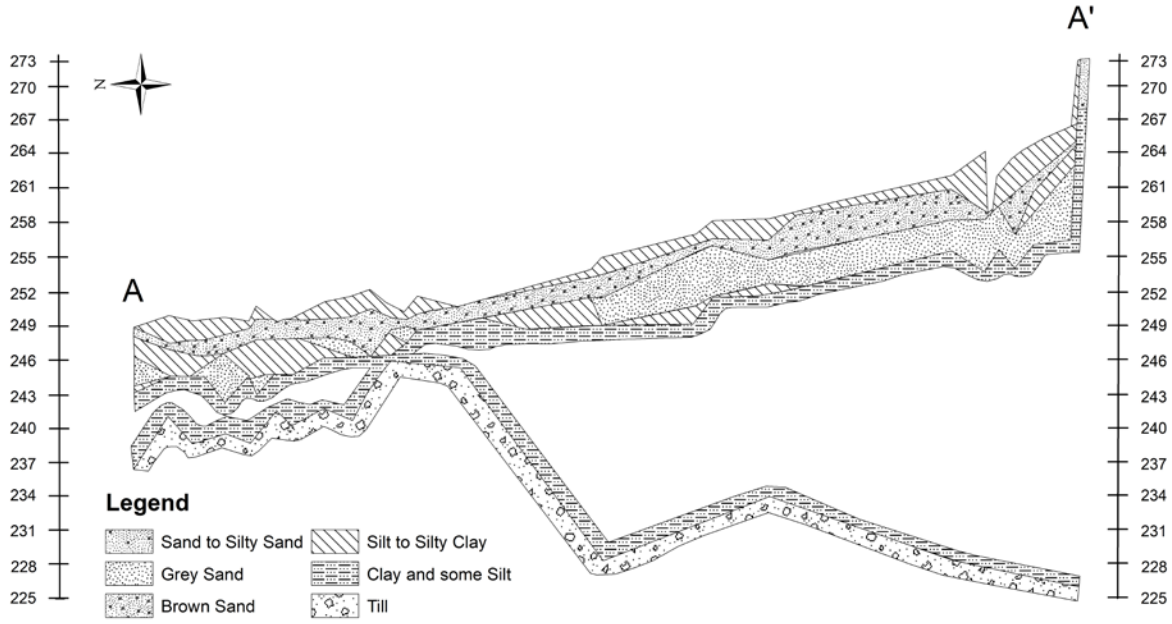

Figure 2.3 Geologic cross-section of the study region from A:A' which is denoted in Figure 2.2 (Adapted from: Gilliland 1965).

2.1.2 Soil types within the study area

The surficial soils in the study area consist of mainly low permeability clays and silts. However, in the areas near the historic tributaries, the stratigraphy becomes more complex and typically consists of a combination of silty or sandy loams, and sand units deposited by historical tributaries (Gilliland 1965; Michalyna and Smith 1972). Generally, the surficial soils are considered flat, with a slope of <2% over the area, and are poor to imperfectly drained (Manitoba Land Resource Unit 1997; Michalyna and Smith 1972). A summary of the common soil types within the study area is given in Table 2.1 and the soils are displayed in Figure 2.4. A full description and analysis of the soils provided in Michalyna and Smith (1972).

In addition to mapping soil location, texture, and chemical features, Michalyna and Smith (1972) also mapped and classified each soil type on the basis of irrigation suitability (Figure 2.5). They classified the soils into four irrigation suitability classes based on the physical, chemical, and other irrigation specific properties. Class 1 soils include fine sandy loam to clay loam textured soils that have good permeability, good water holding capacity, low salt content, low piezometric levels, and good drainage. Class 2 soils include loamy fine sand to clay soils with slight limitations on with respect to the properties listed for class 1. Class 3 soils include sand to permeable clay

textured soils with further issues regarding the irrigation properties, and class 4 soils are considered unsuitable for irrigation due to severe limitations of the properties described above.

Table 2.1 Summary of soil types in the study areas (Michalyna and Smith 1972).

Symbol	Soil Name	Texture	Drainage	Irrigation Class	Conductivity (dS m^{-1})
Da	Deadhorse	Clay	Imperfect	4	1.63
Dc	Deadhorse	Clay Loam	Imperfect	4	1.63
Df	Dugas	Clay	Imperfect	3	1.45
Ga	Gnadenthal	Loam	Imperfect	1	0.80
Hb	Hochfield	Fine Sandy Loam	Moderately Good	2	0.30
Mo	Morris	Clay	Imperfect	4	2.13
Nc	Nuenberg	Loam	Imperfect	1	0.63
Ne	Neuhorst	Clay Loam	Imperfect	2	0.96
Oc	Osborne	Clay	Poor	4	1.13
Pa	Plum Coulee	Clay	Imperfect	4	0.78
Ra	Reinland	Fine Sandy Loam	Imperfect	2	0.45
Rr	Red River	Clay	Imperfect	4	0.60
Wi	Willowbend	Loamy Fine Sand to Clay Loam	Poor	4	0.35

Note: Conductivity values are averaged up to a soil profile depth of 120 cm and are available in Michalyna and Smith (1972).

2.1.3 Salinization processes

Changes in soil salinity can be categorized into two different processes: natural and anthropogenic, or primary and secondary. Primary salinization occurs due to natural processes such as constant upwards flow from a saline aquifer. Such instances have been documented along Lake Manitoba's west side (Grasby 2000), where saline waters occur at the surface. Within the study region, Gilliand (1965) reported a similar situation that occurs within approximately 6.5 kilometres of Lake Manitoba, where the piezometric head within the saline bedrock aquifer exceeds that of the overburden aquifer. It would be expected that the groundwater quality north of that transition point would decline due to increasing salt content (Gilliland 1965).

Secondary salinity is defined as human-induced salinity and has been described by (Henry et al. 1987) as being more related to the soils than the water quality. The reasoning for this is that many saline areas result from a water table within two metres of the surface in soils with ineffective drainage (Carter 1982; Henry et al. 1987; Steppuhn 2013). If the soils are poorly drained, processes such as the capillary rise and evapotranspiration will accumulate salts within the profile (Carter 1982; Henry et al. 1987; McFarlane et al. 2016; Steppuhn 2013). Within the study region, the soil types have been defined by Michalyna and Smith (1972) as being well-drained to poorly drained. However, only eight soil classes have been defined as well-drained, and these soils are not common within the study areas. The majority of the soil types within the study areas are classified as being

imperfectly drained. If these soils are not properly managed, they may be more susceptible to salinization (Michalyna and Smith 1972).

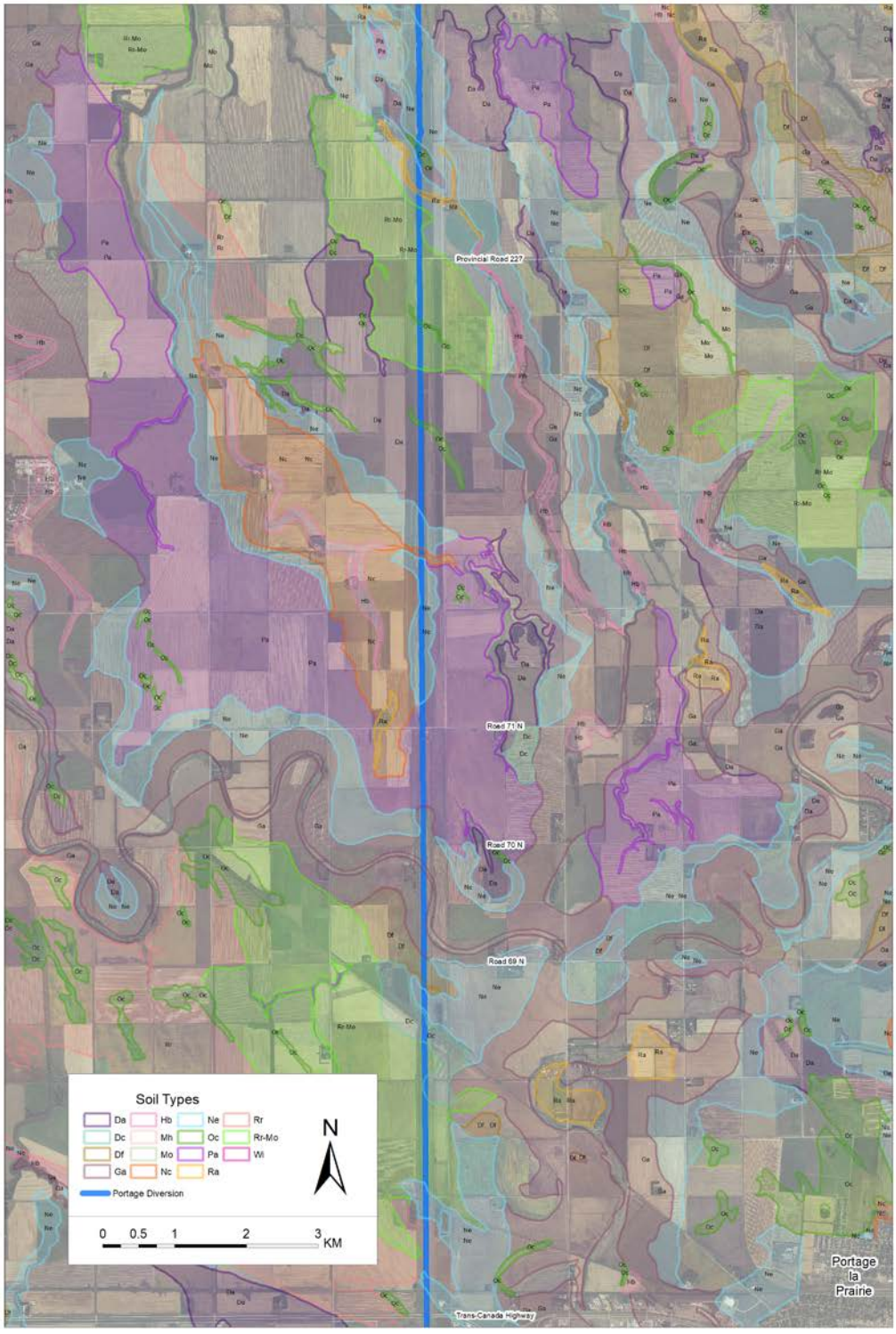

Figure 2.4 Soils map of the study region (adapted from: Michalyna and Smith 1972).

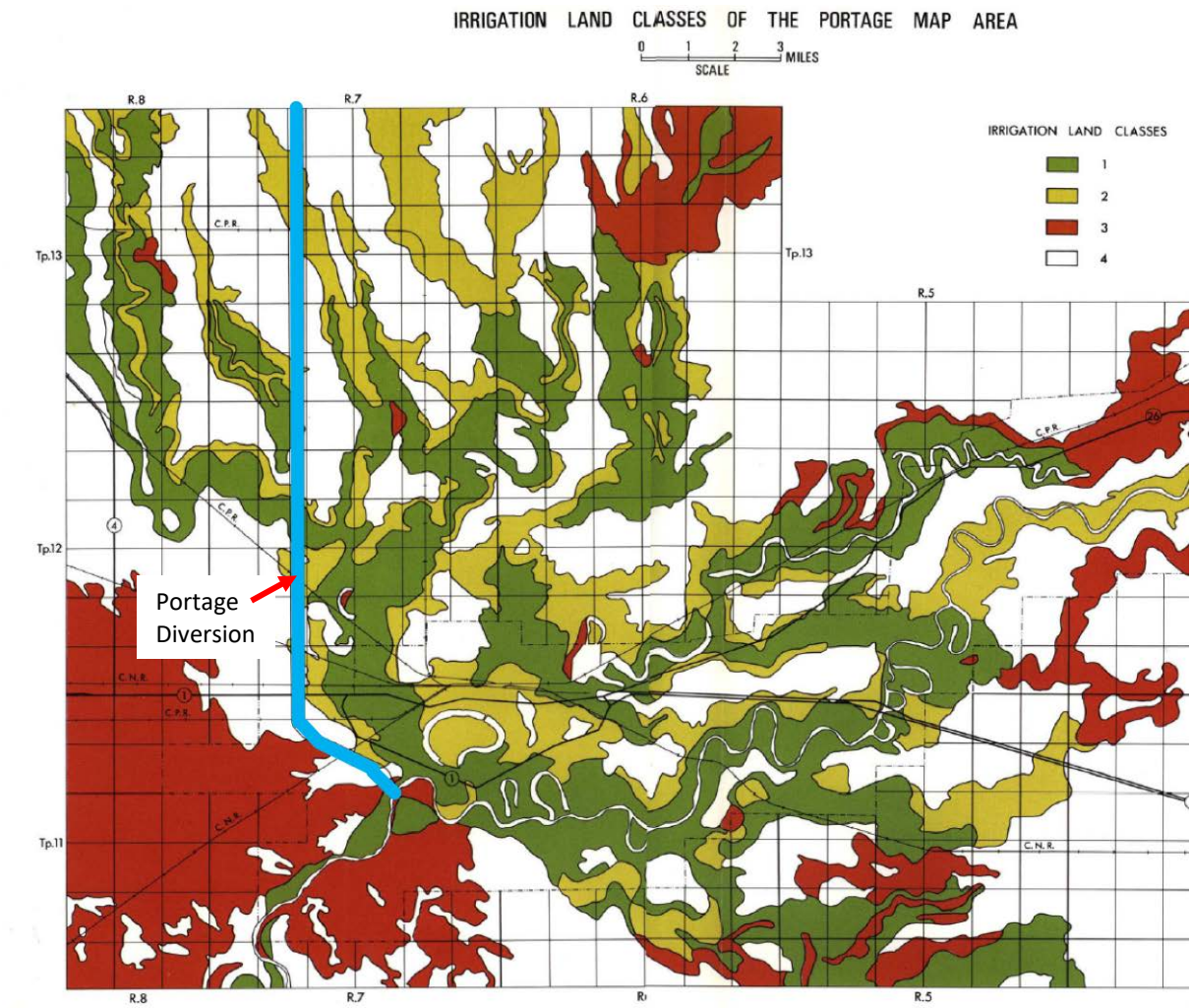

Figure 2.5 Irrigation suitability of the soils within the study region, where irrigation classes 1 and 2 are most suitable for irrigation and classes 3 and 4 are least to unsuitable for irrigation (Michalyna and Smith 1972).

Two examples of secondary salinity sources are excessive irrigation (Lekakis and Antonopoulos 2015; McFarlane et al. 2016; Rhoades et al. 1997), and the removal of deep-rooted perennial vegetation for shallow-rooted crops (Clarke et al. 2002). Excessive irrigation in soils that do not adequately drain can cause an elevated water table that can be susceptible to capillary rise and evapotranspiration (as described above), which are well-understood processes. This issue is further exaggerated in areas where fresh surface water is not present, and poor-quality groundwater is used for irrigation (Latif and Ahmad 2009). Another common problem is the removal of deep-rooted vegetation for shallow-rooted crops. This has been known to cause excess salinization in locations such as in southwest Australia (Clarke et al. 2002) and Alberta, Canada (Stein and Schwartz 1990), where the removal of deep-rooted vegetation causes an increase in the availability

of soil moisture, which can impact the water table and allow the accumulation of salts within the soil profile or the rise of a lower saline aquifer (Clarke et al. 2002; Stein and Schwartz 1990). Excess irrigation is not always guaranteed to increase soil salinity. A case study conducted by Schwartz et al. (1987) in Alberta, Canada demonstrated the influence that a till unit can have on the drainage of near surface soil units where either having high hydraulic conductivities or low hydraulic conductivity with many fractures will allow adequate drainage if the upper soils have a lower hydraulic conductivity than the till. However, in areas where the till has a low hydraulic conductivity and limited fractures, a perched water table can develop and influence soil salinity (Schwartz et al. 1987, 1982).

2.1.4 Socio-economic and seepage impacts of irrigation canals and ditches

There have been a large number of studies of the effects of irrigation canals, ditches and rivers on adjacent agricultural fields reported in the literature (e.g. Joshi and Agnihotri 1984; Skarie et al. 1986; Hollanders et al. 2005; Araki et al. 2011). Irrigation canals can have both a positive and negative effect on adjacent lands. They can provide much needed clean water for irrigation. However, they can also cause various adverse effects due to seepage and poor irrigation practices, which can lead to high water tables in soils that do not adequately drain (Araki et al. 2011; Hollanders et al. 2005; Joshi and Agnihotri 1984; Morway et al. 2013). Irrigation canals can have negative economic effects and adverse effects on local soil quality. Joshi and Agnihotri (1984) suggests that there may be adverse costs to society, changes in productivity, loss of productivity, and may introduce invasive weeds and disease. Akram and Mendelsohn (2017) investigated the water allocation efficiency in a region of Pakistan and determined that irrigation canals are often inefficient and that agricultural producers near the head of the canal may take too much water leaving those downstream with an inadequate supply. The findings of Akram and Mendelsohn (2017) were consistent with those of Latif and Ahmad (2009) also demonstrated that water availability within an irrigation canal can be correlated with increases in soil salinity because closer to the tail of the canal inadequate water supply may result in the agricultural producer using saline groundwater.

Seepage from irrigation canals and rivers can also have negative consequences. Canal seepage can account for loss of available water for the producers. Fernald and Guldan (2006) found that a minimum of 5% of available water was lost through seepage into the adjacent agricultural

fields. However, they theorized that this seepage may also be beneficial in certain situations including the recharge of shallow wells, and dilution of agricultural chemicals or septic leachate. They did fail to mention that this seepage could increase soil salinity through the processes described in section 2.1.3. Other studies have determined that seepage from irrigation canals and ditches can cause increases in soil salinity in adjacent lands, which can lead to reductions in crop yields due to waterlogging, extensive capillary rise, and evapotranspiration (e.g. Joshi and Agnihotri 1984; Chang et al. 1985; Skarie et al. 1986; Araki et al. 2011). Chang et al. (1985) showed that irrigation canals in Alberta, Canada, can increase soil salinity at great distances from the canal and that soil texture was the primary control on the lateral extent. However, after identification of the seepage, many of the canals were lined to mitigate the process. A study by Iqbal et al. (2002) examined the seepage losses of some of the canals within the same area studied by (Chang et al. 1985) after the lining and determined that seepage loss had become negligible. This result demonstrates the efficacy of lining water conveying structures.

Increases in soil salinity due to seepage is not only confined to irrigation canals but can also be attributed to structures as simple as shallow roadside ditches which collect surface runoff, and due to improper drainage the ponded water may seep into the adjacent agricultural fields (Skarie et al. 1986). While ditches can cause issues with adjacent lands we must also consider the positive aspects of them which are primarily for improved agricultural drainage and on a larger scale, flood protection. Improved surficial drainage is essential for increased crop production, decreases crop damage due to wet field conditions. According to (Manitoba Agriculture Food and Rural Initiatives 2008) decreases in crop yields of wheat, oats, barley, and flax by an average of 14, 18, 23, and 4 bu/ac can be expected if excess water is not controlled.

On a larger scale when a flood protection ditch such as a river diversion channel, i.e. the Portage Diversion, non-agricultural benefits must be considered, such as the protection of life and property. Manitoba has an abundance of water especially during spring run off, which has led to numerous large flooding events, most notably the floods of 1826, 1852, 1861, 1950, and 1997 on the Red River, and 1976, 1882, 2014, and 2011 on the Assiniboine River (Westdal et al. 2015). For the years prior to the development of any major flood protection infrastructure (such as the Portage Diversion or Red River Floodway) significant damages occurred during most high water events. For example, the flood of 1826 forced the relocation of the Upper Fort Garry Settlement to the Lower Fort Garry Settlement, the flood of 1950 flooded areas within the Winnipeg city

limits (i.e. Scotia Heights and old St. Vital). On the Assiniboine River, the flood of 1882 caused widespread agricultural damages to the extent that the Manitoba Legislative Assembly created a committee to study the widespread flooding effects along the Assiniboine River (Manitoba Infrastructure and Transportation 2013). The damage caused by these floods clearly demonstrate both the significance and importance of flood protection infrastructure.

2.1.5 Geophysical techniques in agriculture

Geophysical analysis within agriculture typically consists of three types of surveys: electrical resistivity (ER), ground-penetrating radar, and electromagnetic induction and time domain reflectometry (Allred et al. 2008). This section will give a brief overview of both the resistivity and ground-penetrating radar techniques. A more detailed discussion of the EM technique is shown below in section 2.1.5.1. The ER technique measures the resistivity (the inverse of electrical conductivity) of a bulk volume of soil (Allred et al. 2008). The technique has been described by Corwin and Scudiero (2019) as an invasive technique that requires good contact between the electrodes and the soil (though in reality produces very little disturbance of the sub-surface). The accuracy of the measurements can be influenced by the dryness of the soil, stoniness of the soil, poor electrode to soil contact, and in more northern regions, frost in the soils. Electrical resistivity has been successfully used in various studies such as monitoring soil-water relationships in vineyards (Brillante et al. 2014), monitoring soil-water relationships on hillsides (Calamita et al. 2012), and monitoring soil salinity (Allred et al. 2008; Corwin and Lesch 2005a; Visconti and de Paz 2016). Electrical resistivity is a technique equally well suited to the electromagnetic induction technique to gather data on soil conductivity (Corwin and Lesch 2005a; Corwin and Scudiero 2019).

Calamita et al. (2012) examined the efficacy of monitoring soil moisture using ER methods relative to using time domain reflectometry measurements. They determined a non-linear relationship between soil moisture and resistivity, which is consistent with what others have reported (Brillante et al. 2014). The effectiveness of using ER tomography in soil water relationships was examined by Brillante et al. (2014) in a vineyard. They were able to observe water uptake depending on grapevine water status and preferential water paths within the soil. They also acknowledge that ER tomography is a technique that has rarely been used in agriculture and requires more work.

Ground-penetrating radar (GPR) is a non-invasive technique (Liu et al. 2018) that has various uses within agriculture, including measuring microvariability in soil profiles, bedrock depth determination, plant root biomass surveying, identifying subsurface pathways, and determining soil water content (Allred et al. 2008). A review of numerous studies has indicated that the GPR technique is quite effective when defining soil profiles (Doolittle and Collins 1995; Truman et al. 1988), when used in conjunction with EM surveys an increased resolution can be obtained (Inman et al. 2002), and soil water content (Grote et al. 2003; Lambot et al. 2006). Truman et al. (1988) used GPR to estimate soil water content in and compare results with time-domain reflectometry and gravimetric water content measurements. They determined that GPR can be a useful technique for soil water measurements.

2.1.5.1 Electromagnetic induction in soil salinity

Electromagnetic induction (EMI) is a non-invasive methodology used to measure the electrical conductance of a bulk soil mass directly beneath the instrument (Corwin and Lesch 2005a; Corwin and Scudiero 2019; Visconti and de Paz 2016). The technique has been used in various environments to conduct soil salinity surveys in various environments (Hendrickx et al. 1992; Huang et al. 2017; Saleh et al. 2017; Triantafilis et al. 2000, 2001). Commonly used EM Instruments are the Geonics EM-38 and EM-31, with the EM-38 being mainly used in surficial agricultural mapping (Corwin and Scudiero 2019). The instruments function by using both transmitter and receiving coil which have a fixed seperation. Three common configurations include: the V-V configuration (both coil axes are vertical), H-H configuration (both coil axes are horizontal), and V-H configuration (the transmitter coil is vertical and the receiving coil is horizontal). The EM-38 utilizes 1 transmitter and 1 receiver (spaced 1 m apart) and uses the V-V and H-H configurations, the orientations are shown in Figure 2.6. The orientation and distance between the transmitter and receiving coil dictate the depth of exploration of the instrument. The depth of exploration is defined as the depth above which the material provides a cumulative response is 70% (Abdu et al. 2007) as shown in Figure 2.7.

Due to the fixed arrangement of coils in the EM-38 the instrument can only measure one dipole at a time (Corwin and Lesch 2005a). In order to obtain results for two depth ranges, two passes must be made using different dipole configurations (H-H – 0.75 m exploration depth and the V-V – 1.5 m exploration depth). An alternative instrument to the EM-38 is the DualEM 1S,

which provides simultaneous readings with horizontal and vertical receiver dipoles for a vertical dipole transmitter (Abdu et al. 2007; Urdanoz and Aragüés 2011). The ability of the DualEM 1S to provide simultaneous readings is due to it having 1 transmitter and 2 receivers which exist in the V-V (1.5 m exploration depth) and V-H (0.5 m) configurations. The dipole readings of both the Dual EM 1S and EM-38 represent an average weighted response over the sensed depth (Fitterman and Labson 2005; McNeill 1980).

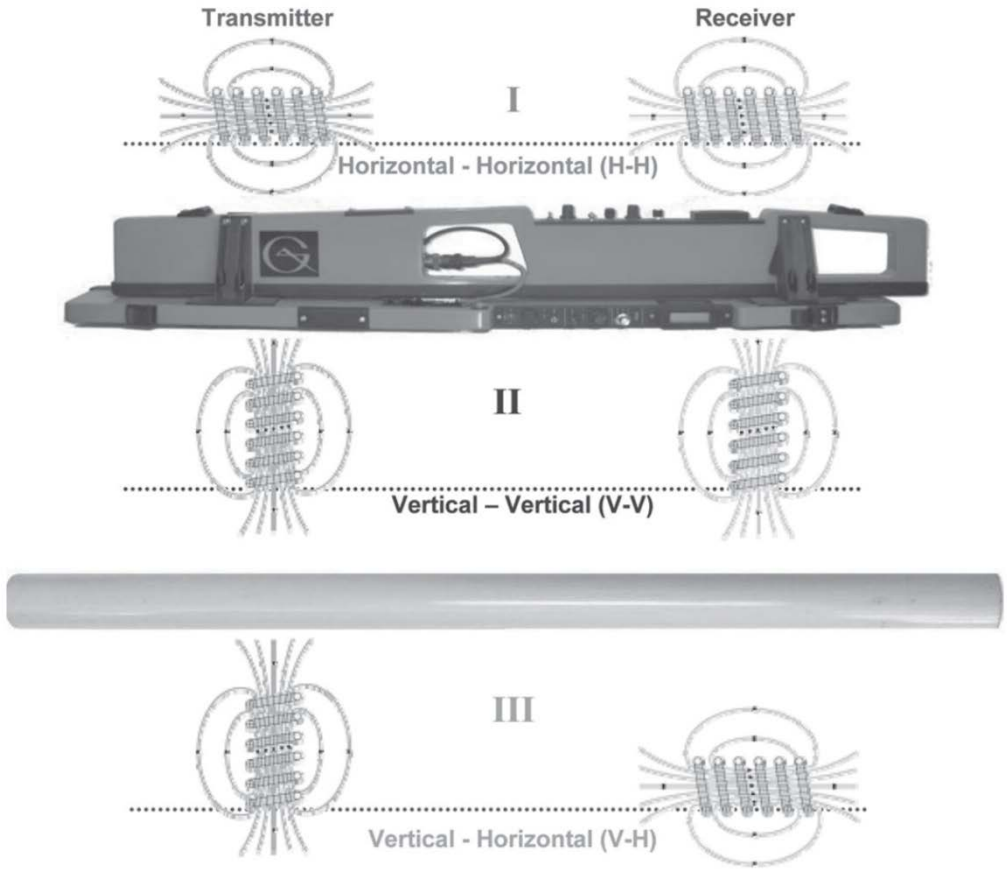

Figure 2.6 Transmitter and receiver orientations for both the Geonics EM-38 and DualEM 1S (Abdu et al. 2007).

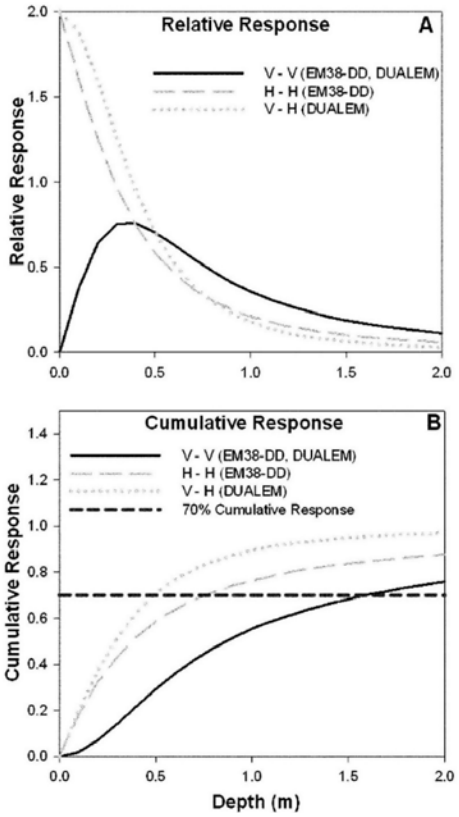

Figure 2.7 A. The relative sensitivity of the EM38 and DualEM; and B. The cumulative response to depth of the EM38 and DualEM orientations (Abdu et al. 2007).

SOURCE: Republished with permission of John Wiley and Sons, from: Comparing bulk soil and electrical conductivity determination using the DUALEM-1S and EM38-DD electromagnetic induction instruments, Abdu, H., Robinson, D. A., and Jones, S. B., volume 71, ©2007. Permission conveyed through Copyright Clearance Center, Inc.

Measurements made by the EM technique are affected by various factors including soil salinity, volumetric water content, pore-water salinity, temperature, organic matter, clay mineralogy, and cation exchange capacity (Cordeiro et al. 2011a, 2011b; Corwin and Scudiero 2019; Sudduth et al. 2003; Visconti and de Paz 2016). These factors control the soil property apparent conductivity (EC_a). The pore water salinity is difficult to characterize without a large number of soil samples from that site (Corwin and Lesch 2005a). In agriculture, the most effective analytical technique to determine soil salinity is to determine the saturated paste extract (EC_e) of each sample (Carter 1982; Gartley 2011; Rhoades 1982; Zhang et al. 2005). However, in certain situations, EC_a alone can be a useful tool to geospatially map fields and to direct soil sampling (Corwin and Lesch 2005a, 2013), EC_a has been successfully used by various studies, including by Johnson et al (2001); Corwin et al (2003); and Fortes et al (2015) as a guide sampling in both soil salinity and irrigation management.

2.1.6 Laboratory techniques to analyze soil conductivity

Soil salinity is the dissolved salt content within soil or water (Sonmez et al. 2008) and can be measured in a variety of ways including the saturated paste extract method which has been regarded as the most accurate and effective technique (Carter 1982; Carter and Gregorich 2008; Gartley 2011; Rhoades 1982; Sonmez et al. 2008; Zhang et al. 2005). This technique approximates the lowest soil-water ratio at which an extract can be sampled. This is ideal as different soil types have different water-holding capacities (Carter and Gregorich 2008). The saturated paste method is described in Rhoades (1996) and Carter and Gregorich (2008). It consists of air drying a 200-400g sample of known water content, adding distilled water the soil and stirring until a paste is formed, leaving the sample to sit for several hours and then extracting a water sample under suction which is analyzed using a conductivity meter. Due to the time and skill involved with the methodology, many laboratories have begun using a fixed ratio methodology (Sonmez et al. 2008). The standard ratios are 1:1, 1:2.5, 1:5, and 1:10 (Carter and Gregorich 2008; Rhoades 1996; Sonmez et al. 2008). The fixed ratio methodology was tested by Sonmez et al. (2008). They salinized sandy, loamy, and clay textured soils over the period of one month using deionized water, tap water, and by adding various amounts of NaCl, KCl, and $CaCl_2$ to tap water to achieve solutions with conductivities of 2, 4, 8, and 16 dS/m. They determined that there is a two-fold dilution factor when soil ratios are increased two-fold; it was noted that this is consistent with the results of Zhang et al (2005).

One of the issues that was not discussed in Sonmez et al (2008) was the effect of sulphate salinity when comparing the fixed ratio method versus the saturated paste method. However, the dissolution effects of gypsum rich soils on the fixed ratio are discussed in Rhoades (1996) as well as Carter and Gregorich (2008). They determined that when using the fixed ratio method, the additional water added beyond saturation will cause additional gypsum to dissolve and overestimate the true soluble salt content of the sample. This phenomenon was also observed by Callaghan et al. (2016) when using the saturated paste method with gypsum bearing soils. However, the saturated paste method uses the lowest soil-water ratio which theoretically should dissolve less gypsum than a fixed ratio method, it was for this reason that the saturated paste method was chosen for the soil analysis.

2.2 The impact of a drainage canal on piezometric levels and soil salinity in adjacent agricultural lands

2.2.1 Model types

A model has been defined by Wang and Anderson (1995) as a tool that can simplify reality and if properly constructed can be a valuable predictive tool. Two common model types are: finite difference models (FDM) and finite element models (FEM), each of these model types are defined by cell shape, and node location (Anderson et al. 2015; Wang and Anderson 1995) where an FDM consists of cubic cells with a single node in the center and a FEM consists of triangular cells with a node on each point (Wang and Anderson 1995). All numerical groundwater models use partial differential equations to describe flow within a porous media (Ashraf and Ahmad 2008). There are many groundwater model software available for use, some commons ones are MODFlow (FDM), FEFlow (FEM), and Hydrus (FEM).

All of the models listed above are capable of modelling both saturated and unsaturated/variably saturated models, with the exception of MODFlow which requires the unsaturated zone package to be installed. Flow through porous media is governed by the combination of Darcys Law and the mass conservation principle. From this, fully-saturated models derive linear equations, and unsaturated/variably saturated models derive non-linear equations (Cattaneo et al. 2016). Simulating flow through unsaturated/variably saturated media is computed by solving the Richards equation (Simunek et al. 2012):

$$\frac{\partial \theta}{\partial t} = \frac{\partial}{\partial x_i}\left[K\left(K_{ij}^{A}\frac{\partial h}{\partial x_j} + K_{iz}^{A}\right)\right] - S \qquad \text{Eq. 2.1}$$

where, h is defined as the pressure head, t is time, θ is volumetric water content, K_{iz}^{A} are components of a dimensionless anisotropy tensor K^A, and K is hydraulic conductivity.

Within equation 2.1, soil water retention θ(h) and hydraulic conductivity K(h) are unsaturated soil properties and are non-linear functions related to pressure head (Simunek et al. 2012). Common analytical techniques for the hydraulic properties, specifically soil water retention, have been defined by various authors including Brooks and Corey (1964), van Genuchten (1980) who used the pore size distribution model described by (Mualem 1976). Vogel and Cislerova (1988) modified the equation by van Genuchten (1980) to allow hydraulic properties

to be near saturation. The Brooks and Corey (1964) equation assumes that an entry pressure is present whereas the van Genuchten (1980) does not, but assumes that there is at least one connected pore pathway that is large enough to negate the entry pressure (Gershenzon et al. 2016).

Determining which soil water retention model to use is based on modeller preference and desired model outcome. However, one of the issues that is common with unsaturated/variably saturated models is model stability and numerical complication. This is a place where the equation by van Genuchten (1980) may be advantageous as it has additional empirical fitting parameters which are not available with Brooks and Corey (1964) equation.

2.2.2 Modelling with data scarcity

Any model is designed with the purpose of being able to replicate and simulate events through calibration and validation processes. Typically, the modeller will use observed data to calibrate the model. A common issue that the modeller may encounter is that there may be insufficient data to adequately develop, calibrate, and validate the model (Switzman et al. 2015). To overcome this issue Switzman et al (2015) utilized a combination of historical regional data, and sparsely locally collected data, and made assumptions on climate, water levels, and discretization. In Rosenthal et al. (1992) a 10 000 km^2 area, which only contained six poorly documented monitoring wells, with virtually no information the regional subsurface geology in the area, was analyzed following the observation of increasing soil salinization. For model generation they inferred stratigraphy from outcrops, deep seated oil wells, and seismic data. Using this technique they determined that the source of brackish water which was different to previous studies.

The value of conducting a sensitivity analysis was demonstrated by Ndomba et al (2008) who used observed and estimated flow data to identify previously unknown important parameters for the model scenario. In another study it was demonstrated that using multiple model parameterizations was more effective than using a simple water balance model when dealing with complex systems involving a lake such as Lake Naivasha, where the lake's exit is through subsurface leakage (Hogeboom et al. 2015).

When modelling with scarce data, the experience and knowledge of the modeller can have a large effect on the results. This was demonstrated by Holländer et al. (2009) where the discharge of an artificial catchment was modeled by ten different modellers using ten different models.

Certain data was withheld within the study, such as discharge values, and certain initial conditions were not properly defined such as volumetric water content. There was a large variation of results between the modellers, demonstrating the importance of the experience and knowledge of the modeller. Similar to the study of Rosenthal et al (1992), who utilized multiple techniques to manage data scarcity, Holländer et al (2016) used multiple techniques to predict recharge estimations in British Columbia using a Hydrus 1D variably saturated model, low cost weather stations, and both soil moisture and temperature data was collected using remote sensors.

The value of using Geographic Information Systems (GIS) within data scarce environments has been shown to be effective in catchment models (Jain et al. 2004), and in rainfall run off modelling when coupled with surface models such as MIKE-Basin and MIKE 11 (Ireson et al. 2006). The results of the rainfall runoff model by Ireson et al. (2006) were further used in multiple aquifer models. One important note made by Ireson et al. (2006) was that while GIS based models can be effective, if the data scarcity is too great, then the model may become ineffective.

3 Effects of salinity and water content on apparent conductivity in an alluvial setting in the Canadian prairies

3.1 Contribution of authors

Jerrold Rentz, P. Geo: Was responsible for collection of all field data, all calculations, creating the first draft of the manuscript, assist in generation of the final copy, answering of reviewers questions, the generation of all salinity maps, and interpretation of the EM Maps.

Dr. Ranjan Sri Ranjan, P. Eng: assisted with initial calculations, interpretations of salinity maps, and reviewing the final copy of the manuscript.

Dr. Ian Ferguson, P.Geo, FGC: Was responsible for expanding upon the first draft and generation of the final copy of the manuscript, answering of the reviewer's questions, the generation of the figures within the article, guidance with geophysical techniques and analysis.

Dr. Hartmut Holländer, P. Eng: assisted with analyzing groundwater chemistry and reviewing the final copy of the manuscript.

3.2 Introductory statement

This chapter of the thesis consists of a combination of materials, including a manuscript titled "Effects of Salinity and Water Content on Apparent Conductivity in an Alluvial Setting on the Canadian Prairies" which has been accepted by the Journal of Environmental Earth Sciences. Additional information that was not provided in the manuscript including details from individual study sites and material that not included in the manuscript due to confidentiality restrictions is included within this chapter. The additional material was prepared exclusively by the Thesis Candidate, and to properly incorporate this information the order of the results were slightly altered.

3.3 Abstract

Electromagnetic induction surveys are commonly used to assess soil salinity. In this study, a DualEM 1S instrument was used to survey an area in southern Manitoba to characterize sulphate-dominated salinity in clay-rich alluvial soils. The efficacy of predicting apparent conductivity (corrected for departure from low induction number responses) was determined by regression analysis of parameters including saturated-paste salinity, pore-water salinity, volumetric water content, porosity and combinations of these terms determined from 542 soil samples at 65

sampling sites. Predictors were depth-weighted using the V-H mode (exploration depth of 0.5 m) and the V-V mode (exploration depth of 1.5 m) of the electromagnetic instrument.

The analysis yielded strong correlations of apparent conductivity (EC_a) with saturated-paste or pore water conductivity, with Pearson r^2 correlation coefficients exceeding 0.75 for the V-H mode and 0.86 for the V-V mode. The strong correlations of EC_a with salinity are explained by moisture conditions being close to field capacity during the survey. These results are similar to those for chloride-dominated salinity. The study yielded less commonly observed results related to the clay-rich soils, including a threshold value of ~10% below which volumetric water content does not affect EC_a, and an improved prediction of EC_a by dividing the porosity data based on clay content. The study results demonstrate the efficacy of using EC_a to parameterize sulphate-dominated salinity in clay-rich soils. They also show that salinity can be estimated relatively accurately from saturated paste conductivity at near field capacity without considering moisture content.

3.4 Introduction

Soil salinity is an ongoing problem for agricultural producers. There are many causes for both primary and secondary development of soil salinity. Primary development is a natural increase in salinity, caused by naturally saline groundwater influencing the upper soils. It is usually a prolonged process associated with a shallow water table and high evaporation levels. Secondary development is defined as anthropogenic soil salinity. It may be caused by a variety of processes including excess irrigation in arid landscapes (e.g., Carter 1982; Steppuhn 2013; McFarlane et al. 2016), use of saline water for irrigation (e.g., Latif and Ahmad 2009), effects from canals (e.g., Sueltenfuss et al. 2013; Akram and Mendelsohn 2017), and inadequate drainage (Hollanders et al. 2005). It has been suggested that increased irrigated farming practices have led to between 20 and 30% of all irrigated land experiencing limited crop production due to secondary salinity (Carter 1982; Lekakis and Antonopoulos 2015).

Various methods have been developed to delineate and monitor the three-dimensional distribution of salinity in agricultural fields (e.g., Corwin and Lesch 2005; Friedman 2005; Visconti, F., and Miguel de Paz 2016; Corwin and Scudiero 2019). Standard methods include time domain reflectometry (Dalton and Van Genuchten 1986; Visconti and de Paz 2016), DC-resistivity measurements (Rhoades 1993; Samouëlian et al. 2005), and non-contact electromagnetic induction

measurements (Corwin and Lesch 2005a; Doolittle and Brevik 2014; Lesch et al. 1998; Rhoades and Corwin 1981; Visconti and de Paz 2016). Electromagnetic induction measurements are commonly made in the low induction number (LIN) range. The electromagnetic skin depth of the signals greatly exceeds the inter-coil spacing in the instrument (Fitterman and Labson 2005; McNeill 1980, 1990). LIN instruments commonly used in agricultural soil studies include the Geonics Limited EM31 and EM38 (Abdu et al. 2007; Cordeiro et al. 2011a, 2011b; Heil and Schmidhalter 2015; Morris 2009; Wollenhaupt et al. 1986) and DualEM instruments (Abdu et al. 2007; Triantafilis and Monteiro Santos 2013). Multi-frequency instruments such as the GEM-300 instrument are also used (e.g., Doolittle et al. 2001; Doolittle and Brevik 2014; Calamita et al. 2015).

Electromagnetic induction measurements give an apparent conductivity (EC_a) of the location of each reading. This reading is apparent as it represents a weighted-average response over the instrument's exploration depth (Fitterman and Labson 2005; McNeill 1980, 1990) and because it corresponds to the response of a uniform single-phase material (Visconti and de Paz 2016). The EC_a measurement depends on factors including volumetric soil-water content (θ), pore-water salinity (EC_w), clay content and cation exchange capacity (Cordeiro et al. 2011a, 2011b; Sudduth et al. 2003; Visconti and de Paz 2016). The most effective laboratory analysis to quantify soil salinity is the saturated paste extract method (Carter 1982; Rhoades 1982; Zhang et al. 2005; Gartley 2011), which yields the electrical conductivity of the extract (EC_e), or via a standardized soil/water ratios such as 1:1, 1:2, or 1:5 (Gartley 2011; Rhoades 1982; Zhang et al. 2005).

Many studies have examined the relationship of EC_a with soil properties, including EC_e, EC_w, moisture content, clay content, soil texture, and temperature. These studies have shown a strong dependence of EC_a on soil conductivity parameters such as EC_e or EC_w. They have demonstrated there may be significant linear (e.g., Sheets & Hendrickx 1995; Khakural et al. 1998) or non-linear (e.g., Nagy et al. 2013; Misra and Padhi 2014) correlations between EC_a and water content. The previous studies have considered both electromagnetic induction measurements (Khakural et al. 1998; Misra and Padhi 2014; Sheets and Hendrickx 1995) and direct contact measurements (Nagy et al. 2013) and used several methods for estimating moisture content.

Several studies have examined the relationship between EC_a and soil parameters (Corwin and Lesch 2005a; Friedman 2005; Knight and Endres 2005; Revil and Glover 1998; Rhoades et al. 1989a, 1976). There are three conduction pathways: conduction through the solid phase, liquid-

phase, and surface conduction at the solid-liquid interface by exchangeable ions due mainly to clay minerals (Rhoades et al. 1989a). In the absence of solid-phase conduction, EC_a (defined as σ_a) can be expressed as:

$$\sigma_a = [a\theta + b]\theta \cdot \sigma_w + \sigma_{surf} \quad \text{Eq. 3.1}$$

where σ_w is EC_w, σ_{surf} is surface conduction, and *a* and *b* are empirical constants related to the electrical connection of pores (Knight and Endres 2005; Rhoades et al. 1976). In soils with tortuous pore connections, *a* is significantly larger than *b* e.g., in clay soils a = 2.1 and *b* = - 0.245 whereas in loamy soils *a* = 1.3-1.4 and *b* = -0.11 to 0.06 (Knight and Endres 2005). For strong interconnection of pores, close to a situation in which equivalent conductive sheets can represent pores, *b* will be dominant. The dual pathway model represented in equation 3.2 can also be written in more complex forms, e.g., allowing for parallel and series solid-liquid conducting pathways (Friedman 2005; Lesch and Corwin 2003; Revil and Glover 1998; Rhoades et al. 1989a).

The EC_a can also be written in a modified form of Archie's Law (e.g., Corwin and Lesch 2005; Nagy et al. 2013):

$$\sigma_a = c\theta^m\sigma_w + \sigma_{surf} \quad \text{Eq. 3.2}$$

in which both *c* and *m* are constants, and *m* is not restricted to integral values. The result for *m* = 1 corresponds to *a* = 0 in equation 3.1 and the result for *m* = 2 corresponds to *b* = 0 in equation 3.1. In some formulations, volumetric water content is replaced by porosity, φ, and water saturation, S_R, terms with different exponents.

Studies have also considered a volumetric water content threshold θ_0 below which the apparent conductivity is independent of θ (Rhoades et al. 1976). At volumetric water content values below the threshold, the conductivity associated with the pore water salinity does not contribute to the overall soil conductivity. If an exponent of 2 is used in equation 3.2, and a threshold term is included in the volumetric water content term, i.e., if θ^2 is replaced with $(\theta-\theta_0)^2$, the resulting equation is:

$$\sigma_a = c\theta^2\sigma_w - 2c\theta\theta_0\sigma_w + c\theta_0^2\sigma_w + \sigma_{surf} \quad \text{Eq. 3.3}$$

This expression is equivalent to equation 3.1 if $a = c$, $b = -2c\theta_0$ and surface conductivity is allowed to depend on EC_e. Negative values for b for clay-rich soils can thus be alternatively interpreted in terms of a threshold volumetric water content. For example, values of a = 2.1 and b = -0.245 correspond a (quadratic) threshold in volumetric water of 0.06. If the threshold is included in a linear θ term corresponding to m = 1, i.e., if θ is replaced with $(\theta-\theta_0)$, then $\theta_0 = -b/a$ (Rhoades et al. 1976). For a = 2.1 and b = -0.245, the corresponding (linear) threshold is 0.12.

In the present study, these relationships for sulphate-dominated salinity in a clay-rich soil in an alluvial setting in the eastern Canadian Prairies were examined. Previous studies on the Canadian Prairies have examined the relationship of EC_a with soil salinity and water content (e.g., de Jong et al. 1979; Read and Cameron 1979; Kachanoski et al. 1988, 1990; Keller and Van der Kamp 1988; Cannon et al. 1994; Mckenzie et al. 1997; Cordeiro et al. 2011b) but most have been concerned with NaCl salinity. There have been several previous studies examining the effect of gypsum on laboratory EC_e conductivity measurements (e.g., Khorsandi and Yazdi 2011; Callaghan et al. 2016) and several studies elsewhere examining the effect of gypsum and sulphate on soil geophysical responses (e.g., Bouksila et al. 2008) including the relationship of EC_a and soil properties (Wollanhaupt 1986; Keller and Van der Kamp 1988; Job et al. 1999; Corwin and Lesch 2005b; Bouksila et al. 2012; Taghizadeh-Mehrjardi et al. 2014). Interest in the electromagnetic delineation of sulphate salinity in the Prairie setting is increased because of the physicochemical behaviour of sulphate salts in soils relative to salts such as NaCl, for example, due to the relative insolubility of gypsum and effects of its precipitation on residual pore-fluid chemistry and pore-geometry (Tanji and Kielen 2002; Visconti et al. 2010). The different electrical mobility of sulphate ions and the interaction of sulphate ions at large concentrations may also lead to differences in ion concentration and ECw relative to other ions.

In this context, the relationship of measured EC_a with EC_e and moisture content in the study area was examined. A secondary question is how effectively EC_a can be predicted from EC_e in the absence of information on water content. In the study, EC_a observations were collected using the two coil configurations of a DualEM 1S instrument. The data were corrected for small departures from the assumed LIN response. Predicted EC_a values were determined from laboratory-measured EC_e using a depth-weighting appropriate for DualEM 1S depth-sensitivity and predictor equations, including those with a surface conduction term (Dalton and Van

Genuchten 1986). Regression analysis is used to examine the relationship and degree of statistical correlation between the observed $EC_{a,}$ and the predicted EC_a and also between observed EC_a and depth-weighted *q*, EC_e, and EC_w parameters. The results of this analysis will be valuable in the future use of electromagnetic measurements in the study area to quantify the salinity level. They will also be useful for optimizing the electromagnetic approach used for mapping salinity in other areas of clay-rich soils.

3.5 Study area

3.5.1 Geology and geohydrology

The study is based on a series of narrow linear sub-areas extending over a north-south distance of 20 km adjacent to a drainage canal in Southern Manitoba, Canada. The study area is located near the base of the Manitoba escarpment on a large alluvial fan with a 30-45 km diameter (Rannie et al. 1989). The area lies near the western margin of the Red River Valley Plain and is flat with slopes of <2% (Manitoba Land Resource Unit 1997; Michalyna and Smith 1972). Across the alluvial fan, the thickness of its deposits varies from around 1.5 to 7.5 m (Fenton and Anderson 1971), but, within the study area, they extend to a maximum depth of 6.1 m.

The alluvial fan deposits overlie offshore silt and clays of glacial Lake Agassiz, which in turn overlies glacial till stratified and undifferentiated drift (Fenton 1970; Fenton and Anderson 1971). The offshore glaciolacustrine deposits form a spatially continuous layer, although some constituent sub-units are discontinuous. The clay was examined during a soil sampling program conducted in association with the current study and was gypsum rich, containing fine gypsum clusters. The thickness of the offshore glaciolacustrine deposits varies with depth to the base controlled by the underlying till elevations (Fenton and Anderson 1971; Gilliland 1965). In the study area, the unit's bottom depth is >8 m (Gilliland 1965). The thickness of the underlying till, which can be subdivided into the lower, middle, and upper sub-units, ranges from 4 m to >30 m across the study area. The till overlies spatially discontinuous deposits stratified and unstratified drift. The total depth to bedrock in the study area ranges from 36 to 42 m. The bedrock consists mainly of the Jurassic Upper Amaranth formation (Fenton 1970; Fenton and Anderson 1971; Nicolas et al. 2010). This formation is dominated by gypsum and anhydrite (present in mineable

quantities in areas to the north with thinner overburden deposits) with minor dolomite and shale (Bannatyne 1959; Fenton 1970; Lapenskie and Bamburak 2016; Moore et al. 2019).

Aquifers identified in the study area include an overburden aquifer and bedrock aquifers (Betcher et al. 1995). In the overburden aquifer, the shallow groundwater flow is dominantly in the surficial sands deposited by historic rivers and creek systems extending from surface to a depth of approximately 7 m. The regional groundwater flow direction is generally north to northwest, initiating at the Assiniboine River and extending to Lake Manitoba (Betcher 1988; Gilliland 1965). The groundwater flow in the unconsolidated sediments is controlled by flow in the basal stratified drift (Cherry et al. 1971). The recharge for this flow occurs in higher elevation areas to the southwest, and the study area lies within the discharge zone. Upwards flow through the shallow overburden layers is interpreted to be caused by lensing-out of the coarse-grained units (Cherry et al. 1971).

A bedrock aquifer occurs in the Middle Ordovician to Middle Devonian carbonate bedrock units located beneath the Amaranth Formation. In the study area, the carbonate aquifer's flow system consists of a regional-scale up-dip flow of saline waters from the Williston Basin (Grasby and Betcher 2002). As a result, the groundwater in the carbonate aquifer is brackish (Gilliland 1965). It is dominated by sodium-chloride type waters with chloride comprising more than 95% of all anion equivalents and only relatively minor concentrations of sulphate are present (Betcher et al. 1995). The carbonate aquifer is separated from the unconsolidated surface sediments by evaporites in the Amaranth Formation, acting as an aquitard (Betcher et al. 1995). However, at a regional scale, there is an upward hydraulic gradient from the bedrock aquifer to the surface (Gilliland 1965), resulting in some areas of enhanced sodium-chloride soil salinity in the region.

3.5.2 Soils

Soil sampling within the study area sites shows the near-surface materials correspond to the alluvial fan setting with surface textures, including silt loams, clay loams, silts, and minor tributaries of the alluvial fan, fine-grained sands (Michalyna and Smith 1972). The land in the study area is used mainly for annual crops, including various varieties of beans, canola, corn, potatoes, wheat, and forage crops, including alfalfa (Manitoba Land Resource Unit 1997). Over most of the study area, the drainage is classed as imperfect, meaning that water is removed from the soil sufficiently slowly that the soil remains wet for a significant part of the growing season

(Manitoba Land Resource Unit 1997). Soil-waters from the study area have a median pH of 8 and exhibit a pattern of increasing TDS with increasing pH. These observations align with the soil classification in the study area and adjacent areas as alkaline (Manitoba Agriculture 2008).

Manifestations of strongly salt-affected soils in the study area include negatively impacted crop growth. In some of these locations, salt crystals, interpreted to be gypsum, are visible in surface soils (Figure 3.1). Soils occurring in different parts of the study area, including those from the Gnadenthal, Morris, and Plum Coulee groups, are all reported to have gypsum crystals in the C horizon (Michalyna and Smith 1972), supporting the interpretation of the crystals observed at the saline sites in the study area as being gypsum. However, sodium or magnesium salts may also be present. Saline variants of the Gnadenthal and Red River groups outside the study area are noted as containing magnesium sulphate. The presence of salts is also noted in the Osborne group in the vicinity of the study area. The engineering sulphate hazard in a number of these soils reaches moderate levels and becomes severe in the soils (Michalyna and Smith 1972).

Figure 3.1 Photograph from an area of high salinity showing a surface soil sample speckled with fine-grained crystals that are interpreted to be gypsum**.**

3.5.3 Sulphate salinity in groundwater and soil-water

Groundwater and soil-water studies show the enhanced salinity in the study area is characterized by high sulphate levels. Cherry et al. (1971) examine the distribution of groundwater salinity in the area. As the groundwater flows laterally through the stratified drift at the base of the overburden, it undergoes an increase in total dissolved solids (TDS) related to the concentration of Na^+, Ca^{2+}, Mg^{2+}, Cl^- and SO_4^{2-} ions. Further increases in Na^+, Mg^{2+}, and SO_4^{2-} occur as the water moves upwards through the lacustrine clay deposits. This process is interpreted as related to exchange reactions with montmorillonite (Cherry et al. 1971). Immediately below the water table, the concentration of TDS is typically in the range 5-10 $g.L^{1,}$ with the concentration increasing to 10-15 $g.L^{-1}$ at depths exceeding 15 m. The concentration of SO_4^{2-} below the water table is 5-10 $g.L^{-1}$ reaching values of >10 $g.L^{-1}$ in some locations (Cherry et al. 1971).

Analysis of the groundwater from monitoring wells of the study area shows areas of elevated soil salinity are correlated with high groundwater salinity and increased SO_4^{2-}, Ca^{2-}, Na^+, Mg^{2+} concentrations with negligible Cl^-, HCO_3^-, and CO_3^{2-} (Figure 3.2) conforming to the findings of Cherry et al., (1971). At some locations in the study area, SO_4^{2-} concentrations reach values of 20 $g.L^{-1}$ (Figure 3.2). Analyses of ionic concentrations in groundwater from the study area using the hydrogeochemical model PHREEQC (Parkhurst and Appelo 2013) and Pitzer aqueous model (Plummer et al. 1988) indicate the groundwater is either near to saturated or supersaturated, with gypsum and near to saturated with anhydrite (Rentz et al. Accepted(a)).

The concentrations of sulphate ions in the soil-water and sulphate minerals in the soil can be attributed to interactions between the phreatic and vadose zones e.g., associated with capillary processes occurring when the water table is close to the surface. As shown in Fig 3.2, the soil-water is also dominated by sulphate. Comparison of the groundwater and soil-water conductivity indicates lower values in the soils than in the groundwater, likely due to the infiltration of fresher surface water in the soil. Spatial variations in the zone of oxidation may also affect the sulphate distribution (e.g., Keller and Van der Kamp 1988). Furthermore, localized concentrations of sulphate may have resulted from the lateral movement of groundwater associated with microtopography. Keller and Van der Kamp (1988) interpret large accumulations of sulphate below the soil zone at a Saskatchewan site as being caused by such processes.

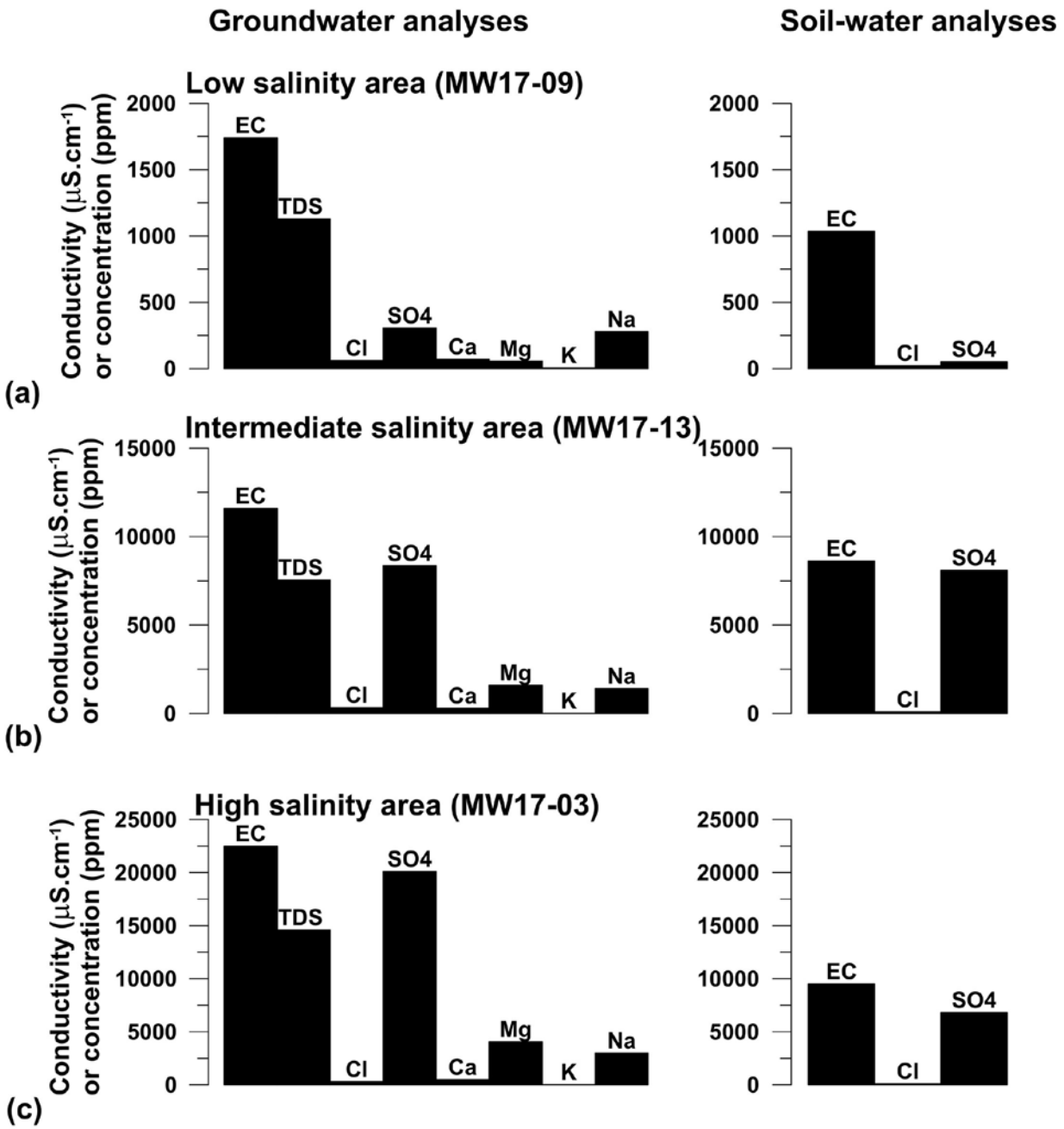

Figure 3.2 Groundwater and soil-water samples from three locations in the study area that exhibit relatively (a) low, (b) intermediate and (c) high levels of salinity. The groundwater samples correspond to freshwater, brackish water, and saline water, respectively, using Hem's classification (Hem, 1985). Each soil sample is from a location that is close to the corresponding groundwater monitoring well and has similar soil: for MW17-09, the soil sample is 200 m from the monitoring well; for MW13, it is 5 m; and for MW17-03, it is 45 m. Groundwater sampling was done using procedures outlined in ASTM D4448-01 (ASTM, 2013), and samples were analyzed at a private laboratory. For MW17-09 and MW17-03, the soil-water results are an average of individual results for 8 depths over the upper 120 cm, and for MW17-13, they are for a single sample at approximately 2.1 m depth.

3.6 Materials and methods

3.6.1 Instrumentation

Electromagnetic induction surveys were conducted using a DualEM-1S (DualEM Inc., Milton, ON, Canada). A DualEM-1S is similar to the commonly used Geonics EM-38 conductivity meter (Geonics Ltd., Mississauga, On, Canada). The instruments operate optimally in areas of low to moderate conductivity where they remain in the low induction number (LIN) range (Fitterman and Labson 2005; McNeill 1990). A LIN response occurs when the electromagnetic skin depth at the signal frequency greatly exceeds the instrument's inter-coil spacing. The DualEM-1S instrument operates at a 9 kHz frequency. It senses the apparent conductivity of the subsurface soils simultaneously over two depth ranges. One using a vertical dipole transmitter and receiver pair (V-V mode) with a 1 m coil spacing and another a vertical-horizontal dipole receiver pair (V-H mode) with a 1.1 m coil spacing (e.g., Abdu et al. 2007) in order to analyze the typical root zone. At LIN the depth sensitivity of the V-V mode is:

$$S_{V-V}(r,z) = 4\left(\frac{z}{r}\right)\left(4\left(\frac{z}{r}\right)^2 + 1\right)^{-3/2} \quad \text{Eq. 3.4}$$

where z is the depth and r is the coil spacing (Abdu et al. 2007; Fitterman and Labson 2005). The depth sensitivity for the V-H mode is:

$$S_{V-H}(r,z) = 2\left(4\left(\frac{z}{r}\right)^2 + 1\right)^{-1/2} - 8\left(\frac{z}{r}\right)^2\left(4\left(\frac{z}{r}\right)^2 + 1\right)^{-3/2} \quad \text{Eq. 3.5}$$

Figure 3.3 shows the depth-sensitivity function for the instrument for the two modes of operation. The sensitivity may also be expressed as the cumulative sensitivity above or below a specified depth (Figure 3.3a). In a layered medium, the LIN V-H mode is more sensitive to the very near-surface conductivity and has an exploration depth of 0.5 m. The LIN V-V response provides deeper penetration, with an exploration depth of 1.5 m (e.g., Abdu et al. 2007). For the field data collection, the DualEM-1S was coupled with an Allegra CX data collector (Juniper systems Inc., Logan, UT, USA).

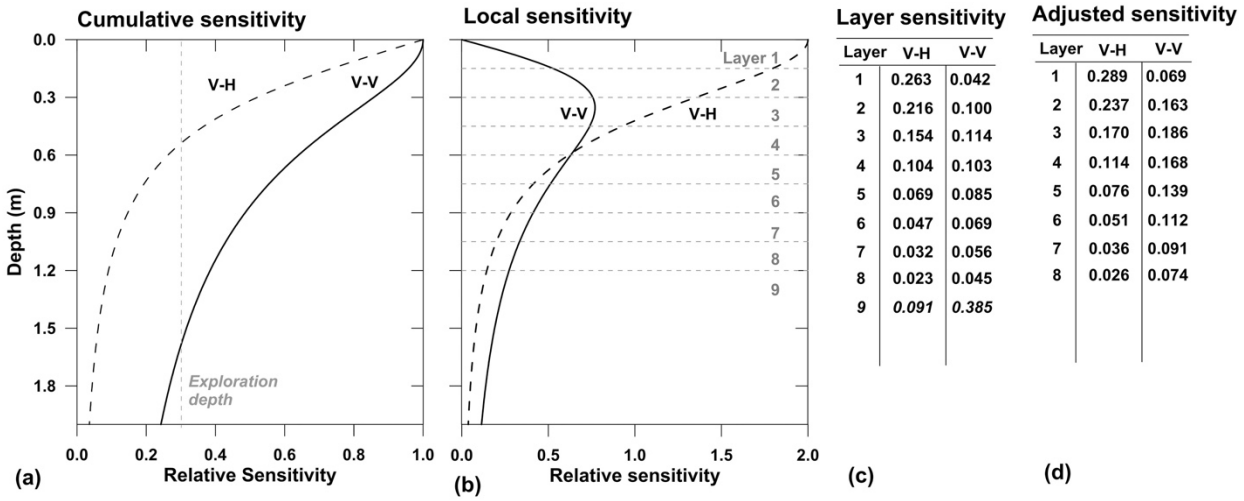

Layer	V-H	V-V
1	0.263	0.042
2	0.216	0.100
3	0.154	0.114
4	0.104	0.103
5	0.069	0.085
6	0.047	0.069
7	0.032	0.056
8	0.023	0.045
9	*0.091*	*0.385*

Layer	V-H	V-V
1	0.289	0.069
2	0.237	0.163
3	0.170	0.186
4	0.114	0.168
5	0.076	0.139
6	0.051	0.112
7	0.036	0.091
8	0.026	0.074

Figure 3.3 Depth sensitivity of DualEM-1S when operated at LIN in a layered medium. a Cumulate sensitivity shown for the sensitivity at depths larger than the specified value. Vertical dashed line show the exploration depth above which material contributes 70% of the response. b Relative sensitivity of the V-V and V-H modes. Horizontal lines define the layers used in the present study. Layer 9 corresponds to all depths greater than 1.2 m. c Sensitivity of the V-H and V-V modes to the individual layers. d Adjusted sensitivity values with the total sensitivity of the upper 8 layers adjusted to 100%.

3.6.2 Electromagnetic survey

The study was conducted in 14 sub-areas. Each area consisted of a narrow strip of length between 1.2 to 3.5 km and width 400 m adjacent to the east or west side of the drainage canal. Study sites were located on a combination of crown and private land. Restrictions placed on publication of site locations from some farms preclude inclusion herein of a detailed site map. The sites were selected based on two features: sites where the local producers have perceived increases in soil salinization and geologic features such as former creeks and riverbeds throughout the area.

The electromagnetic field data collection took place between October 9, 2016, and November 15, 2016. The DualEM-1S instrument placed in a sled was towed behind an all-terrain vehicle (ATV) at a speed of 5 km/h. The data logger was mounted on the ATV. The survey of each site was completed in a grid pattern, with V-H and V-V readings collected every 10 m along north-south lines separated by approximately 30 m in the east-west-direction. Measurement locations were recorded using a GPS feed into the Allegra CX system. V-H and V-V measurements were made at a total of 14,215 locations providing 28,230 EC_a data values.

3.6.3 Correction of data for departure from LIN

The calibration of electromagnetic induction instruments such as the DualEM-1S for operation in the LIN range means that the instruments may provide less accurate readings in areas

of high soil conductivity (Abdu et al. 2007; Fitterman and Labson 2005; McNeill 1980, 1990). The electromagnetic skin depth decreases in proportion to the inverse square root of the ground conductivity so that in areas of high conductivity the skin depth will no longer greatly exceed the coil spacing and the induction number will no longer be low. Figure 3.4 shows the theoretical departures of the DualEM-1S readings from the true conductivity of a uniform half-space as the conductivity increases. The deviation below 1.0 $dS.m^{-1}$ (at an induction number of 0.008) is negligible. At higher values of conductivity, the deviation increases, especially for the V-V configuration. At a true conductivity of 10 $dS.m^{-1}$ (at an induction number of 0.025) the V-V configuration will provide a value that is 2.7% below the correct value and the V-H configuration will provide a value that is 0.02% too low.

Theoretical departures of the true values' responses can be used to estimate a correction factor for EC_a data collected in areas of increased conductivity (Figure 3.4b). Strictly, the correction factors will yield the true EC_a only for measurements above a uniform soil. In a layered environment, the exact factor will depend on the conductivity in each layer. However, if the vertical variation in conductivity is not extreme, application of the correction factors will yield responses that are closer to the true (LIN) values than uncorrected EC_a values.

The observed ECa values measured at the soil sampling sites in the survey were corrected using the factors shown in Figure 3.4b. The V-V ECa values at these locations are <3 $dS.m^{-1}$ so the maximum correction factor applied causes a change in the response of <12%. The observed V-H ECa values are <2.5 $dS.m^{-1}$ so the correction factors for this mode cause negligible (<1%) change to the ECa values. However, the correction was still applied for completeness.

3.6.4 Soil sampling

In order to examine the spatial correlation of EC_a readings and soil properties including the EC_e, soil sampling was conducted at a total of 65 locations with between 3 and 6 locations in each sub-area. The locations for the soil sample cores were determined using in-field evaluation of the recorded EC_a values and sampling was completed on the same day as the electromagnetic survey. The locations were chosen using two basic criteria rather than a statistical approach, such as implemented in the ESAP-RSSD software (USDA-ARS, Riverside, CA, USA). Sample sites were chosen to be representative of low, intermediate, and high EC_a responses for each survey sub-area (generally in the 0-30, 30-70, and 70-100 percentile ranges of EC_a values respectively) and to be spaced spatially as widely as possible. A total of 542 soil samples were collected using

a 1.2 m hand auger. Soil samples were collected every 0.15 m to a maximum depth of 1.2 m. The samples were stored in sealed bags for subsequent laboratory analysis.

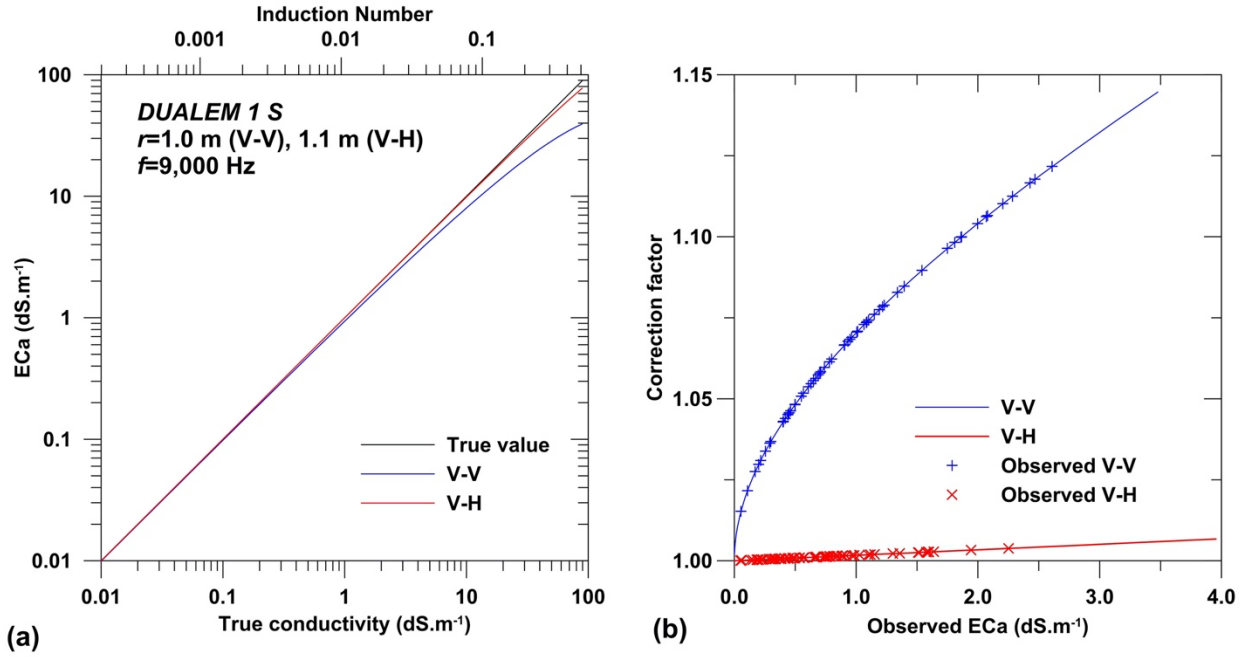

Figure 3.4 LIN approximation and correction for DUALEM 1 S instrument. a Departures of instrument ECa reading over a uniform Earth from the true conductivity. Top axis show the corresponding induction number for the V-V mode. Note that the V-V configuration has much larger departures from the true reading than the V-H mode. **b** Correction factor used to multiply observed the observed EC_a to yield the true conductivity. Individual symbols show the correction factors for the data measured in the present study.

3.6.5 Laboratory analysis

Soil samples were analyzed at a commercial analytical lab in Calgary, Alberta and at the University of Manitoba, Department of Biosystems Engineering, Soil and Water Engineering Laboratory. At the commercial laboratory, they were evaluated for analytes including: EC_e, chloride, sodium, pH, sodium adsorption ratio (SAR), saturation percentage (SP), and, where analyzed, soluble sulphate, magnesium, and calcium (Carter and Gregorich 2008). Lab procedures for EC_e followed those described in Miller and Curtin (2008). Samples were dried for 24 hours at 105°C and then ground. The ground material was saturated using deionized water to create a saturated paste which was then allowed to equilibrate for a minimum of four hours while being checked to ensure that no additional water or soil was required. At the University of Manitoba, samples were analyzed for gravimetric soil water content (θ_g) following the procedure outlined by

Topp et al. (2008). A sample with a mass between 30 to 50 g was weighed, dried at 105°C for a minimum of 24 hours, and then re-weighed, allowing calculation of the water content.

Additional soil and water parameters were derived from the measured quantities. Porosity (φ) was not measured in the laboratory it was determined from the saturation percentage using:

$$\varphi = \frac{SP \cdot \rho_g}{(\rho_w + SP \cdot \rho_g)} \quad \text{Eq. 3.6}$$

where ρ_g is the average particle density which was taken to be 2.65 g.cm^{-3} and ρ_w is the water density (e.g., Rhoades et al. 1989b; Rhoades 1993). Following standard approaches (e.g., Carter and Gregorich 2008), the bulk density ρ_b was obtained using:

$$\rho_b = (1 - \varphi)\rho_g \quad \text{Eq. 3.7}$$

and was used with the gravimetric water content to calculate the volumetric water content:

$$\theta = \theta_g \cdot \rho_b \quad \text{Eq. 3.8}$$

The degree of water saturation S was obtained using:

$$S = \frac{\theta}{\varphi} \quad \text{Eq. 3.9}$$

and the paste conductivity ECe was converted to pore-water conductivity (EC_w, σ_w) using

$$\sigma_w = \frac{ECe}{S} \quad \text{Eq. 3.10}$$

The propagation of errors from the SP measurements into derived results was examined using a 65-point data set and three statistical replications. Hypothetical 5% errors in the SP data result in 1.7% errors in derived porosity, 3.1% errors in derived volumetric water content, 4.8% errors in derived water saturation, and 7.4% errors in derived pore-water conductivity. Based on the multiplicative relationships in equations 3.8 to 3.10, errors in the measured gravimetric water content and paste conductivity will cause errors of the same relative magnitude in the quantities

derived from them. These results indicate that there should be no strong compounding of errors in derived quantities.

3.6.6 Depth weighting

To compare an observed EC_a value with the EC_e values (or an alternative parameter) determined from soil samples from the same location, it is necessary to weight the EC_e values for different depths using the same relative weighting as the depth sensitivity of the EC_a measurement. The sensitivity of a layer is defined by the difference in the cumulative sensitivity of the top and bottom layers. These values are shown in Figure 3.3 for the sampling layers used in this study. There are different approaches for handling the depth range beneath the deepest sample. One approach is to assume that the EC_e value determined in the deepest layer sampled is representative of the material at greater depth. A second approach, used by Wollenhaupt et al. (1986), is to adjust the sensitivities in the sampled layers by a common factor so they sum to 1. This approach was used in the current study with the total sensitivity of the upper 8 layers being adjusted so that they total to 1 (Figure 3.3). With this adjustment, the weighted response of the V-V configuration of values from the response of individual layers R_i is:

$$R_{W:V-V} = 0.068R_{0-15\text{cm}} + 0.163R_{15-30\text{cm}} + 0.186R_{30-45\text{cm}} + 0.168R_{45-60\text{cm}} + 0.139R_{60-75\text{cm}} + 0.112R_{75-90\text{cm}} + 0.091R_{90-105\text{cm}} + 0.074R_{105-120\text{cm}} \quad \text{Eq. 3.11}$$

and for the V-H configuration it is:

$$R_{W:V-H} = 0.289R_{0-15\text{cm}} + 0.237R_{15-30\text{cm}} + 0.170R_{30-45\text{cm}} + 0.114R_{45-60\text{cm}} + 0.076R_{60-75\text{cm}} + 0.052R_{75-90\text{cm}} + 0.036R_{90-105\text{cm}} + 0.026R_{105-120\text{cm}} \quad \text{Eq. 3.12}$$

3.6.7 Linear regressions

Linear regressions were used to examine the spatial correlation of observed V-V and V-H EC_a values and predicted conductivity values based on the weighted averages of EC_e calculated using equations 3.11 and 3.12. In order to accommodate a surface conduction term in the regression both the slope and intercept were fitted. Additional regressions were done to examine the correlation of observed EC_a with weighted values of other soil and water parameters and combinations of these terms. Single-parameter variables used in these tests were pore fluid salinity

(σ_w), volumetric water content (θ), porosity (φ), and saturation (S). Regressions were also done using the product of EC_w and volumetric soil water content ($\sigma_w \cdot \theta$), the product of EC_w and the square of volumetric soil water content ($\sigma_w \cdot \theta^2$), and with a threshold value included in the previous parameter. The combined parameter terms correspond to individual terms in Eq. 1 (e.g., Rhoades et al. 1976; Dalton and Van Genuchten 1986). The quality of each correlation was examined using the squared (Pearson) coefficient of determination (r^2), root mean squared error (RMSE), and mean absolute error (MAE). Statistical significance of the results was assessed using the two-tailed critical t-test (e.g., Davis 1986). More detailed investigations of some of the relationships observed in the initial regressions was done using regressions of subsets of the full data set and contour maps of EC_a versus multiple parameters.

3.7 Results

3.7.1 Distributions of paste extract and soil moisture parameter values

In order to assess the spatial correlation of the observed EC_a values with the different soil properties, it is necessary for there to be significant spatial variation in these properties (θ_m, SP, and EC_e). Figure 3.5 shows the distribution of properties measured in the laboratory analyses as a function of depth. The saturation percentage exhibits an approximately normal distribution. The measured values are high reflecting a high clay content in the soil (e.g., Rhoades et al. 1989b). The values show a significant decrease with depth from a mean value of 0.71 in the upper 15 cm to a value of 0.55 at 120 cm depth. This variation indicates a changing soil texture and a decrease in clay and/or silt content with increasing depth. The change is associated with an increase in the width of the distribution with depth indicating that near-surface materials are much more homogeneous across the study sites, probably due to agricultural activities that have modified the shallow parts of the soil. The gravimetric water content also has an approximately normal distribution. It defines a decrease in the mean value in the upper 60 cm from 0.37 in the upper 15 cm to 0.28 at 60 cm depth and relatively constant at greater depth.

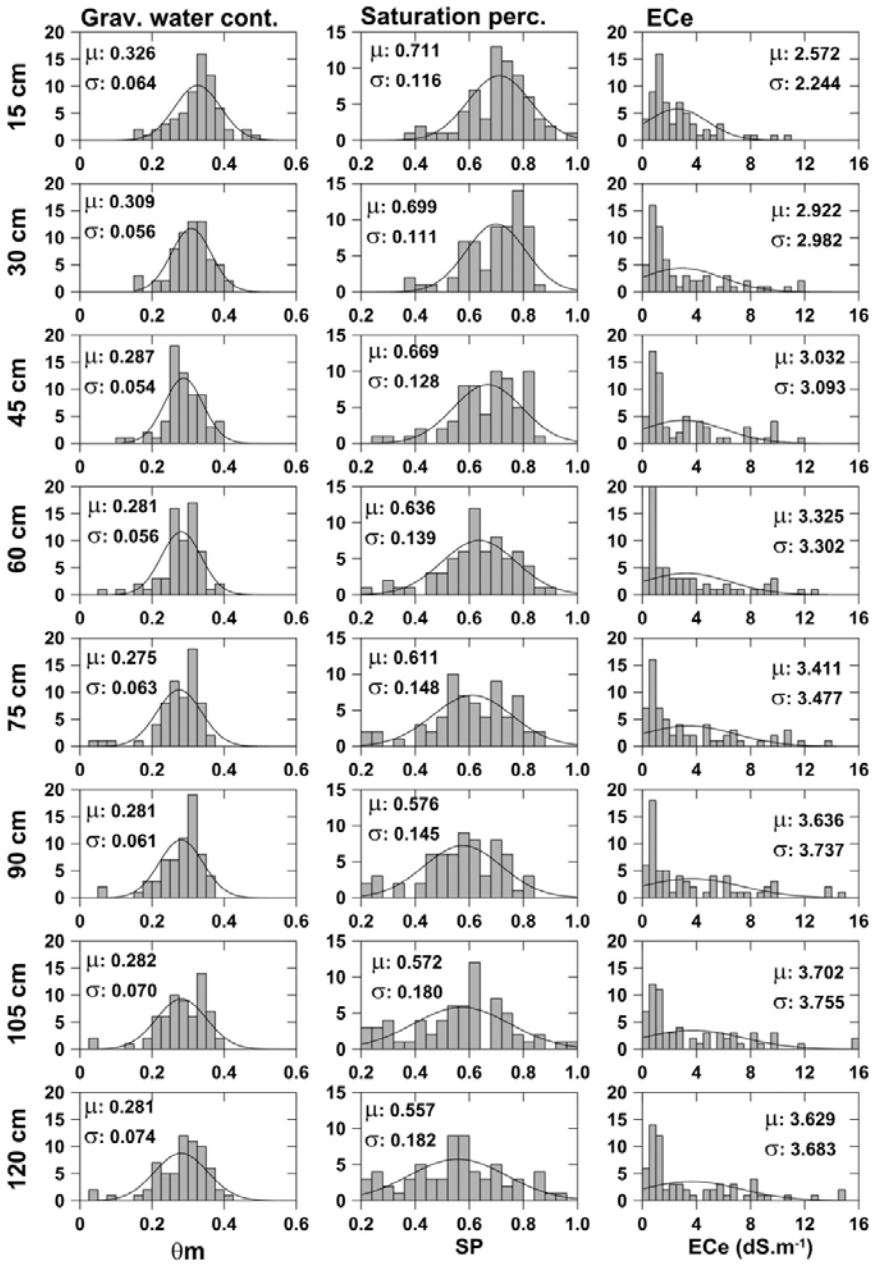

Figure 3.5 Histograms of properties derived directly by laboratory measurements for the full suite of 65 soil samples at each depth. Each panel also shows a normal distribution fitted to the observed distribution and the mean and standard deviation of the observed values.

In contrast to the approximately normal statistical distribution for saturation percentage and gravimetric water content, saturation paste measurements have a strongly positively-skewed distribution. A background normal distribution can explain the observed variation in EC_e with anomalously large values present at around 20% of the sample locations. The mean value of EC_e and the skew of the distribution increase significantly from 15 cm to 30 cm depth and are more

constant at greater depth. Overall, the paste extract values vary between 0.2 and 16 $dS.m^{-1}$ and the mean value at each depth increases from 2.57 $dS.m^{-1}$ in the upper 15 cm to 3.76 $dS.m^{-1}$ at 90 cm depth. The relative moderate vertical variations in EC_e suggests that the bulk conductivity does not vary greatly with depth and supports the approach adopted to correct the observed EC_a values to equivalent LIN results.

Figure 3.6 shows histograms of quantities derived from the laboratory measurements using equations 3.6 to 3.10. The porosity values are very high as expected based on the corresponding high values of saturation percentage with both parameters indicating a high clay content in the soil. The volumetric water content is relatively constant with depth, decreasing from 0.298 near the surface to 0.273 at 60 cm depth before increasing slowly again with depth. The relative water saturation, calculated using equation 3.9, shows a similar trend to the volumetric water content. Saturation values are around 50%. For the clay-rich soils in the study area, the field capacity, equal to about 50% of saturation percentage (Amezketa 2007; Lesch and Corwin 2003; Miller and Curtin 2008) may provide a better measure of the maximum water capacity than the relative saturation. Comparison of the saturation percentage and the volumetric water content results shows that the field capacity decreases from 94% at the surface to a minimum of 78% at 45 cm depth before increasing again to 100% at 100 cm depth. Pore-water conductivity values show the same strongly positively-skewed distributions as the paste extract conductivity. Average EC_w values at each depth increase from 5.7 $dS.m^{-1}$ near the surface to 7.5 $dS.m^{-1}$ at depth. The maximum value of the individual samples at each depth is between about 24 and 30 $dS.m^{-1}$.

The significant lateral variations in EC_e and EC_w, reflected by the high ratio of the standard deviation to the mean value for these parameters, indicate that the soil conductivity data from the sampling study provides an excellent framework for examining the relationship of EC_e and EC_a. The other soil parameters including volumetric water content, porosity, and relative water saturation exhibit smaller relative lateral variations across the study sites. For these parameters, at shallow depths, the standard deviation is about 10% of the mean value and at depth of 1 m it increases to about 20% of the mean value. These lateral variations still provide an adequate data set for examining the soil parameters affecting EC_a. However, their smaller range relative to the conductivity parameters decrease the statistical confidence in the correlations involving the parameters.

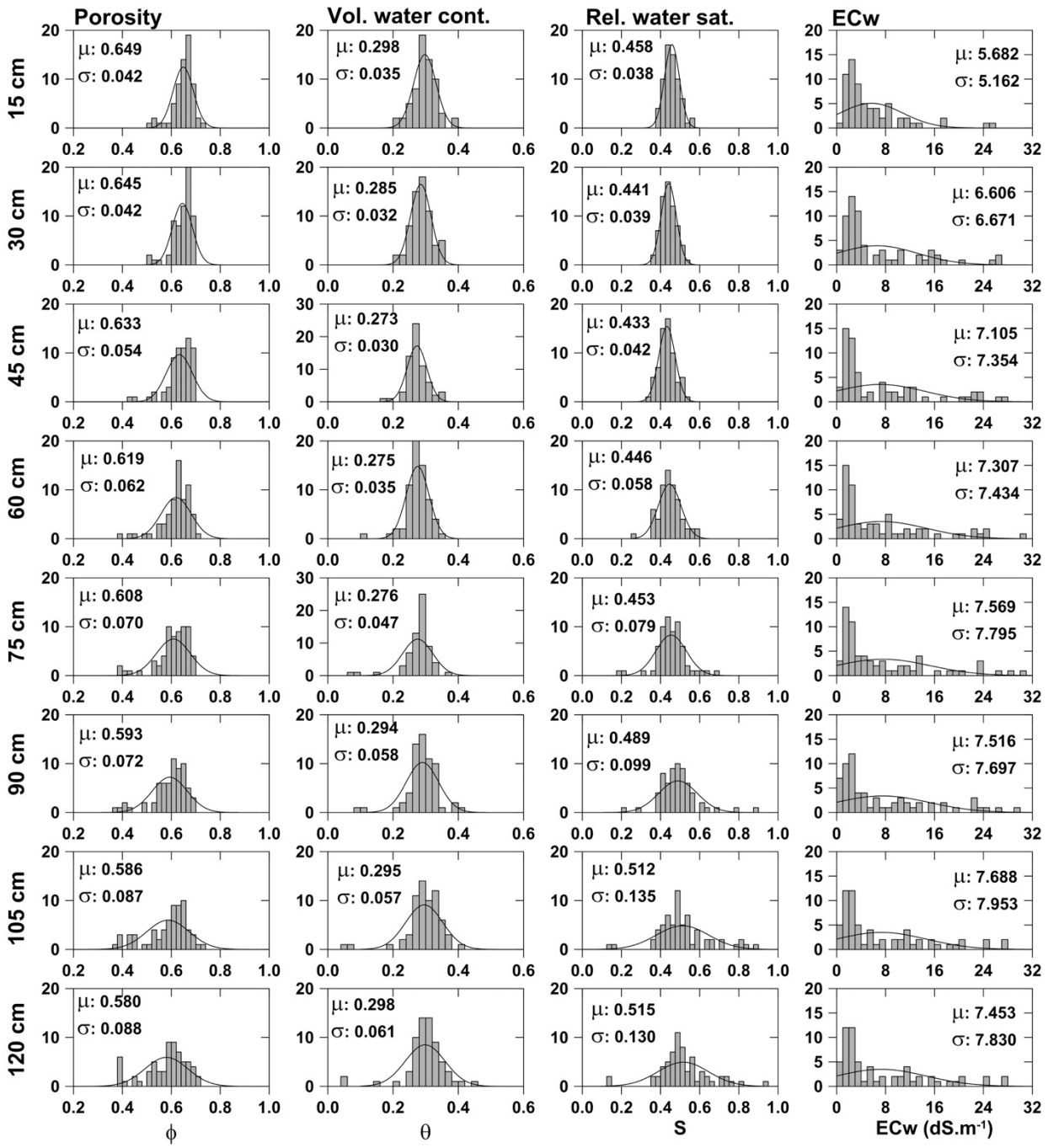

Figure 3.6 Histograms of properties derived from laboratory measurements for the full suite of 65 soil samples at each depth. Each panel also shows a normal distribution fitted to the observed distribution and the mean and standard deviation of the observed values.

3.7.2 Regression results for EC_e and EC_w

Regression analysis was conducted on the seven weighted predictor parameters in order to examine the influence of each on the prediction of EC_a. For both V-H and V-V modes, there is a strong linear relationship between the observed EC_a values and correspondingly-weighted EC_e

values. The Pearson correlation coefficients for V-H and V-V modes of 0.78 and 0.87 are statistically significant at the 99% confidence level (Tables 3.1 and 3.2). The calculated RMSE and MAE values indicate that the EC_a in the study area can be predicted from weighted EC_e values with an accuracy of approximately 0.2 $dS.m^{-1}$. The linear regressions define slopes of 0.152 and 0.219 and intercepts of 0.284 and 0.336 $dS.m^{-1}$ for the V-H mode V-V mode respectively (Figure 3.7). The intercepts of the fitted lines correspond to surface conduction term in equations 3.1 and 3.2.

Table 3.1 Correlations between ECa and weighted predictors for V-H measurements.

Predictor	Coefficient of determination (r^2)	RMSE ($dS.m^{-1}$)	MAE ($dS.m^{-1}$)
EC_e	0.78*	0.22	0.17
EC_w (σ_w)	0.75*	0.24	0.18
Vol. water content (θ)	0.21***	0.41	0.32
Porosity (φ)	0.30**	0.40	0.31
Saturation (S)	0.002	0.47	0.37
EC_w x θ ($\sigma_w \cdot \theta$)	0.79*	0.22	0.16
EC_w x θ^2 ($\sigma_w \cdot \theta^2$)	0.81*	0.29	0.23

*Significant at 99% confidence level
** Significant at 95% confidence level
***Significant at 90% confidence level

Examination of the misfit in the EC_a-weighted EC_e regressions shows there is a systematic misfit at low conductivity values (weighted $EC_e < 2$ $dS.m^{-1}$) in which the observed EC_a values lie below the linear trend defined by the rest of the data. This same feature is observed in the results for EC_w (Figure 3.7b). It is examined in more detail below. There is no significant systematic misfit at larger conductivity values in the V-V response suggesting the method used to correct the data for the departures from the low induction number range was effective.

Table 3.2 Correlations between ECa and weighted predictors for V-V measurements.

Predictor	Coefficient of determination (r^2)	RMSE ($dS.m^{-1}$)	MAE ($dS.m^{-1}$)
EC_e	0.87*	0.26	0.20
EC_w (σ_w)	0.86*	0.27	0.22
Vol. water content (θ)	0.14	0.67	0.54
Porosity (φ)	0.27**	0.62	0.48
Saturation (*S*)	0.002	0.72	0.57
EC_w x θ ($\sigma_w \cdot \theta$)	0.87*	0.25	0.19
EC_w x θ^2 ($\sigma_w \cdot \theta^2$)	0.88*	0.25	0.19

*Significant at 99% confidence level
** Significant at 95% confidence level
***Significant at 90% confidence level

Regression results for EC_w are very similar to those for EC_e and are again significant at the 99% confidence level. However, for both the V-H and V-V mode the correlation coefficients for the EC_w regressions are slightly lower than for the EC_e regressions and the RMSE and MAE values are slightly higher. In principle, there should be a stronger relationship between EC_w and EC_a than between EC_e and EC_a since the pore-fluid conductivity appears directly in the formula for EC_a (equations 3.1 and 3.2). The EC_a relates to the salinity of the pore-fluids (measured by EC_w) rather than total salt content of the sample (measured by EC_e). The saturation is used to convert the measured EC_e to EC_w (equation 3.10). The saturation does not vary very strongly in the survey area, for example the mean value at different depths only varies between 0.46 and 0.52 (Figure 3.6). It is derived from other measured parameters (using equations 3.6 to 3.9) that its values may contain cumulative errors with magnitudes significant relative to the spatial variations. These factors explain the observation that the EC_a-EC_w correlations are slightly inferior to the EC_a-EC_e ones. Superior results may be obtained if the saturation is measured directly.

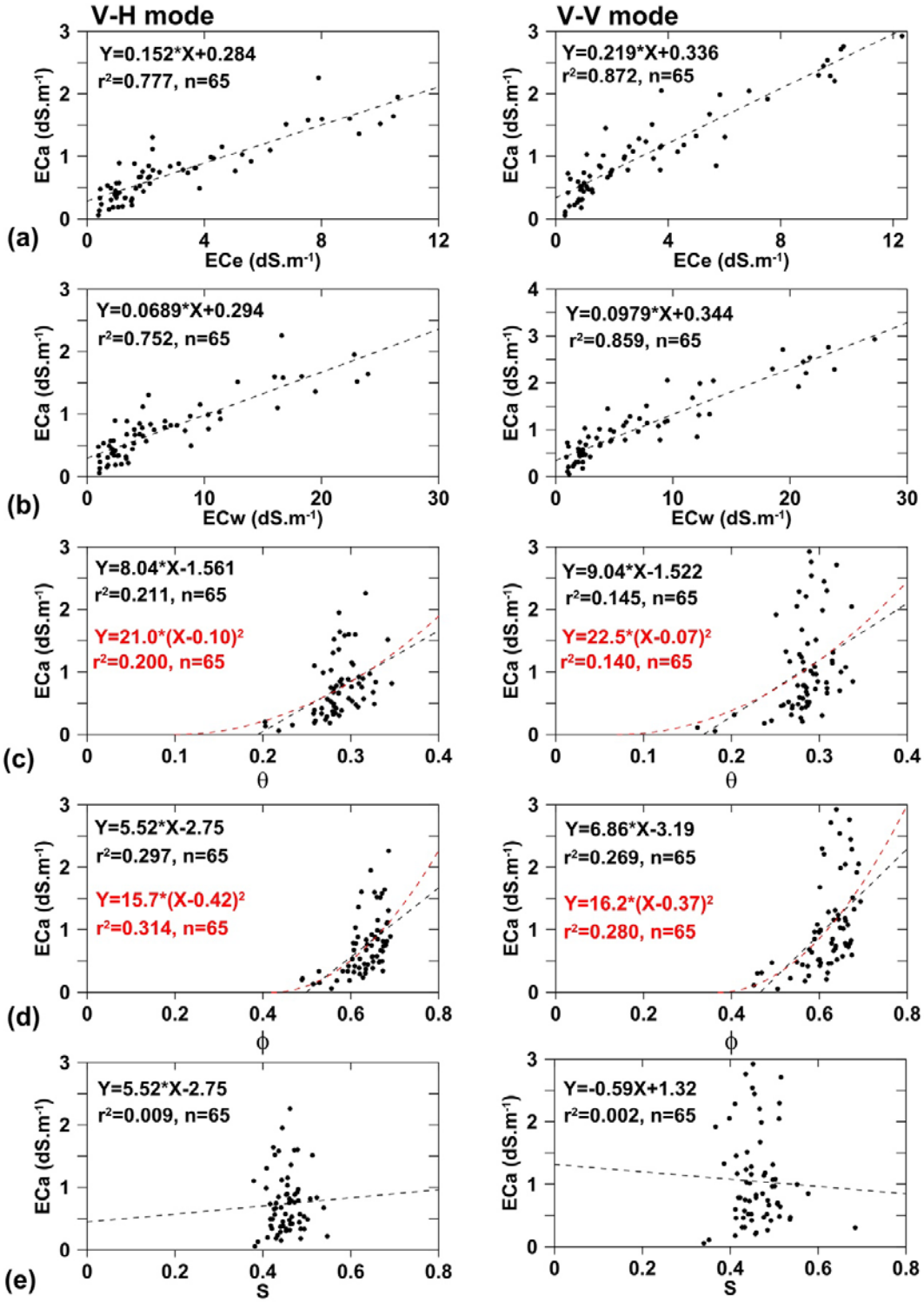

Figure 3.7 with single-parameter variables: a weighted ECe, b weighted ECw, c weighted volumetric water content, d weighted porosity, and e weighted relative water saturation. The weighting is matched to V-H or V-V mode respectively. Dashed black line shows least-squares fitted linear trend and annotations show equation of the fitted trend, squared correlation coefficient and number of samples. Dashed red line and red labels for the weighted volumetric water content and porosity results show the fit for a quadratic function.

3.7.3 Regression results for other parameters

The regression results for EC_a with saturation (S) as the independent variable show no statistical correlation (Table 3.1 and 3.2, Figure 3.7e). As discussed above, this result may be explained by the limited range of saturation values and the presence of small errors in the saturation data arising from its indirect method of determination.

In contrast to the results for the saturation, regression results for EC_a and porosity show moderate correlation, with Pearson correlation coefficients for V-H and V-V data of 0.30 and 0.27 respectively, values significant at the 95% confidence level. The RMSE and MAE are in the range 0.3-0.4 $dS.m^{-1}$ for the V-H mode and 0.5-0.6 $dS.m^{-1}$ for the V-V mode indicating that the porosity provides a poor prediction of EC_a compared to EC_e or EC_w. The regression plot shows that the fitted data define a vertically-extended cloud of values with strongly increasing EC_a at porosity values of 0.6-0.7 (Figure 3.7d). The observation can be explained by the combined effect of porosity and EC_e on apparent conductivity. Samples with low to moderate EC_e define a minimum EC_a response corresponding to the base of the cloud of data points. However, a number of the samples with porosity values of 0.6-0.7 also exhibit very high EC_e values causing the EC_a response to extend vertically upwards from the base of the cloud of data.

The volumetric water content depends on both the porosity and saturation. Regression of the EC_a and volumetric water content yields fairly similar results to those for the porosity, suggesting that porosity is the primary control for the volumetric water content for the sample set examined. This result is consistent with the water content of the soils being close to field capacity. The correlation coefficients for volumetric water content are slightly lower than for the porosity, which is likely due to inaccuracies in the saturation values.

For both porosity and volumetric water content, the data exhibits a threshold effect in which the fitted line in the EC_a regressions intersects the horizontal axis (Figure 3.7c, d). Rhoades et al. (1976) discussed this threshold effect. The data set examined in this study included no samples with weighted porosity values less than 0.45 but sites with porosity just above this value exhibit very low EC_a (<0.2 $dS.m^{-1}$, Figure 3.7d). For volumetric water content the corresponding smallest values in the data set are 0.18-0.20 and samples with water content just above this limit again have very low EC_a (<0.2 $dS.m^{-1}$, Figure 3.7c).

The data for porosity and volumetric water content were fitted with quadratic functions with each parameter including a threshold value (Figure 3.7c, d). For the optimal threshold, the

regression results have similar statistical significance as the linear function. There is insufficient range in the parameters in the data set (e.g., Figure 3.6) to allow accurate discrimination between the linear and quadratic fits. Because of the relatively poor fit to the data the accuracy with which the threshold can be estimated is also poor. However, the values yielding the highest Pearson coefficients for the V-H and V-V modes are 0.10 and 0.07 for the volumetric water content and 0.42 and 0.37 respectively for the porosity.

3.7.4 Regression results for combined parameters

It is possible to examine the combined effects of fluid conductivity and volumetric water content by considering regressions of EC_a with the product of EC_w and volumetric soil water content ($\sigma_w \cdot \theta$) and with the product of EC_w and the square of volumetric soil water content ($\sigma_w \cdot \theta^2$) (Figure 3.8). These combined parameters represent constituent parts of equation 3.1 or the response in equation 3.2 for exponents of 1 and 2. For both V-H and V-V modes these regressions yield correlation coefficients that are consistently higher than those obtained for EC_w considered individually, and yield RMSE and MAE values that are consistently lower. For example, for the V-H mode the correlation coefficient, RMSE, MAE for the product of EC_w and volumetric soil water content ($\sigma_w \cdot \theta$) are 0.79, 0.22 $dS.m^{-1}$ and 0.16 $dS.m^{-1}$ compared with the results for EC_w alone of 0.75, 0.24 $dS.m^{-1}$ and 0.18 $dS.m^{-1}$. The results demonstrate that although regressions using volumetric water content as a single parameter do not produce highly significant results, the water content does have a significant influence on apparent conductivity.

Regression results for ($\sigma_w \cdot \theta$) and ($\sigma_w \cdot \theta^2$) are statistically quite similar (Figure 3.8a, b). For example, for the V-H mode the Pearson correlation coefficient, RMSE, MAE for ($\sigma_w \cdot \theta$) are 0.79, 0.22 $dS.m^{-1}$ and 0.16 $dS.m^{-1}$ compared with results for ($\sigma_w \cdot \theta^2$) of 0.81, 0.29 $dS.m^{-1}$ and 0.23 $dS.m^{-1}$. Additional tests using fractional powers of θ between 1 and 2 yield similar statistical fits. As noted above, the reason for this result is that there is insufficient variation in the volumetric water content in the data set, relative to the mean value, to allow the determination of the exact power-law dependence of EC_a on volumetric water content. Regressions were also done with a threshold in the volumetric water content (Figure 3.8c) to reflect the results for the water content noted above (Figure 3.7c). The results show that the statistical fit is only weakly dependent on the exact value of the threshold. However, the highest correlation coefficients are determined for the V-H mode for a threshold of 0.08 and the V-V mode for a threshold of zero.

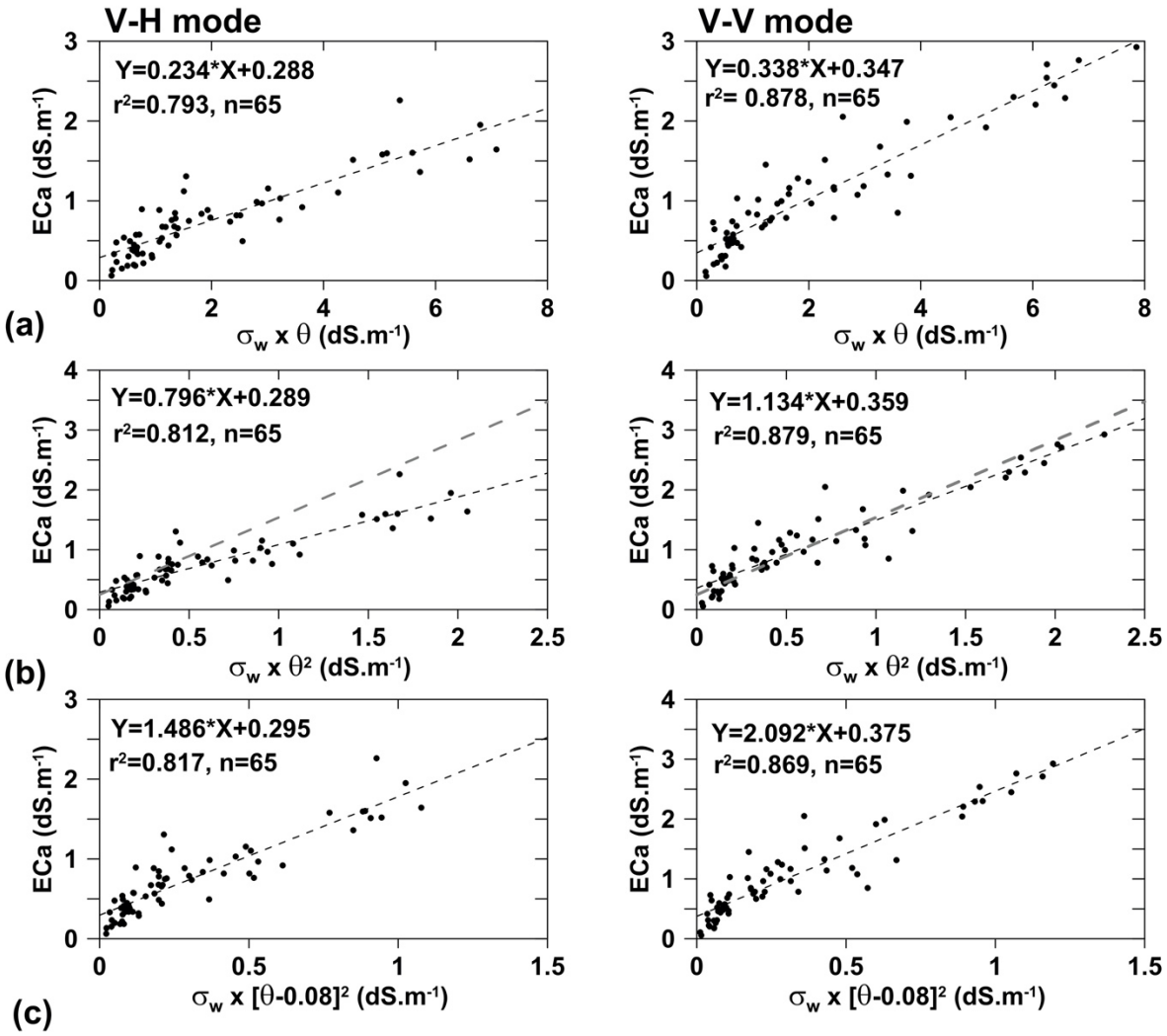

Figure 3.8 Regression of LIN-corrected V-H mode (left column) and LIN-corrected V-V mode (right column) ECa with combined-parameter variables **a** weighted ECw x θ (σw·θ), **b** weighted ECw x θ2 (σw·θ2) and **c** weighted ECw x [θ-θ0]2 (σw·[θ-θ0]2) with θ0 = 0.08. Weighting is matched to V-H or V-V mode respectively. Short dashed black line shows least-squares fitted linear trend and annotations show equation of the fitted trend, squared correlation coefficient and number of samples. Long dashed grey line in (b) shows the equation determined by Dalton and Van Genuchten (1986) i.e., $\sigma_a = 1.29\sigma w\theta^2+0.25$ dS.m^{-1}.

The linear trends defined in Figure 3.8 demonstrate very good fits to the whole EC_a data set. The EC_w and volumetric water content parameters can explain 82% of the variance in the V-H data and 88% of the variance in the V-V data. However, all results in Figure 3.8 include a similar systematic misfit at low conductivity values, as observed for the EC_e and EC_w regressions. This misfit limits the amount of variance that can be explained in the regressions and contributes to the lack of sensitivity to the volumetric water content threshold. It suggests the presence of two

different controlling relationships for EC_a within the sample data set and is examined in more detail below.

Figure 3.9 shows contour plots of V-H and V-V apparent conductivity versus EC_w and porosity. The results confirm the influence of both parameters on EC_a. The increase in EC_a with distance to the right on the plot reflects the strong increase in EC_a with increasing EC_w. Although the trend is not as simple, it is also evident that there is an increase in EC_a along the vertical ordinate on each plot showing the increase in EC_a with increasing porosity. This trend is clearest at low values of EC_e (reflecting the limiting trend at the lower limit of the data in Figure 3.7c). The trend is noisier but present at higher values of EC_w. Plots using EC_e rather than EC_w as the first independent variable and/or volumetric water content rather than porosity as the second independent variable show similar trends.

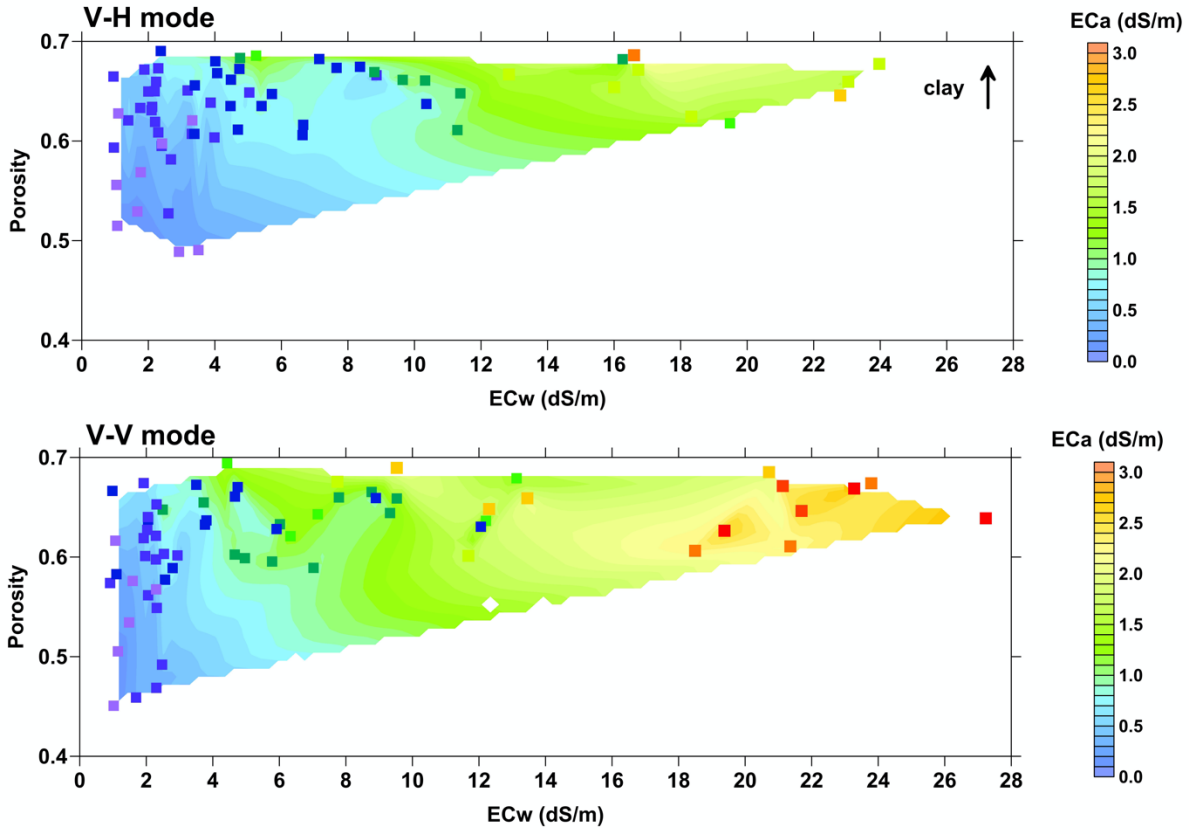

Figure 3.9 Contour plots of the ECa response at sample locations as a function of weighted ECw and weighted porosity values. Upper panel shows V-H response and lower panel shows V-V response. The contour maps were each constructed using a 100x100 point grid produced using natural neighbor interpolation. Dark symbols show the actual data points plotted using a more intense colour scale.

3.7.5 Dependence of results on porosity and clay content

Regression results for EC_e, EC_w, $(\sigma_w \cdot \theta)$ and $(\sigma_w \cdot \theta^2)$ suggest the presence of two trends in the data, one at lower values of conductivity and one at high values (Figure 3.7 and Figure 3.8). In order to test whether the clay content of the soil can explain the observations, the results were sorted according to the porosity and the regression repeated for subsets of the data corresponding to lower porosity (and lower clay content) and higher porosity (and higher clay content). Testing indicated that fits with similar regression equations and statistics could be obtained for a range of porosity cut-offs. However, results are presented here for the case of 19 samples in the low porosity range. This limit corresponds to a maximum weighted porosity of 0.617 for V–H data and 0.601 for V-V data.

Regressions for the subdivided data sets are shown in Figure 3.10. Inspection of the lower porosity results showed that the intercept for a general linear fit is close to zero. So, for the final regressions the low porosity data were fitted with a trend passing through the origin. The regressions for the subdivided data set provide a good fit to the data. Although the statistical fits for the high porosity data are slightly lower than for the full data set, the results show that two trends can explain the systematic misfit effects observed in Figure 3.7. The EC_a is best explained by a low-porosity (low clay content) low-conductivity trend with zero surface conduction and steeper slope, and a high-porosity (high clay content) high-conductivity trend with statistically-significant surface conduction and a gentler slope. The steeper slope for the low porosity data corresponds to a more rapid increase in apparent conductivity per unit increase in salinity than for the high porosity data set. It may relate to either tortuosity of pores being less, or the dissolved ions having larger effective mobility, than in the higher-porosity clay-rich soils. Surface conduction terms for the high porosity data set are significantly higher than for the combined data set, consistent with the presence of a higher clay-content. For the V-H mode, the regressions shown in Figure 3.10c indicate the surface conduction for high porosity data is 0.37 $dS.m^{-1}$ and for the V-V mode, the regressions shown in Figure 3.10d indicate that it is 0.44 $dS.m^{-1}$.

The subdivided data set was also tested to see if it permitted a more accurate definition of the optimal threshold value for volumetric water content. The results could not provide very accurate estimates for the threshold. However, they did provide sufficient resolution to suggest that the threshold for the low porosity data for both the V-H and V-V modes is close to zero. A threshold of zero yields the highest correlation coefficients in EC_a - $[\theta-\theta_0]^2$ regressions. For the

high porosity data set, the corresponding thresholds were 0.17 for V-H and 0.08 for V-V. These results indicate that the threshold effect is related to the clay-rich soils.

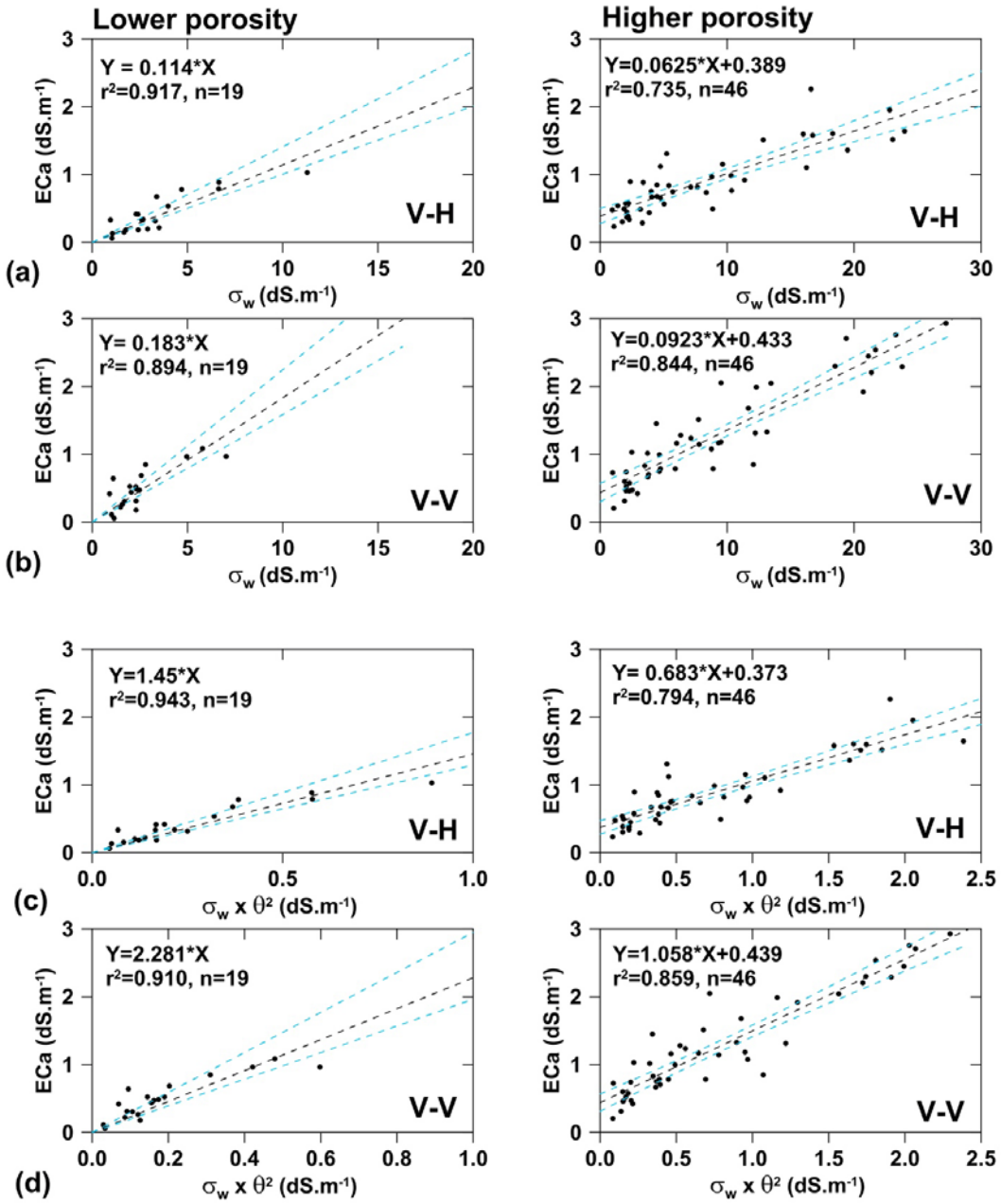

Figure 3.10 Porosity-sorted regression of LIN-corrected ECa data with **a** V-H weighted ECw, **b** V-V weighted ECw, **c** V-H weighted ECw x θ2, and **d** V-V weighted ECw x θ2. Left panels show results for 19 lowest porosity-samples for the corresponding mode with the linear trend constrained to pass through the origin and right panels show results for 46 highest-porosity samples with the linear trend including a non-zero intercept. Short dashed black line shows least-squares fitted linear trend and annotations show equation of the fitted trend, squared correlation coefficient and number of samples. Blue dashed lines are 95% confidence levels.

3.8 Application of results

3.8.1 Conversion of apparent conductivity results to salinity

The strong correlations of EC_a with EC_e or EC_w observed in this study mean that it is possible to use maps of the EC_a results to infer the spatial distribution of salinity across the study area. In general, this approach would require the maps of EC_a and also maps of moisture content and possibly soil type. However, for the present study, the EC_a depends only weakly on the moisture content and soil texture, making it possible to simply correct the measured EC_a values for their departure from a LIN response and convert the corrected EC_a values directly to an equivalent EC_e. The resulting value of EC_e represents a weighted EC_e value over the depth range of the instrument used to collect the EC_a data. In the study area, the EC_e does not vary strongly with depth, so it will be close to an arithmetic average over the exploration depth.

Figure 3.11 shows an example for one of the sub-areas surveyed in the study. The DualEM 1S V-H and V-V EC_a values were first corrected for the departure from a LIN response. This correction causes minimal change to the V-H mode results but increases the largest V-V values by about 12%. The corrected EC_a responses were then converted to equivalent EC_e responses for the upper 0.5 m and 1.5 m. The regression equations from the fit to the full V-H and V-V data sets (shown in Figure 3.7a) were used for the conversion.

As expected from the consistency of soil parameters with depth observed at the sampling sites (Figure 3.5 and Figure 3.6) there is a high correlation between the V-H and V-V derived EC_e maps. The V-V responses exhibit higher values of greater spatial continuity of areas of enhanced EC_a. The larger values of EC_a for V-V translate to larger values for the equivalent EC_e over the upper 1.5 m relative to the 0.5 m result. The relative amount of area with different salinity levels can be assessed using a salinity or a crop response classification scheme as shown in Table 3.3.

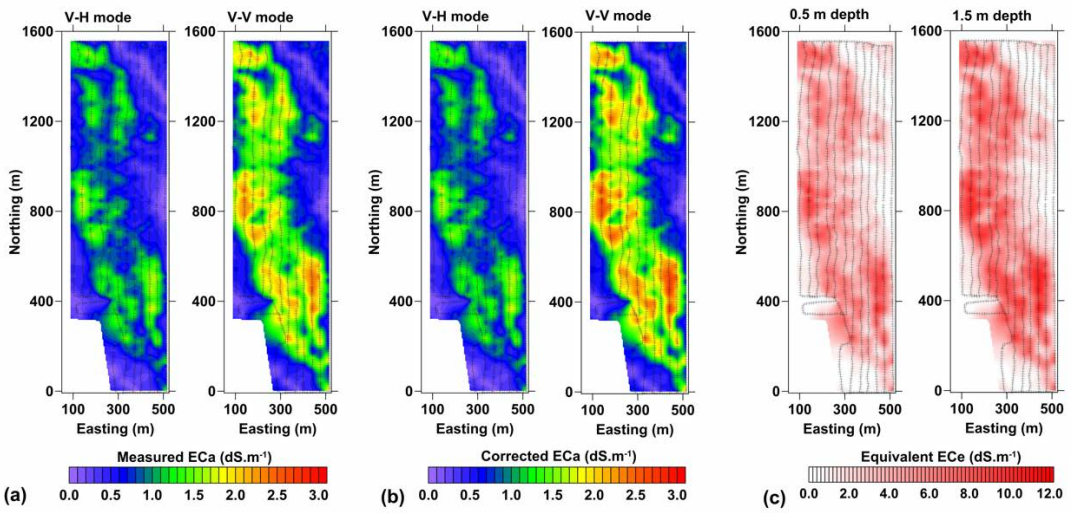

Figure 3.11 Conversion of measured EC_a values into equivalent EC_e maps for one sample sub-area of the study. **a** Measured V-H and V-V EC_a values. **b** V-H and V-V EC_a values corrected for departure from LIN responses. **c** Equivalent EC_e maps for the upper 0.5 m and the upper 1.5 m computed using the linear regression results for the full data set (shown in Figure 3.7. Each map is based on 1630 original data points. Gridded data with a 5 m spacing was produced using kriging and a manually-fitted exponential variogram with a length scale defined by the data of 105 m for the V-H mode and 120 m for the V-V mode. Black crosses show the location of individual data points. Distance axes are shown in UTM14 N coordinates relative to a reference point at the southwest corner of the sub-area.

Table 3.3 Percentage of sub-area with different levels of salinity.

EC_e ($dS.m^{-1}$)	Salinity classification* and crop response**	V-H % (top 0.5 m)	V-V % (top 1.5 m)
0-2	Non Saline. Almost negligible crop effects.	35.5	31.1
2-4	Slightly saline. Yields of very sensitive crops restricted.	28.9	18.6
4-8	Moderately saline. Yields of most crops restricted.	33.9	41.3
8-16	Strongly saline. Only tolerant crops yield satisfactorily.	1.6	9.0
>16	Extremely saline. Only very tolerant crops yield satisfactorily.	0.0	0.0

* Salinity classification scheme given in Corwin and Scudiero (2019) (from U.S. Salinity Laboratory Staff 1954)
** Crop response classification scheme from Miller and Curtin (2008) (modified from Bernstein 1975)

The accuracy of the EC_e maps can be estimated from the regression results (Figure 3.8) which suggest that, at any specific location, the maximum error in the EC_e value (equivalent to the horizontal offset of points from the fitted trend lines in Figure 3.8a) is about 1 $dS.m^{-1}$. These errors will average to zero over the whole study area. The main systematic error in the EC_e maps will

occur in low salinity areas, as at low levels of salinity the fitted regression trends slightly overestimate the conductivity. However, in many situations the low salinity areas will be outside the main focus of the study so the small overestimation will often not be a problem. In a situation of strong vertical variation in EC_e the use of a half-space model for the LIN correction will also introduce errors. However, because of the relatively small variation of EC_e with depth in the study area (Figure 3.5) this effect will be very small for this study.

As discussed by many other authors, when EC_a-derived EC_e maps are based on appropriate calibration procedures, the results have many advantages compared to direct sampling methods (Corwin and Lesch 2005a; Corwin and Scudiero 2019; Samouëlian et al. 2005; Uribeetxebarria et al. 2018; Visconti and de Paz 2016; Watson et al. 2017). In particular, the results were acquired with much less time and cost than required for a detailed soil-sampling survey. The EC_a-derived maps also have the advantage that the EC_e is spatially averaged over the lateral sensitivity range of the DualEM 1S instrument, reducing small-scale (<2 m) spatial variability in the salinity values. One disadvantage of the EC_a-derived salinity maps is that they will not account for undissolved salt in the soil. In the current study the resulting EC_e maps for each of the surveyed sub-areas will be used to quantify the amount of salt present, to assess the relationship between the salt content and observed plant growth, and if needed, to assist in planning of remediation approaches. In locations of high salinity, where SO_4^{2-} is the dominant dissolved ion, the survey results could be used to map the concentration C of sulphate in the pore water. The contribution of SO_4^{2-} to EC_w is EC_w ($dS.m^{-1}$) ~$1.6x10^{-3} \cdot C(mg.L^{-1})$ (e.g., McNeill 1980; Tycholiz et al. 2016). However, as noted above, this result will underestimate the total sulphate present in the soil because of the additional undissolved sulphate. The survey results will also be used to investigate the local controls on the distribution of the salinity, e.g., to examine correlations with micro-topography and soil oxidation conditions (e.g., Keller and Van der Kamp 1988).

3.8.2 Electromagnetic induction survey results of individual fields

Soil salinity surveys were conducted on 14 fields (Table 3.4), ECa overview maps and field specific maps are given in Appendix A. To analyze the fields for salinity the EC_a values were calibrated using depth weighted EC_e values from the corresponding sampling location. Linear regressions were performed on each individual survey area to extrapolate the calibration

throughout the data sets. Using this data EC_e equivalent maps were produced using ArcMap 10.3 through raster and kriging processes.

Laboratory saturated paste conductivity values ranged from <0.10 $dS.m^{-1}$ to 14.78 $dS.m^{-1}$ for the V-H configuration (Appendix B) and <0.10 $dS.m^{-1}$ to 11.56 $dS.m^{-1}$ for the V-V configuration (Appendix B). Soil salinity can be divided into five different severity categories based on the EC_e values: non-saline 0-2 $dS.m^{-1}$; slightly saline 2-4 $dS.m^{-1}$; weakly saline 4-8 $dS.m^{-1}$; moderately saline 8-16 $dS.m^{-1}$, and strongly saline >16 $dS.m^{-1}$ (Scianna 2002). All but two of the fields contained areas of slightly saline soils (2-4 $dS.m^{-1}$) and five fields contained soils where EC_e values exceeded 4 $dS.m^{-1}$. Results from the five fields will be analyzed below, Additional EC_e maps of the remaining fields are given in Appendix B.

Table 3.4 General information on surveyed fields stratigraphy from: Michalyna and Smith (1972).

Field	General Coordinates (UTM)	General Stratigraphy	General Surface Features
29-13-7W	14 U, 543929m E 5552749m N	Da; Pa; Ra; Ne	Cross-cut by historic tributary
16-12-7W	14 U, 544727m E 5540432m N	Ne; Wi; Dc; Df	Cross-cut by historic tributary and adjacent to borrow pit
5-13-7W	14 U, 543962m E 5546281m N	Nc; Hb; Ne	Cross-cut by historic tributary (did not extend to Portage Diversion)
32-12-7W	14 U, 543992m E 5544933m N	Nc; Hb; Ra	N/A
5-12-7W	14 U, 544557m E 5536782m N	Rr; Ne	Adjacent to borrow pit
4-12-7W	14 U, 544821m E 5536856m N	Ne	Adjacent to borrow pit
N4-12-7W	14 U, 544574m E 5537610m N	Rr-Mo	Adjacent borrow pit
8-12-7W	14 U, 544572m E 5538519m N	Rr-Mo; Oc	N/A
W20-12-7W	14 U, 544054m E 5542393m N	Ga; Wi; Ne	Cross-cut by historic tributary
E20-12-7W	14 U, 544505m E 5542124m N	Ga; Wi; Ne	Cross-cut by historic tributary
29-12-7W	14 U, 544043m E / 5543452m N	Ga; Nc	N/A
9-12-7W	14 U, 544799m E / 5538504m N	Ne; Rr-Mo; Df; Ga	N/A
21-12-7W	14 U, 544812m E / 5541883m N	Ga; Wi; Ne	Cross-cut by historic tributary
S8-13-7W	14 U, 543943m E / 5547962m N	Da; Ne	N/A

3.8.2.1 Section 29-13-7W

The surveyed area within section 29-13-7W contains four soil types, the Gnadenthal Loam, the Deadhorse Clay, the Plum Coulee Clay, and the Reinland Fine Sandy Loam (Michalyna and Smith 1972). The areas containing the highest levels of both EC_a and derived EC_e values are generally contained within both the Deadhorse Clay and the Plum Coulee Clays (Figure 3.12). Michalyna and Smith (1972) noted that throughout the region if both the Deadhorse Clay and Plum Coulee clays were in close proximity that a saline phase may exist. However, Michalyna and Smith (1972) did not map these soils within this section as being saline.

Laboratory derived EC_e analysis of the field yielded values between 0.2 $dS.m^{-1}$ up to 16 $dS.m^{-1}$ (Table 3.5) and a visual comparison of the V-V and V-H maps indicates lower salinity near the surface than at depth. The observed depth-distribution of salinity may be caused by a relatively stable moisture regime with slow upwards migration of salt from depth. Additionally, it appears that areas of higher salinity are located adjacent to what may be two historic tributaries. In this case it is possible that subsurface silt and sand lenses may extend off these sand structures into the field promoting an increase in soil salinization.

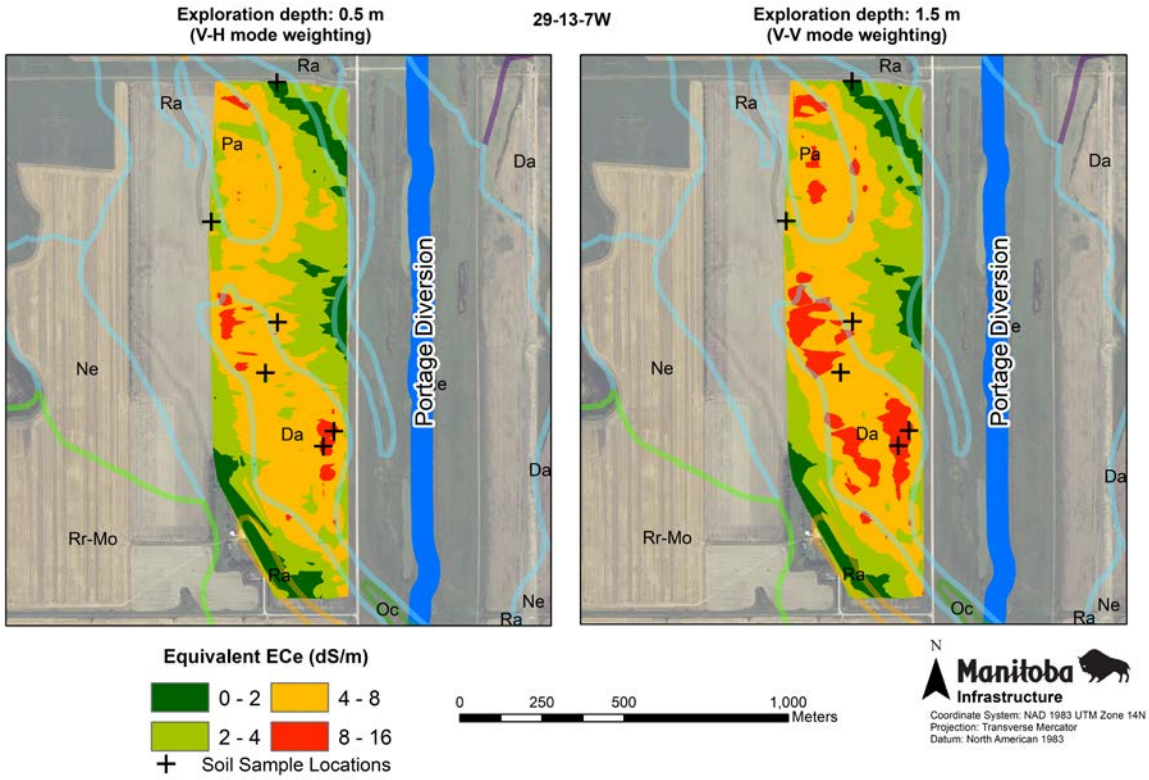

Figure 3.12 Soil salinity survey of Section 29-13-7W showing both V-H and V-V mode.

Table 3.5 Summary of Chemical Analysis from the surveyed fields with ECe values >4 $dS.m^{-1}$.

Field	Electrical Conductivity ($dS.m^{-1}$)	Chloride (ppm)	Calcium (ppm)	Magnesium (ppm)	Sodium (ppm)	Sulphate (ppm)
29-13-7W	0.2 – 16.0	6.7 – 840	9.4 – 520	4.6 – 2400	10.0 – 1600	NA
16-12-7W	1.2 – 14.0	6.3 – 1800	NA	NA	NA	1300 - 9000
5-13-7W	0.5 – 16.0	14.0 – 2300	44.0 – 590	21.0 – 2600	17.0 – 1700	NA
32-12-7W	0.5 – 11.0	8.1 – 370	28.0 – 480	9.9 – 1300	13.0 – 1500	NA
5-12-7W	0.8 – 12.0	6.3 – 1800	NA	NA	NA	1300 - 9000

3.8.2.2 Section 16-12-7W

Section 16-12-7W comprises three soil types. The primary soil type is the Neuhorst Clay Loam, with smaller areas of the Dugas Clay, and a combination of the Willowbend Fine Sand and Willowbend Clay Loam present (Michalyna and Smith 1972). The areas containing the highest levels of ECe are contained within the Neuhorst Clay Loam and are located adjacent to a large borrow pit that is located opposite a mile road to the field (Figure 3.13). Borrow pits can be a cause of increases in soils salinity due to increased amounts of evapotranspiration around the pit (Anderson 1988).

Laboratory EC_e analysis of the field yielded values between 1.2 $dS.m^{-1}$ to 14 $dS.m^{-1}$ (Table 3.5). A visual comparison of both the V-V and V-H maps indicates that there is increased near surface salinity than at depth. A visual examination of near-surface soil samples noted that white crystals were present which were interpreted to be gypsum (Figure 3.1). The presence of such crystals may be indicative of an upwards migration of salt within the profile.

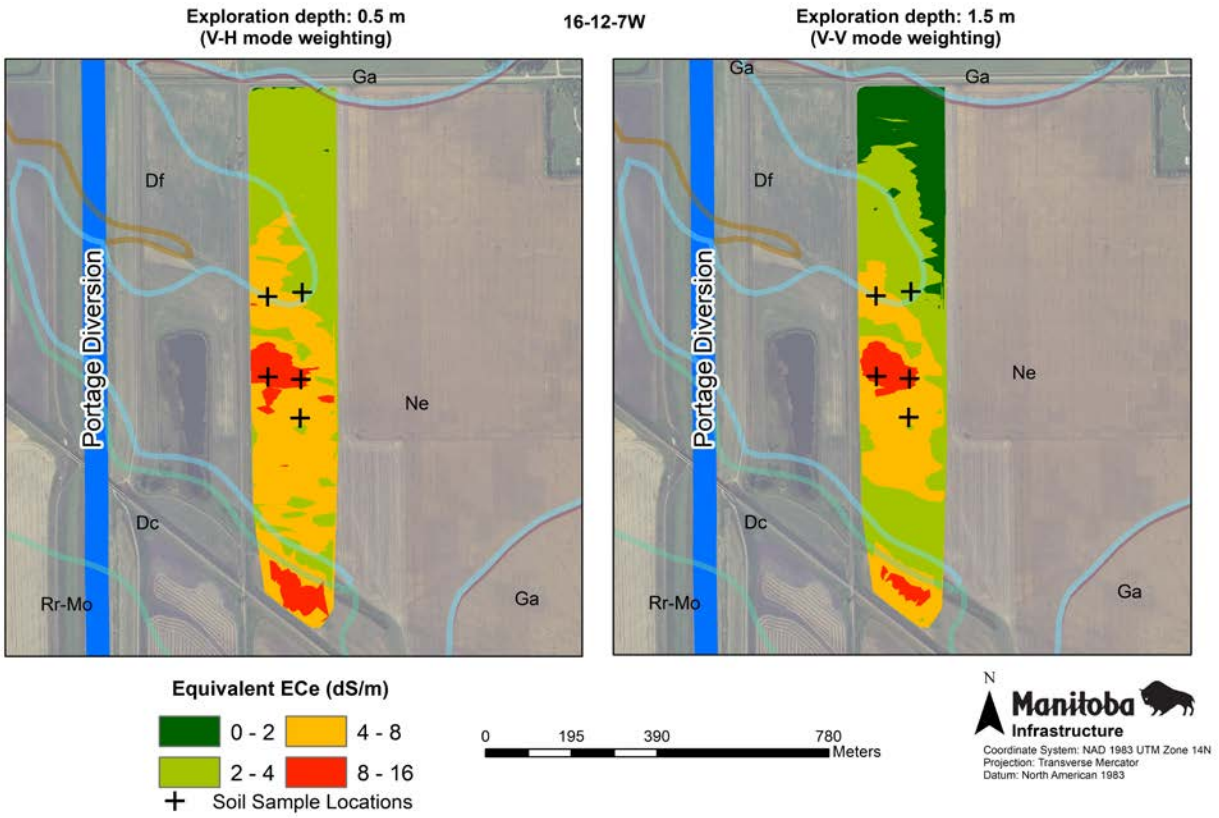

Figure 3.13 Soil salinity survey of Section 16-12-7W showing both V-H and V-V mode.

3.8.2.3 Section 5-13-7W

Section 5-13-7W comprises primarily the Neuhorst Clay Loam and Nuenberg Loam, with lesser amounts of the Hochfield Fine Sandy Loam, and Willowbend fine Sand to Clay Loam (Michalyna and Smith 1972). Areas of highest measured EC_e are located adjacent to the Portage Diversion dike and the Hochfield Fine Sandy Loam which transects the Portage Diversion (Figure 3.14).

Laboratory EC_e analysis of the field yielded 0.5 $dS.m^{-1}$ to 16 $dS.m^{-1}$ (Table 3.5). A visual comparison of the V-V and V-H maps indicates that there is less salinity near the surface than at depth. This may be indicative of elevated piezometric levels which may be promoting an upwards migration of salt. Additionally, areas of elevated EC_e are located adjacent to the Hochfield Fine Sandy Loam which may be a historic tributary, subsurface sand and silt lenses may extend from the tributary into the field promoting increases in salinity.

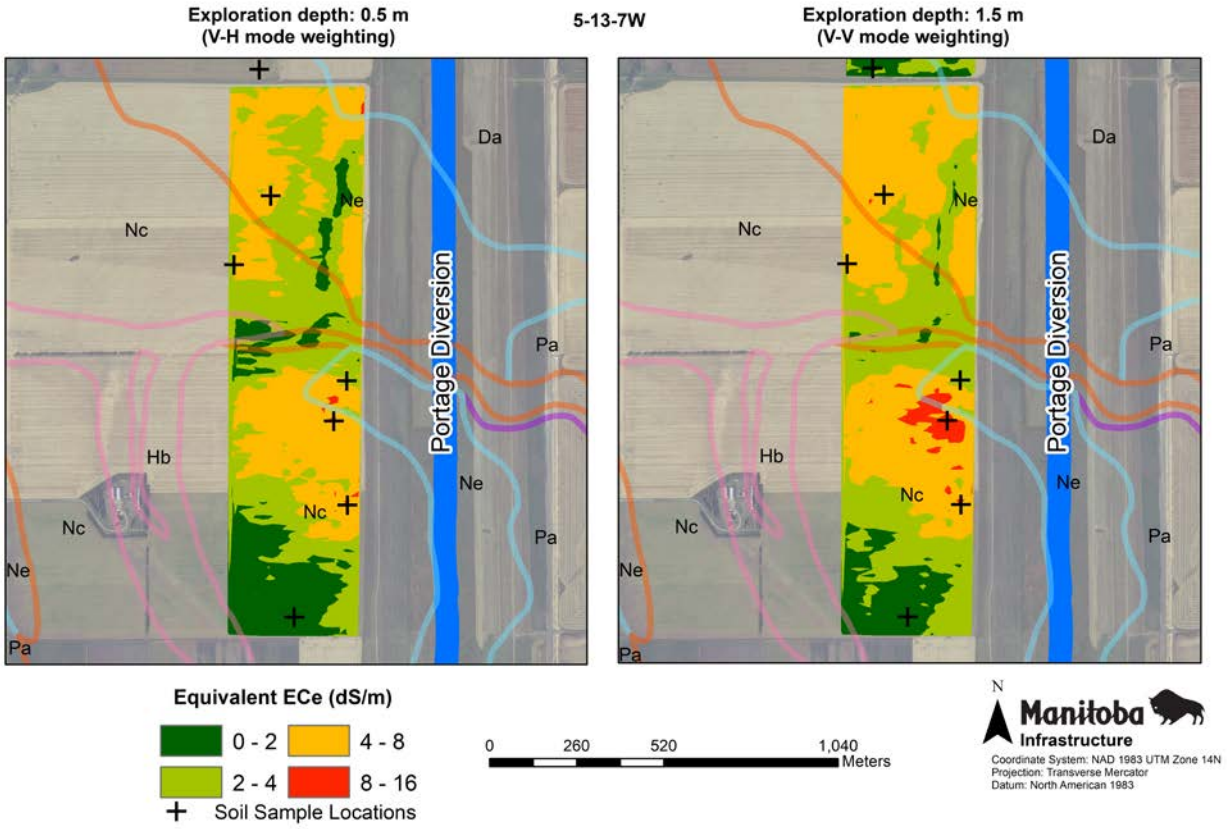

Figure 3.14 Soil salinity survey of Section 5-13-7W showing both V-H and V-V mode.

3.8.2.4 Section 32-12-7W

Section 32-12-7W comprises primarily Nuenberg Loam with smaller areas of the Hochfield Sandy Loam and Reinland Fine Sandy Loam (Michalyna and Smith 1972). The area of highest EC_e values is located near the center of the site (Figure 3.15). Laboratory EC_e analysis of the field yielded 0.5 $dS.m^{-1}$ to 11 $dS.m^{-1}$ (Table 3.5). A visual comparison of the V-V and V-H maps indicates that there is moderate salinity at both the near-surface and at depth.

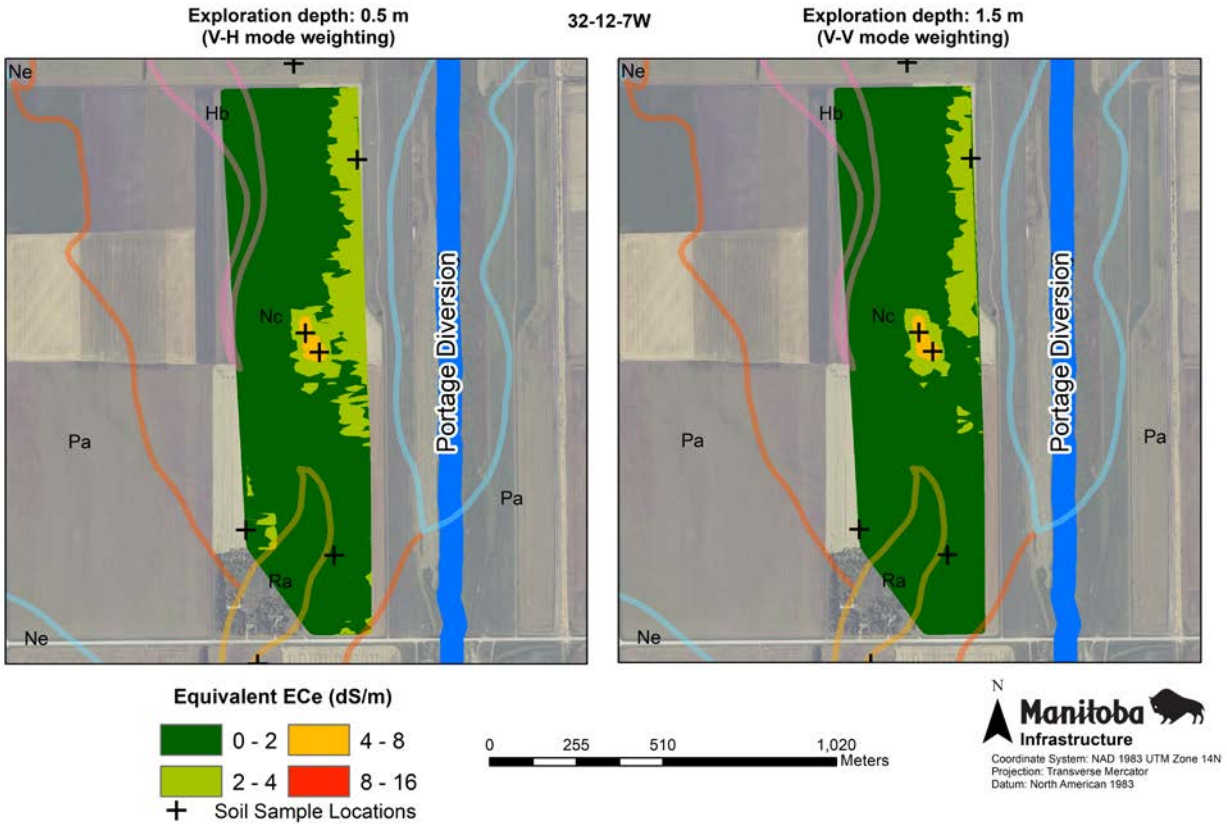

Figure 3.15 Soil salinity survey of Section 32-12-7W showing both V-H and V-V mode.

3.8.2.5 Section 5-12-7W

Section 5-12-7W comprises both the Red River Clay and Neuhorst Clay Loam (Michalyna and Smith 1972). The highest EC_e values are located in the northern area of the field by a borrow pit, and adjacent to the Portage Diversion dike (Figure 3.16). Laboratory EC_e analysis of the field yielded 0.8 $dS.m^{-1}$ to 12 $dS.m^{-1}$ (Table 3.5). A visual comparison of the V-V (1.5 m exploration depth) and V-H (0.5 m exploration depth) maps indicate a small extent of moderate salinity in the shallow root zone with a larger extent at depth which may be indicative of an upwards migration of salt.

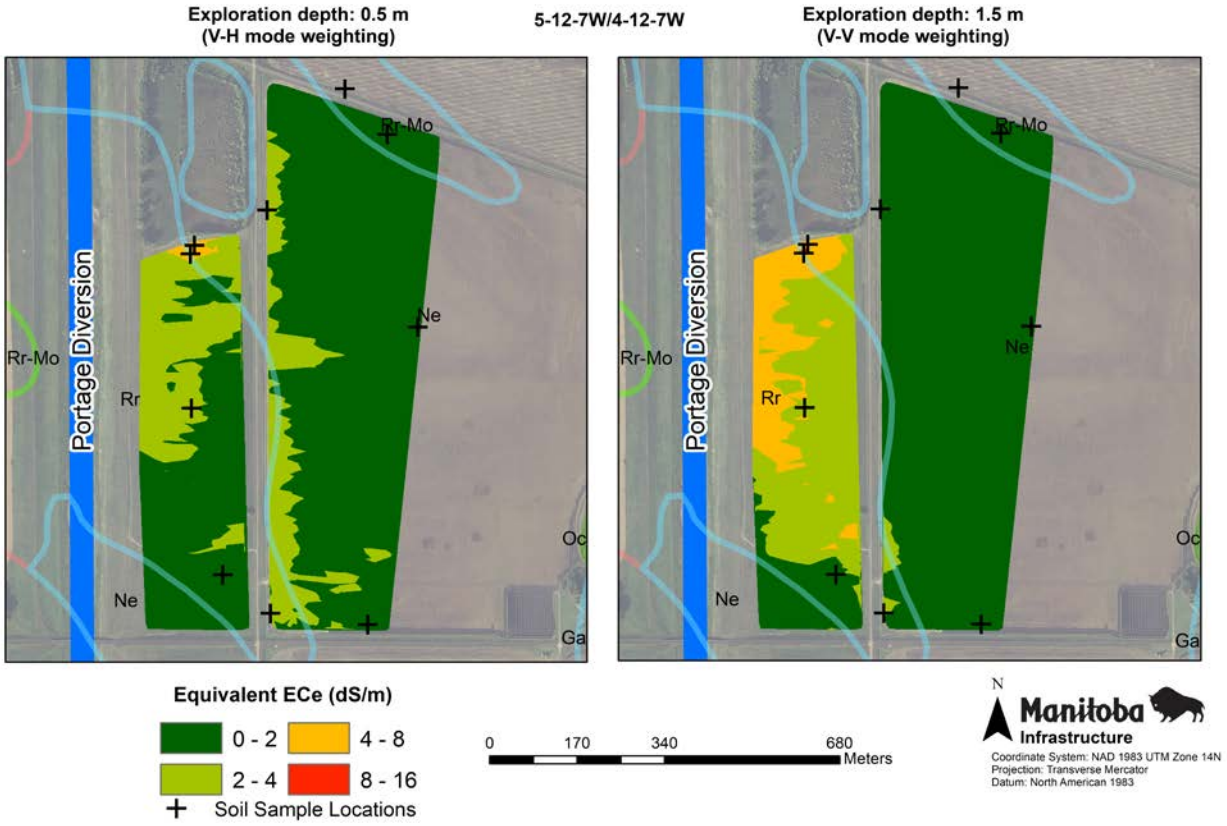

Figure 3.16 Soil salinity survey of Sections 5-12-7W and 4-12-7W showing both V-H and V-V mode.

3.9 Discussion

3.9.1 Review of apparent conductivity prediction results

Results of this study show that depth-weighted saturated paste extract values, when used alone, provide a good prediction of the apparent conductivity across the study area (Figure 3.7a, Table 3.6). For the full data set, a linear trend based on these values explains 78% of the variance in the V-H EC_a data and 87% of the variance of the V-V EC_a data. RMSE and MAE values indicate that the EC_a in the study area can be predicted from weighted EC_e values with an accuracy of about 0.2 $dS.m^{-1}$ (Tables 3.1 and 3.2). Conversion of the EC_e results to equivalent pore-water conductivity reduces the statistical fit only slightly and suggests the presence of small errors in the saturation values, which were determined indirectly in this study.

Depth-weighted volumetric water content values, when used alone, provide a poor prediction of apparent conductivity with only marginal statistical significance (Tables 3.1 and 3.2). However, when the parameter is included with the pore water conductivity, the combined

parameter can explain slightly more variance of EC_a values than the saturated paste extract conductivity. For the whole data set, a linear trend based on $\sigma w\theta^2$ values can explain 81% of the variance in the V-H EC_a data and 88% of the variance of the V-V EC_a data.

Table 3.6 Summary of relationships determined between ECa, ECe, ECw and volumetric water content.

Data set	V-H result		V-V result	
	Function ($dS.m^{-1}$)	r^2	Function ($dS.m^{-1}$)	r^2
Full data set (n = 65)	$0.152 \cdot EC_e + 0.284$	0.777	$0.219 \cdot EC_e + 0.336$	0.872
	$0.0689 \cdot EC_w + 0.294$	0.752	$0.0979 \cdot EC_w + 0.344$	0.859
	$0.796 \cdot EC_w\theta^2 + 0.289$	0.812	$1.13 \cdot EC_w\theta^2 + 0.359$	0.879
Lower porosity (n = 19)	$0.144 \cdot EC_w$	0.917	$0.183 \cdot EC_w$	0.894
	$1.45 \cdot EC_w\theta^2$	0.943	$2.28 \cdot EC_w\theta^2$	0.910
Higher porosity (n = 46)	$0.06652 \cdot EC_w + 0.389$	0.735	$0.0923 \cdot EC_w + 0.433$	0.844
	$0.683 \cdot EC_w\theta^2 + 0.373$	0.794	$1.06 \cdot EC_w\theta^2 + 0.439$	0.859

Note: all functions are significant at 99% confidence level

The study results provide a strong indication of threshold effects in volumetric water content (e.g., Figure 3.7c). Multiple methods were tried in order to make an accurate and independent determination of both c and θ_0 or both a and b.

(i) An approach similar to that shown in Rhoades et al. (1976) was applied in which quadratic functions were fitted to $(EC_a - \sigma_{surf})/EC_e$ versus θ. The method yielded results with low r^2 values corresponding to large uncertainty estimates on the fitted coefficients.

(ii) Using a similar approach, regressions of EC_a with $[\theta - \theta_0]^2$ were done for a range of threshold values. The results yielded correlated values of c and θ_0 and low r^2 values indicating large uncertainty estimates on both c and θ_0.

(iii) Finally, a full grid search was conducted over a and b using a MATLAB code to determine the values or a and b that explained the maximum variance in the V-H, V-V or combined V-H and V-V EC_a data sets. The method yielded negatively correlated solutions for a and b with no single combination of values explaining significantly more variance than individual linear or quadratic terms. The multiple solutions are related by:

$$c = a + 2b \qquad \text{Eq. 3.13}$$

where c is the quadratic coefficient if $b = 0$.

The poor results obtained from all methods applied show that the data set does not include a sufficient range of water content values to allow accurate and independent determinations of either c and θ_0 or a and b. Therefore, results for apparent conductivity are given simply here in the form of equation 3.2 (Table 3.6). Equivalent values of a and b or c and θ_0 can be calculated with the introduction of additional constraints.

Finally, the study shows that for the full data set, the linear trends used to predict EC_a from the saturated paste extract conductivity, pore-water conductivity, or combined parameters overestimate the observed EC_a at low values of conductivity. The EC_a variations can be explained by the presence of a steeper trend, with zero surface conductance, for samples with lower porosity and a gentler trend, with significant surface conductance, for samples with higher porosity values. The lower porosity data set corresponds to samples with low clay content and the high porosity data set corresponds to clay-rich samples.

The coefficients of the independent variable shown in Table 3.6 are lower than those in which EC_a and EC_e are determined for the same temperature. Soil temperature was not measured during the electromagnetic survey. Based on previous studies in the region (e.g., Ferguson and Desrosiers 1998) and the warm fall weather before the survey, it is estimated fairly reliably at 10±2°C over the depth-range of the measurements. For NaCl solutions, conductivity increases by 2% per °C (e.g., McNeill 1990; Corwin and Lesch 2005a; Knight and Endres 2005; Visconti, F., and Miguel de Paz 2016). Assuming a similar temperature for sulphate-dominated solutions, the 15°C difference between the actual soil temperature and the 25°C reference for the EC_e laboratory measurements means that the coefficients determined in the study will be 30% lower than temperature-corrected values.

3.9.2 Comparison of EC_a-EC_e and EC_a-water content correlations obtained in other studies

Statistical fits determined in the present study can be compared with results of previous field and laboratory studies that related apparent conductivity to saturated paste conductivity, pore-fluid conductivity and/or water. Wollenhaupt et al. (1986) used a similar regression approach to the present study to examine the linear relationship between EC_a and weighted EC_e values using EM38 measurements in fine loamy soils from North Dakota. Their weighted EC_e values were much higher than in the current study with maximum values of about 80 $dS.m^{-1}$. In their

regressions, they treated weighted EC_e as the independent variable and observed EC_a as the dependent variable. Their results indicated that for the EM38 V-V mode, which has similar depth-sensitivity to the DualEM 1S V-V mode the EC_a was able to predict 92% of the variance of EC_e. This result is similar to the 87% prediction of EC_a from EC_e in the present study.

Numerous other studies in Canada and elsewhere have demonstrated similarly strong statistical relationships between EC_a and EC_e (Amezketa 2007; Bouksila et al. 2012; Lesch et al. 1992; Read and Cameron 1979). In general, these studies have involved relatively high pore-water salinity, fairly uniform levels of soil moisture, or both. The soil moisture condition minimizes the EC_a signal due to variations in moisture content allowing for stronger correlations with EC_e or EC_w. High moisture contents may also partially reduce the effects of soil texture. As a result of relatively low spatial variation in soil moisture in these studies, they have also commonly yielded poor statistical correlation between EC_a and moisture content (e.g., Read and Cameron 1979; Amezketa 2007).

In contrast, other studies have yielded lower correlations between EC_a and EC_e and stronger correlations between EC_a and θ. For example, Kachanoski et al. (1988) determined for soils in southern Ontario, Canada, that EC_a values measured by EM38 and EM31 instruments yield correlation coefficients between EC_a and pore-water conductivity of only around 0.25 but correlations between EC_a and water-content of 0.77. These authors note possible effects of the broad sensitivity functions of the electromagnetic instruments on their results. However, they attribute most of the low correlation of EC_a with soil moisture conductivity to low salinity of the pore fluids and low moisture content (Kachanoski et al. 1988, 1990). Other studies have shown moderate to very strong correlations of EC_a and moisture content can occur in locations having strong variation in moisture content and/or low to moderate soil conductivity (e.g., Sheets, R & Hendrickx 1995; Khakural et al. 1998; Job et al. 1999; Nagy et al. 2013; Misra and Padhi 2014).

The present study indicates moderate to strong correlations between EC_a and EC_e ($r^2>0.77$) and weak to very weak correlation of EC_a and moisture content ($r^2<0.21$). The results occur even though the salinity levels are only low to moderate (with a mean EC_e of ~3.5 $dS.m^{-1}$). They can be attributed to the limited spatial variation in water content across the study area at the time of the survey and soil sampling. The observation is in turn explained by the water content being close to field capacity. As noted above, the mean saturation percentage and water content values suggest the soils at different depth was at between 78% and 100% of the field capacity at the time of the

study. The observed strong correlations between EC_a and EC_e are thus in agreement with previous recommendations. For electromagnetic induction methods to provide an optimal mapping of salinity the soil moisture needs to be close as possible to a uniform level such as maximum field capacity (e.g., Rhoades et al. 1976; Lesch et al. 1992; Samouëlian et al. 2005; Amezketa 2007; Bouksila et al. 2012).

As a corollary, although soil salinity is only moderate in the current study area, the relatively high, uniform water content means the EC_a data set less suitable for examining the effects of soil moisture or mapping the spatial variation in soil moisture. For example, the available data do not allow accurate determination of the coefficients of a multiple term power relationship between EC_a and water content even when the data set is sub-divided to account for effects of soil texture.

3.9.3 Comparison of physical relationships with other studies

It is instructive to compare relationships for EC_a determined in the present study with results from previous studies. Rhoades et al. (1976) used laboratory measurements to fit EC_a values with an equation of the form of equation 3.1. They determined values for the quadratic coefficient of θ, *a*, ranging from 1.287 in sandy loam to 2.134 in clay. Other studies have also determined coefficients in this range (e.g., Dalton and Van Genuchten 1986; Kachanoski et al. 1988). These studies have also determined values of values for the linear coefficient, *b*, and negative values of *b*, the corresponding threshold value θ_0. Rhoades et al. (1976) list values of *b* ranging from -0.064 to -0.245 corresponding to (linear) water content thresholds of 0.05 to 0.12, Dalton and Van Genuchten (1986) determined a value of b = -0.116 corresponding to a (linear) threshold of 0.09 and Kachanoski et al. (1988) determined a high value for the water content threshold of 0.25.

A larger number of previous studies have determined the surface conductivity term. For example, Rhoades et al. (1976) determined values of 0.18 to 0.45 $dS.m^{-1}$, Wollenhaupt et al.'s (1986) results for the EM38 horizontal and V-V modes correspond to values of 0.27 and 0.31 $dS.m^{-1}$ respectively, Dalton and Van Genuchten (1986) determined a value of 0.25 $dS.m^{-1}$, and Kachanoski et al. (1988) determined a value of 0.14 $dS.m^{-1}$. Overall, the value is expected to increase with increasing cation exchange capacity or clay content (e.g., Friedman 2005). Although the surface conduction increases with some other chemical properties such as exchangeable

sodium percentage, studies have found it to be relatively independent of the EC_w (e.g., Rhoades et al. 1976).

The quadratic coefficients determined in the present study (Table 3.6) are significantly lower than typical values for a noted above, especially the values of *a* applicable for clay rich soils. After correction for temperature effects, the coefficients for the full data set are $c = 1.137$ for V-H data and $c = 1.614$ for V-V and the coefficients for the high porosity data set are $c = 0.978$ for V-H data and $c = 1.514$ for V-V data. Only the results for the low porosity data set lie in, or close to, the expected range. These observations can be explained by the presence of threshold effects in volumetric water content and provide additional support for the presence of threshold effects in both the full data set and the high porosity data set.

If a threshold effect is present, the value of *c* determined from an EC_a data fit represents the combined effect of the individual *a* and *b* coefficients. The grid search results described above defined the relationship between *c* and *a*, *b* in equation 3.13: $c = a+2b$. If the threshold is zero ($b = 0$) then $a = c$ but if the threshold is non-zero ($b<0$) then $a>c$. The internal relationship between *a* and *b* is defined by the linear or quadratic threshold coefficient. It can be combined with equation 3.13 to calculate the exact relationship between *a* and *c*. For example, for a quadratic threshold coefficient of 0.1, $a = 1.4c$.

The temperature-corrected coefficients determined in this study can be compared with the expected value for a clay rich soil of $a = 2$ to provide an independent estimate of the water content threshold. In order for the observations to yield a coefficient of $a = 2$, the corresponding thresholds required for the full data set, are 0.08 for V-H and 0.05 for V-V and the thresholds required for the high porosity data set are 0.13 for V-H and 0.06 for V-V. These results are remarkably close to the relatively low-accuracy thresholds estimated from regressions of EC_a with $[\theta-\theta_0]^2$. The latter yielded maximum correlation coefficients for the full data set at thresholds of 0.10 for V-H and 0.07 for V-V and the high porosity data set of 0.17 for V-H and 0.08 for V-V. The results provide firm support for water content thresholds of around 10%, below which the exact water content does not affect the apparent conductivity. The thresholds are higher for the high porosity data set because of the removal of the effects of the low threshold data in the low porosity data set. The higher values for the V-H data than the V-V data set may be due to the greater sensitivity of the V-H response to near-surface depths where saturation percentage data suggests a higher clay content.

The surface conductivity values estimated in this study for the high porosity data set were 0.373 $dS.m^{-1}$ for the V-H mode and 0.439 $dS.m^{-1}$ for the V-V mode. These values are for a soil temperature of about 10°C. The values are relatively high compared with those in other studies, indicating the soil's relatively high clay content and cation exchange capacity. The higher value for the V-V mode indicates an increase in surface conduction with depth. This trend is the opposite of expected from percentage saturation results considered in isolation, which suggests a decrease in the clay content with increasing depth. The result may be due to a minor contribution of water to the surface conduction and the increasing water content with depth.

3.9.4 Effects of sulphates on apparent conductivity

The results of this study show that despite the sulphate-dominated salinity and high clay content of the soils, the relationships of EC_a to EC_e and water content are similar to those observed in previous surveys (Table 3.6). However, it is useful to examine some of the results of the study in the context of the pore fluid and soil compositions.

Figure 3.2 shows the correlation between EC_w and pore fluid composition for water samples of varying salinity from the study area. It shows that pore fluids are dominated by the chloride content at low salinity and sulphate at intermediate to high salinity. The transition between the different pore-fluid composition with increasing salinity appears to have no significant impact on the study result. The results for higher levels of salinity in the study, (i.e., the extension of the data points towards the right hand sides of Figures 3.7a, b, 3.8, 3.9, and 3.10) are based on sulphate-dominated pore fluids. However, they are consistent with results for the lowest salinity levels, which corresponds to more chloride-rich pore-fluids. Although there are two trends present in the EC_a-EC_w relationships (e.g., Figure 3.10) the data points do not divide into individual trends for low and high EC_w as would be expected if the ionic composition affected the EC_w-EC_e relationship. As shown in Figures 3.8 and 3.10, there are data points at EC_w values of less than 5 $dS.m^{-1}$ falling onto both the trend defined lower porosity samples as well as the trend for higher porosity samples. The spread in this response can be attributed to changes in the soil rather than the pore fluid composition.

The presence of gypsum in soil samples may affect the determination of EC_e and EC_w values. Khorsandi and Yazdi (2011) found that for soils containing gypsum different relationships existed between EC_e determined using aqueous extraction from saturated pastes and conductivity

determined using various soil/water extract or suspension ratios such as EC1:5. In some cases, the fitted relationship between these parameters included a constant indicating an offset between the values. The relationships were affected by the soil texture but not in a consistent manner. The study results suggest varying degrees of the dissolution of solid-phase gypsum during the different conductivity determination procedures. Callaghan et al. (2016) provided a more rigorous examination of this process. They showed that the effects of dissolution of solid gypsum on the measured EC_e increase as the soil becomes less saline. For EC_e <3 $dS.m^{-1}$ the EC_e modeled in the absence of excess gypsum dissolution was up to 52% lower than the measured value.

The results of the present study do not provide any clear evidence of gypsum dissolution effects in the EC_e determination, even though the soils from the most saline areas contain visible salt crystals (Figure 3.1). Such effects may be manifest as a downward curvature of the EC_a versus EC_e or EC_w data at larger values of EC_e (due to regressions based on the laboratory-measured EC_e overestimating the amount of sulphate sensed by field EC_a readings). As shown in Figure 3.10 there is no evidence of such curvature in the V-H or V-V data. It is possible, that there could be a consistent overestimation of EC_e at all salinity levels, changing the slope of the fitted trend, but this would require solid gypsum to have been present in all of the soil samples. Also, as discussed above, the EC_a-EC_w slopes that were determined are close to expected values for a clay-rich soil with a threshold moisture content effect, so any overestimation of EC_e must be relatively minor. One possible reason for the absence of stronger effects is that electromagnetic survey measurements were made under moisture conditions near field capacity minimizing the differences between moisture conditions between the field survey and laboratory determination of EC_e.

3.9.5 Effects of clay on apparent conductivity

Soil samples analyzed in the study area have very high saturation percentages and corresponding high values for the porosity calculated from the saturation percentage using equation 3.6 (Figure 3.5 and Figure 3.6). Soils in the surrounding region and within the study area have been classified as montmorillonite (Michalyna and Smith 1972). The clay mineralogy of the soil samples was not determined in the present study. However, the very high plasticity in field soil samples and the high measured values of saturation percentage, suggest a significant montmorillonite component.

The results from the study are generally consistent with those from other studies of clay-rich soils. For example, slopes of the regression fits are consistent with the regression coefficients and water content thresholds determined in other studies (e.g., Rhoades et al. 1976). The surface conduction terms fitted in the study (0.373 $dS.m^{-1}$ for the V-H mode and 0.439 $dS.m^{-1}$ for the V-V mode) are relatively high values. However, they are consistent with the presence of montmorillonite soils, which will have a high cation exchange capacity (Michalyna and Smith 1972). The present study is consistent with earlier studies done on montmorillonite soils alone and soils with montmorillonite and sulphate salinity (e.g., Corwin and Lesch 2005b). For example, relatively weak dependence of the measured EC_a on water content is consistent with studies showing that the resistivity of montmorillonite-rich clay is relatively weak at moisture contents exceeding about 0.2 (e.g., Kibria and Hossain 2012).

It is of note that slope of the regression fits for the high porosity data set have slopes that are about 50% smaller than for the low porosity data set for regression involving both EC_w alone and the $EC_w \cdot \theta^2$ combination (Figure 3.10, Table 3.6). This result indicates that for the more clay-rich soils there is a smaller overall increase in apparent conductivity per unit increase in EC_e and/or water content. This effect is explained by the large specific surface areas of the clays involved and the corresponding need for more water and salt to form a continuous saline surface water film (e.g., Kibria and Hossain 2012).

One aspect considered in studies of the conductivity of clay soils is the degree to which the surface conductivity term is independent of EC_w (e.g., Rhoades et al. 1976; Friedman 2005). The two trends evident in the EC_a versus EC_w data (Figures 3.8 and 3.10) in this study cannot be explained by EC_w-dependent surface conduction. Linear regression of the parameter $EC_w (\theta-\theta_0)^2$ (which contains an implicit EC_w dependent term, $\theta_0^2 EC_w$) to either V-H or V-V EC_a data resolves an independent constant term that is similar to the surface conduction term obtained when fitting $EC_w\theta^2$. The result indicates that the surface conductivity term for the data set examined and the moisture contents involved is relatively independent of EC_w.

3.9.6 Additional electromagnetic induction surveys results

3.9.6.1 Soil salinity index

Soil salinity can have varying effects on crop growth based on crop type (Tanji and Kielen 2002). The primary negative effect is an increase of osmotic pressure which causes a decrease in

water uptake by the roots (Henry et al. 1987). This effect in turn will starve the plant of water and nutrients and over a larger scale will cause decreased crop yields. The rate at which various crops are affected can vary greatly. Generally vegetables (soybeans, corn, etc.) do not tolerate increases in salinity and require low conductivity soils, whereas grains and forages tend to be more tolerant to soil salinity (Mckenzie 1988; Tanji and Kielen 2002).

Some common crops grown within the study region are beans, corn, potatoes, oats, canola, wheat, and onions/shallots. Of these the most sensitive to soil salinity are beans, corn, potatoes, and onions/shallots. Tanji and Kielen (2002) compiled numerous studies that described soil salinity thresholds for various crops and the rate at which decreases in yield may be observed based on soil conductivity. For instance beans may be affected at soil conductivity levels as low as 1.0 dS/m, corn at 1.7 dS/m, onions/shallots at 1.2 dS/m, and potatoes at 1.7 dS/m (Tanji and Kielen 2002). It was also reported that productivity of these crops would decrease at the following rates 19%, 12%, 16%, and 12%, respectively, per increase of 1.0 dS/m. Based on these values, soils which are considered non-saline (Scianna 2002) can still have negative impacts on crop productivity due to low conductivity values, thus every field within the study region may be impacted by low levels on conductivity depending what crops are grown.

3.9.7 Effects of microtopography on salinity

The potential effects of microtopography on soil salinity relates to piezometric levels within the field in question. In both fields 29-13-7W and 5-13-7W on the western side of the Portage Diversion there is a distinct correlation between elevated soil salinity (EC_e derived) and topography (Figures 3.17 and 3.18). There are several processes that can possibly influence increases in soil salinity in low lying areas. Firstly, elevated levels of surface runoff may accumulate within the low-lying areas. Secondly, piezometric levels will be closer to surface in low lying areas versus areas of even slightly higher topography, this is caused because piezometric levels and surface elevation are not 1:1. For example, if we assume that the piezometric level is at an elevation of 250 m, and there is a topographic high next to a topographic low with elevations of 251 and 250.5, then the piezometric level is 0.5 m closer to surface within the topographic low.

Due to this discrepancy in piezometric levels, the third process which is evapotranspiration, may have a greater effect soil salinity within the topographic lows due to the increase in soil saturation near surface. In areas where the groundwater is naturally saline this will be a greater

concern as salt precipitation will be closer to surface within the low areas. Both fields in sections 29-13-7W and 5-13-7W may be impacted by microtopography, areas of increased EC_e tend to be located within topographic lows.

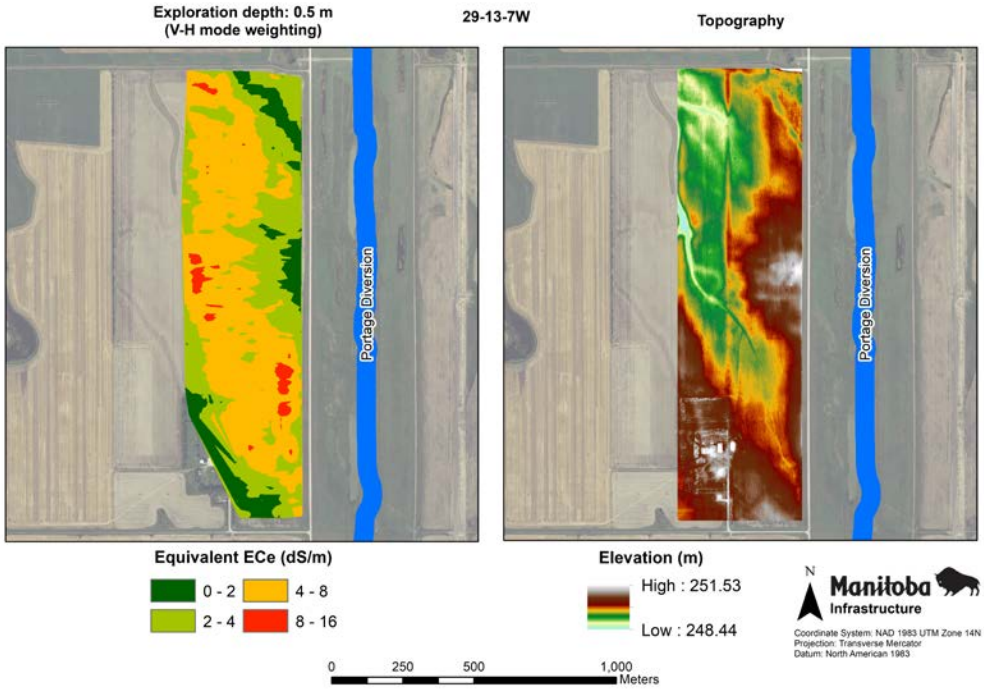

Figure 3.17 A comparison between the soil salinity analysis from the V-H mode to microtopography in Section 29-13-7W.

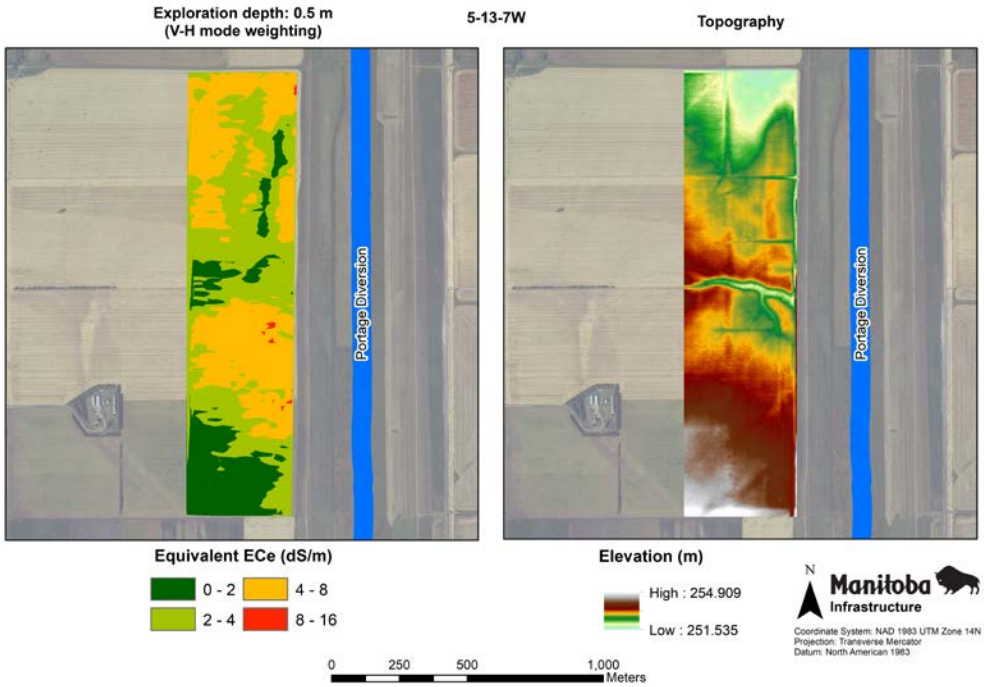

Figure 3.18 A comparison between the soil salinity analysis from the V-H mode to microtopography in Section 5-13-7W.

3.10 Conclusions

Electromagnetic inductions surveys using a DualEM 1S were conducted in alluvial soils in an agricultural area in southern Manitoba, Canada over a number of narrow sub-areas extending over a distance of 20 km. Geological and hydrogeological conditions around the study area cause upward flow of groundwater through montmorillonitic glaciolacustrine clays resulting in sulphate-dominated salinity. Gypsum crystals are visible in the soil in the most saline areas. In this study, DualEM electromagnetic survey results were used along with 542 soil samples covering 8 depths from 0 - 130 cm at 65 sites to conduct a soil salinity survey on 14 fields and define the relationships between the measured EC_a values, salinity and moisture content of the soil.

The electromagnetic survey collected EC_a data using the V-H mode (exploration depth of 0.5 m) and V-V mode (exploration depth 1.5 m) of the DualEM 1S instrument. Measured data were corrected for their departure from a LIN response using a uniform half-space model for the conductivity. For the low to moderate EC_a values measured, this correction results in minimal change to V-H EC_a values and a 12% increase to the largest V-V EC_a values. Laboratory analyses of the soil samples included EC_e, composition, gravimetric water content, and saturation percentage. These measurements were combined using standard procedures to yield porosity, volumetric water content, relative water saturation, and EC_w. Overall the soil parameters indicate relatively high clay content (based on average saturation percentages with increasing depth of 0.71 to 0.56) and relatively uniform volumetric water content of around 0.27-0.30. Although the calculated water saturation is only at a moderate level (around 0.45-0.52) comparison of the saturation percentage and volumetric water content indicates that the moisture content of most samples was relatively close to field capacity. Corrected EC_a values and soil parameters were compared using linear and quadratic regressions of V-H and V-V EC_a with values of soil parameters depth-weighted using the sensitivity of the corresponding instrument response.

3.10.1 Field surveys

Salinity surveys of the 14 fields indicated that each one comprises areas of slightly saline soils. Depending on the crop grown on these fields there may be decreased yields on each field as certain crops are susceptible to soil conductivities below 2 $dS.m^{-1}$, this means that crops such as: corn, beans, onions/shallots, and potatoes that are grown in soils that are considered non-saline to

slightly saline (Scianna 2002) may experience decreased yields. Of the 14 fields, five contained areas of conductivity >4 $dS.m^{-1}$ to a maximum of 16 $dS.m^{-1}$. Within these fields it is expected that if the crops previously mentioned were grown, there would be substantial decreases to crop yield based on the electrical conductivity tolerances given by (Tanji and Kielen 2002). Within two of the five fields there is a distinct correlation with microtopography a soil conductivity. It is believed that this correlation may be driven by the difference in surface elevation to groundwater elevation where the areas of low topographic elevation experience elevated groundwater levels which would cause increases in evapotranspiration, capillary rise, and increase in surficial water ponding due to surface run off.

Additionally, the area of saline soil in Section 16-12-7W is located adjacent to a borrow pit that was dug in the 1960's or 1970's. There is conflicting anecdotal information on the borrow pit. It is assumed that the water elevation in the borrow pit is roughly approximate to the local groundwater levels with minor influence from surface runoff and precipitation. It is believed that the area of saline soils adjacent to the borrow pit is associated with increased amounts of evapotranspiration around the borrow pit (Anderson 1988). This process is similar to that described by Skarie et al. (1986) around drainage ditches and by Jolly et al. (2008) around wetlands.

3.10.2 Statistical analysis

Regressions of EC_a with either EC_e or EC_w provide a strong prediction of observed EC_a values with Pearson r^2 correlation coefficients exceeding 0.75 for the V-H mode and 0.86 for the V-V mode. Conversely, linear regressions with volumetric water content yield poor prediction of EC_a values with linear and quadratic functions yielding maximum correlation coefficients of 0.21 for the V-H mode and 0.145 for the V-V mode. The data are unable to discriminate whether a linear or quadrative function provides a better fit to the EC_a data but in both cases the data plots provide strong evidence of a threshold in the water content below which changes in the water content do not affect the EC_a. Although the water content considered in isolation provides poor statistical prediction of the EC_a, contour plots show that it does have an effect on the EC_a and when it is included in a combined regression parameter $EC_w \cdot \theta^2$ correlation coefficients are higher than when EC_w is considered alone.

The strong correlations of EC_a with salinity (EC_e or EC_w) and the weak correlations of EC_a with moisture content can be explained by the moisture conditions of the fields during the

survey. As the moisture content was close to field capacity it was relatively uniform providing the desired conditions for EC_a to relate to EC_e or EC_w. Conversely, the relatively uniform moisture content provided poor conditions for relating EC_a to moisture content, e.g., discriminating between linear and quadratic relationships.

Overall, the results of this study are consistent with those expected for chloride-dominated salinity. However, a number of the observations required explanation in terms of the clay-rich soil. The regressions of EC_a with volumetric water content and the slopes of the fits of EC_a with $EC_w \cdot \theta^2$ are consistent with threshold effects of round 10% in the volumetric water content. The threshold effect is equivalent to the occurrence of both quadratic and linear dependence of EC_a on θ and is expected for clay rich soils. In addition, the division of the data set into lower porosity and higher porosity subsets, providing a separation of clay-poor and clay-rich samples provides an improved representation of the observed EC_a at lower conductivity values.

The regression fits obtained in the study can be used to accurately predict EC_e from LIN-corrected EC_a values for the 0.5 m and 1.5 m depth range for the DualEM 1S instrument. The resulting maps provide a framework for additional research including understanding the geological and hydrological processes providing local controls on the salinity and for quantifying the total salt content of the shallow soil layers.

4 Hydrogeological investigation of soil salinity adjacent to a flood protection infrastructure

4.1 Contribution by authors

Jerrold Rentz, P. Geo: Was responsible for collection of all field data, all calculations, modelling (groundwater and chemical), creating the first draft of the manuscript, respond to reviewer and editor comments, generate the final copy of the manuscript.

Dr. Ranjan Sri Ranjan, P. Eng: Assisted with the interpretation of the groundwater chemistry, interpretation of the modelling results, and final review of the manuscript.

Dr. Hartmut Holländer, P. Eng: Assisted with the groundwater modelling, interpretation of the groundwater chemistry, interpretation of the modelling results, and review of the manuscript throughout various stages.

4.2 Introductory statement

This chapter of the thesis consists of a manuscript titled “Hydrogeological investigation of soil salinity adjacent to a flood protection infrastructure” which has been accepted by the Journal of Environmental Earth Sciences, for the purposes of the Thesis, minor alterations were made to the text and some figures. The manuscript describes a “study area”. This is a sub area of the total study area described within Chapter 3 which due to confidentiality restrictions could not be identified within the manuscript. The study area described within Chapter 4 is Section 29-13-7W and the “drainage canal” is the Portage Diversion.

4.3 Abstract

Groundwater modelling is a commonly used technique to determine the influence of surficial processes on subsurface aquifers. In this study, a groundwater monitoring study was conducted on an agricultural field adjacent to a large drainage canal to determine the effects of the canal's operation as it relates to soil salinity during periods around flood events. The groundwater monitoring program consisted of twenty standpipes instrumented with groundwater pressure transducers that took four daily measurements. A finite element model was generated using data collected from the 2017 flood year to determine the effect of the flood on the local groundwater regime within one area consisting of four standpipes.

Analysis of the model calibration yielded good to excellent results using the Nash-Sutcliffe Model Efficiency technique, with three of the four standpipes. The salt content within the model area was primarily gypsum initially derived from the underlying till and bedrock units. Model analysis indicated that various processes might impact soil salinity, including canal seepage, evapotranspiration, and excessive snowmelt/recharge. The largest flood event on record for the canal was used in the calibrated model to determine the maximum extent of influence the canal has on the adjacent lands. The maximum extent of impact was found to be 112 m in the alluvial sediments and 240 m within a separate surficial sand structure.

4.4 Introduction

Soil salinization is the process by which various salts are transported and accumulate within the soil profile (Araki et al. 2011; Greenway and Munns 1980). It is often naturally caused by saline water discharge near the surface of a soil profile (Stein and Schwartz 1990), which can be considered primary salinization. Primary salinization is defined as being caused by natural processes. Conversely, secondary salinization is caused by anthropogenic-triggered changes in the soil water balance, such as excess irrigation in soils with impaired drainage (Carter 1982; Lekakis and Antonopoulos 2015; McFarlane et al. 2016; Steppuhn 2013) or the removal of vegetation, which decreases evapotranspiration and increases groundwater recharge (i.e., the Australian wheat belt).

It is estimated that approximately 20% of irrigated land worldwide is salinized to some degree (Lekakis and Antonopoulos 2015). Excess irrigation does not have to be the sole source of additional water. Instances involving seepage arising from surface water in drainage/irrigation canals and ditches have also been documented to increase local soil salinization through a rise in the water table (Araki et al. 2011; Chang et al. 1985; Skarie et al. 1986). Seepage leads to a rise in the water levels towards the soil surface, creating a hydraulic connection to the saline groundwater below. This process could lead to secondary salinization of near-surface soils. Due to the potential economic impact of this phenomenon, the monitoring of groundwater in these locations becomes increasingly essential.

Hydraulic and geochemical changes in groundwater on agricultural lands can be determined by collecting groundwater data using various methods, including standpipe

piezometers, pneumatic piezometers, or vibrating wire piezometers. The observed data can then used during groundwater modelling to identify the relative importance of processes that affect the soil water balance (e.g. Sperling et al. 1989; Bates et al. 2000; Alexander and MacQuarrie 2005). However, a common issue is that there may be insufficient data to adequately develop, calibrate, and validate such models (Switzman et al. 2015). They demonstrated that groundwater modelling could be successful when combining regional historical data combined with sparse locally collected data and assumptions on climate, water level time series, and discretization. Hogeboom et al. (2015) showed that multiple model parameterizations (low leakage and high leakage models) were more effective than using a simple water balance model in identifying processes in complex systems.

One example of this is identifying the processes that influence the accumulation and removal of salts from Lake Naivasha in Kenya. Lake Naivasha is a freshwater lake with no surface outlets to remove salts and other chemicals. The only outlet is groundwater transport, which prevents the accumulation of these chemical constituents within this water body. During the simulation of the behaviour of groundwater-surface water interactions in this system, Ndomba et al. (2008) managed data scarcity by conducting a sensitivity analysis using both observed and estimated flow data. Using this process, they were able to determine an essential set of parameters required to model the behaviour of the system, which was previously unknown. A critical parameter in the investigation of this *a priori* prediction is the knowledge and experience of the modellers since they have a more significant impact on the model prediction than the parameterization or even the model choice (Bormann et al. 2011; Holländer et al. 2009, 2014). However, this evaluation of *a priori* predictions showed that all groups that joined the evaluations used physically based models since the modeller as at least the control over the used processes, which is not the case when using stochastically based models.

Additionally, Holländer et al. (2016) were able to predict both short- and long-term recharge estimations using the physically-based model HYDRUS-1D with a combination of tools including low-cost weather stations and soil moisture data. Often this data and processes are integrated into Geographic Information Systems (GIS). For example, Jain et al. (2004) successfully integrated catchment models into GIS to model runoff. Ireson et al. (2006) further integrated GIS with surficial models (MIKE-Basin and MIKE 11) to simulate a rainfall-runoff model, which was additionally used in multiple groundwater models using the Aquifer Simulation Model. Ireson et

al. (2006) also noted that while using GIS-based models can be useful, the model may be ineffective where data obtained from the field are limited.

In the present study, which is similar to that of Ireson et al. (2006), GIS was used along with two different models to evaluate the extent of any influence on the groundwater adjacent to a drainage canal in southern Manitoba in a data-scarce environment. The purpose of this study was to determine if a drainage canal built for flood protection purposes may be contributing to increased soil salinization of lands adjacent to the canal.

4.5 Study area

4.5.1 Location and site description

This study was carried out in southern Manitoba in the Portage la Prairie and Delta Marsh area on the southern shore of Lake Manitoba, Manitoba, Canada (Figure 4.1). The site was initially selected due to landowner concerns about increased soil salinization that is believed to be caused by the drainage canal operation.

In the fall of 2016, an extensive electromagnetic induction survey of various sites was conducted in this region (Rentz et al. Accepted(b)). The study area revealed anomalies of low to moderate salinity. A further investigation continued with a test hole drilling program implemented to characterize the soil types within the anomalies and install groundwater monitoring wells. A total of twenty-one test holes were completed using both hollow- and solid-stem augering over five separate areas in which twenty standpipes were installed. One site, which was monitored by four standpipes, showed a potential influence from the drainage canal. This area was chosen for the present study. Further details about the study area and the electromagnetic survey can be found in Rentz et al. (Accepted(b)).

4.5.2 Climate and precipitation

The Köppen-Geiger classification defines the Canadian Prairies as having a climate that ranges from dry to semi-arid to humid continental (Kottek et al. 2006). Within the study area, the climate ranges from DFA to DFB (Fang et al. 2007; Michalyna and Smith 1972; Peel et al. 2007), indicating a relatively low annual precipitation, long cold winters, and warm to hot summers. Total

measured precipitation for the 2017 year was determined to be 318.2 mm, with a ten-year average (2008 – 2018) of 466.6 mm (Environment Canada 2019a).

4.5.3 Regional geology and geohydrology

Geologically, the area is located on an alluvial fan that is approximately 30-45 km in diameter (Rannie et al. 1989), which extends off the Manitoba escarpment base. The fan consists of various alluvial sediments, including clays, silts, and sands whose thickness ranges from 1.5 to 7.5 m (Michalyna and Smith 1972; Rannie et al. 1989; Rentz et al. Accepted(b)). The silts and sands are typically associated with historic tributaries of the Assiniboine River (Michalyna and Smith 1972; Rannie et al. 1989; Rentz et al. Accepted(b)). The alluvial fan sediments overlay a glaciolacustrine clay unit and both stratified and undifferentiated glacial till. The total thickness of the sedimentary units is up to 83 m (Fenton 1970; Fenton and Anderson 1971; Gilliland 1965).

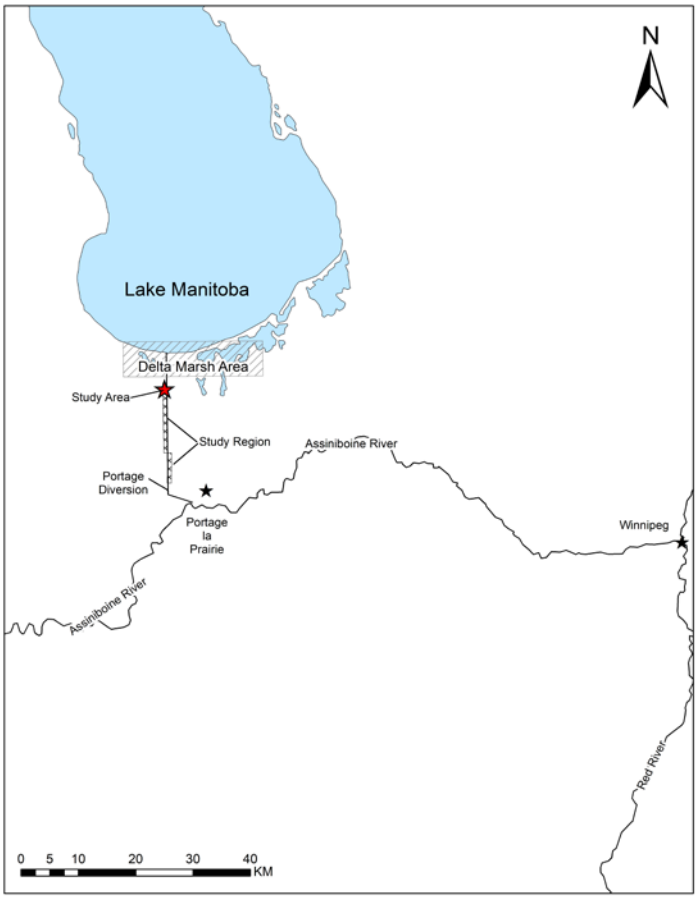

Figure 4.1 Map showing the location of Delta Marsh (hatched) and the general study area.

The regional groundwater flow is to the northwest from the Assiniboine River towards Lake Manitoba (Gilliland 1965). Three aquifers have been defined within the region with groundwater flow through an overburden aquifer, a till aquifer, and a bedrock aquifer (Betcher et al. 1995; Cherry et al. 1971; Gilliland 1965; Grasby and Betcher 2002). The overburden aquifer extends from surface to a depth of approximately 7 m and is contained within the surficial sand units, which were deposited by historic rivers such as the Willowbend (at present known as the Assiniboine River), and its tributaries (Gilliland 1965; Rannie et al. 1989). Groundwater flow within the till is controlled by the lensing and pinching out of coarse-grained material, which is also responsible for both upwards and downwards flow gradients (Cherry et al. 1971), where lens pinch outs are the source of upwards flow.

The bedrock aquifer is contained within the carbonate units beneath the Amaranth Formation, which is a unit within Williston Basin, and mineralogically is dominated by gypsum and anhydrite (Gilliland 1965; Grasby and Betcher 2002). Flow from within the aquifer has been determined to originate within the topographic highs within the United States of America (Bachu and Hitchon 1996; Grasby et al. 2000). Regionally, around Lake Manitoba, groundwater in the bedrock aquifer is believed to have a large component of upward flow, which is supported by the presence of saline groundwater springs along the western side of Lake Manitoba (Grasby 2000) and the occurrence of gypsum in the overburden soils in this region (Gilliland 1965). A more detailed description of the area's regional geology and hydrogeology is described in Rentz et al. (Accepted(b)).

4.5.4 Overburden

Due to the nature of alluvial fans, the sediment types within the study area are quite complex. They comprise seven different discontinuous soil types (Table 4.1) that range from clays to fine sands (Michalyna and Smith 1972). These cover an area of 1.94 km^2, which gently slope in a northwesterly direction (Michalyna and Smith 1972). A subsurface investigation was conducted that resulted in the installation of piezometers using a combination of solid- and hollow-stem auger drilling techniques. Geotechnically, it was determined that the total alluvial sediment and glaciolacustrine clay thickness in the area is approximately 6.1 m. The alluvial sediments comprise both interbedded low-intermediate plasticity clays and fine-grained sands. These materials overlie

a silt till. A digital elevation model was developed for the study area using LIDAR with 1 m resolution with an elevation error of +/- 7 cm.

Table 4.1 Summary of agricultural soil types within the study area, where hydraulic conductivity was analyzed throughout the soil profile (Michalyna and Smith 1972).

Soil Name	Approx. Area km^2	Hydraulic Conductivity (m/s)
Red River - Morris Osborne Clay (RR-MO)	0.43	<3.5E-7
Neuhorst Silty Clay Loam (NE)	0.95	4.9E-7 - 1.8E-5
Reinland Fine Sandy Loam (RA)	0.13	1.8E-5 - 1.1E-4
Deadhorse Silty Clay (DA)	0.17	<3.5E-7 - 9.9E-7
Plumcoulee Clay (PA)	0.08	<3.5E-7 – 3.5E-6
Red River Clay - Saline Phase (RRS)	0.18	1.4E-7 - 1.6E-6

4.5.5 Soil salinity

The model area was previously surveyed for soil salinity up to a distance of 400 m from the canal dike (Rentz et al. Accepted(b)). Salinity impacts were observed using electromagnetic induction (EM) coupled with saturated paste soil analysis (ECe). Saturated paste salinity values ranged from non-saline (0-2 dS/m) to strongly saline (8-15 dS/m) (Gartley 2011) with maximum regressed ECe values of 10.8 dS/m within the top 0.5 m soil profile and 10.6 dS/m within the top 1.5 m (Figure 4.2). Areas of weakly (2-4 dS/m) to strongly saline (8 -15 dS/m) soils are located within the alluvial soils where the non-saline soils are situated in sandy loams.

4.5.6 Drainage canal

A large drainage canal lies to the east side of the study area used primarily for flood protection during the spring to divert water from the Assiniboine River to Lake Manitoba. The canal has a low flow channel, which can be used for conveying irrigation water during the summer. At the study site, the canal is diked, unlined, and approximately 375 m in width from dike crest to dike crest, with a dike elevation of 3 m above the surface. Water in the low flow channel consists of a combination of surficial runoff, groundwater discharge, and inflow from Lake Manitoba in the northern part of the channel if the lake level exceeds the channel elevation. The maximum capacity that the canal has controlled during a flood event was approximately 963 m^3/s, which occurred in

both 2011 and 2014. Most recently, the canal discharged a flow of 699 m^3/s in the spring of 2017. The duration of flood events is generally less than four weeks per year.

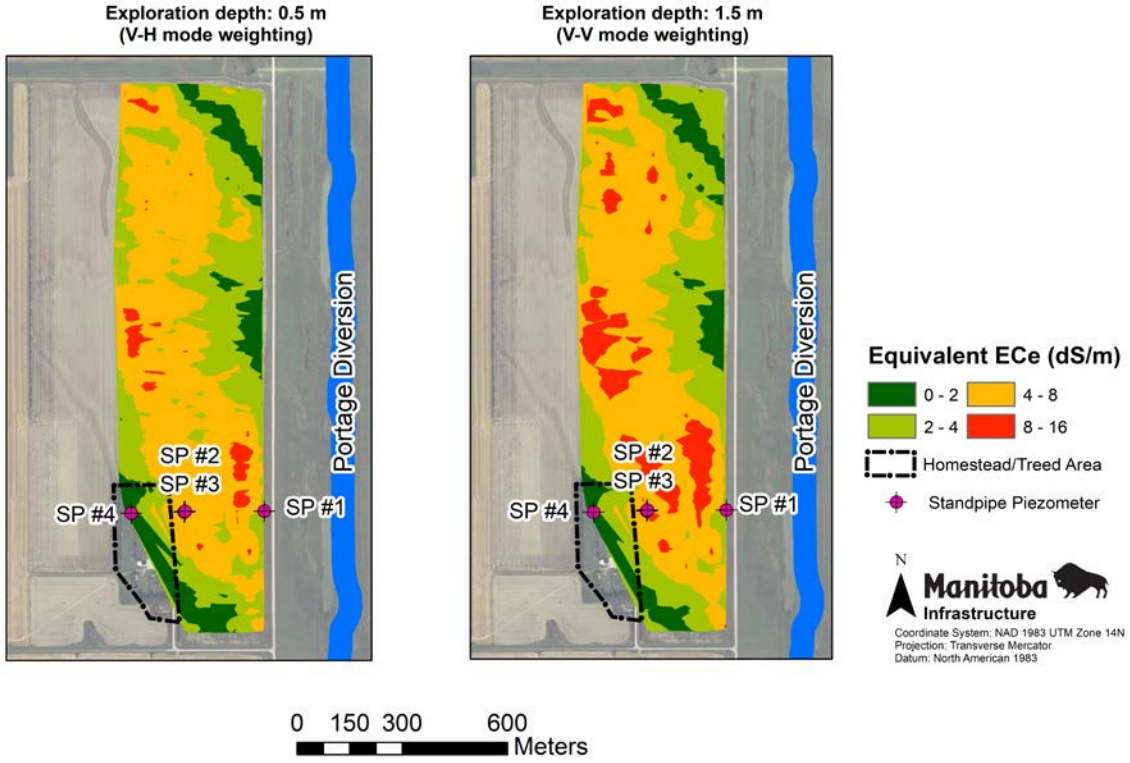

Figure 4.2 Electromagnetic induction survey of the study area illustrating areas of low to high concentrations of salinity.

4.6 Methodology

4.6.1 Field program and data collection

Test holes were drilled using either a solid- or hollow-stem auger. During drilling, soil samples were collected at 1.5 m intervals, with selected samples being analyzed for gravimetric water content, particle size, and the plasticity index. Twenty standpipes (SP) were installed within five areas with standard pressure transducers that collected data every 6 hours (0:00, 06:00, 12:00, and 18:00) daily. One area (Figure 4.1) that was selected for more detailed investigations contained four standpipes. Two standpipes were installed in the upper alluvial sediments (SPs #1 and #2), one in the surficial sand aquifer (SP #4), and one that was nested in the deeper glaciolacustrine clay (SP #3) to evaluate if an upwards hydraulic gradient is present within the clay and alluvial

sediments. Data collected from the SPs from March 2017 until October 2019 are given in Figure 4.3.

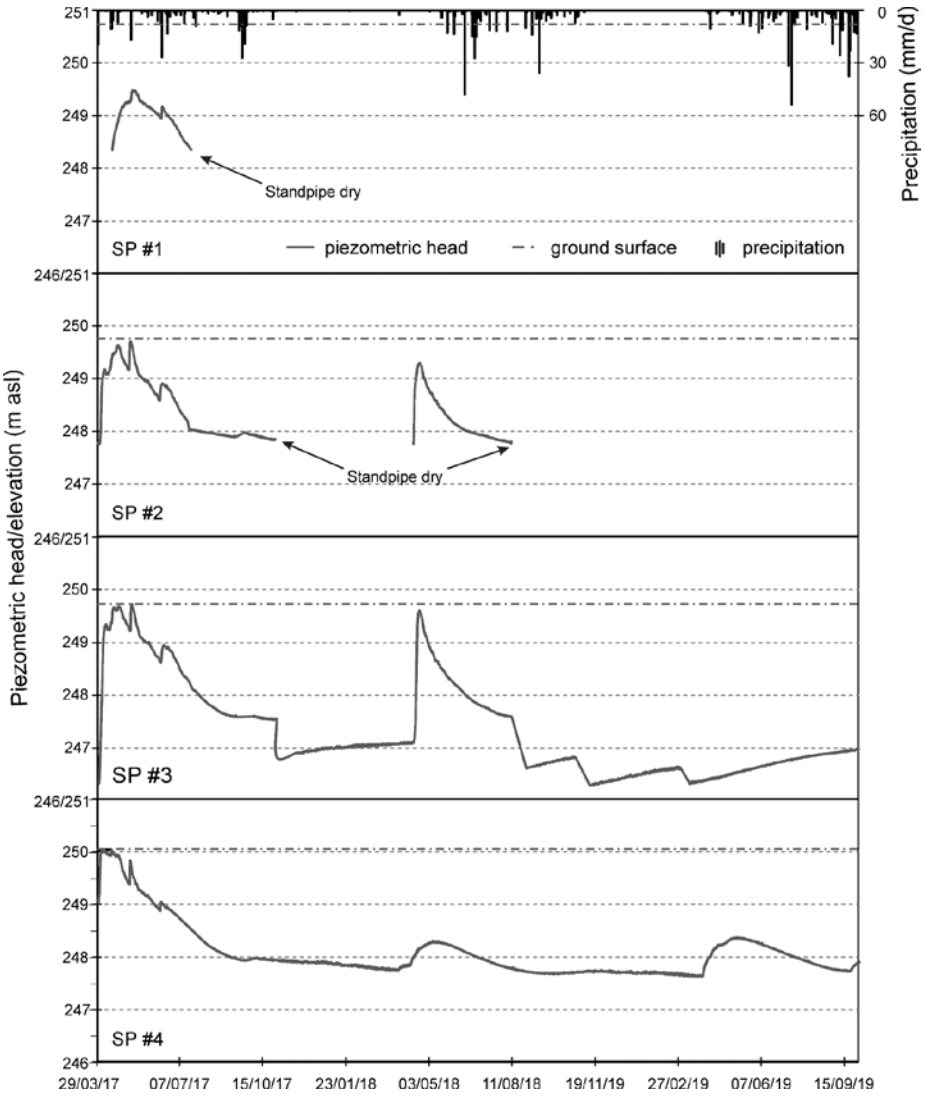

Figure 4.3 Observed piezometric head and precipitation data within the study area.
Note: SP #3 displays sharp decreases in the piezometric head due to water sampling events.

4.6.2 Assessment of the hydraulic conductivity of the aquifers

In-situ hydraulic conductivity (K) measurements were made using each of the standpipes, except for SP #1 to estimate the local hydraulic conductivity in the adjacent sediments. SP #1 remained dry, except for a short period in the spring of 2017. The unconfined aquifer slug-test methodology described in Bouwer and Rice (1976) was used during the analysis. A 4 L slug of

water was injected instantaneously into the piezometers in the alluvial sediments, and 8 L was injected into the sand aquifer to initiate an increase in water level. The water level rise and fall as a function of time were measured using a standard pressure transducer. The analysis results were compared to those of Michalyna and Smith (1972) for the corresponding soil units.

4.6.3 Water Sampling, chemistry, and hydrogeochemical modelling

Water sampling was conducted seasonally from March 2017 until March 2019 with events occurring in the spring, summer, and fall of 2017 and 2018 and one separate winter sampling event at the beginning of March 2019. All standpipes were sampled unless dry. Only SP #4 was sampled in fall 2018 and winter 2019. Water samples were collected following the procedures outlined within ASTM D4448-01 (ASTM, 2013) and were analyzed at a private laboratory for standard salinity parameters including pH, electrical conductivity (EC), chloride, calcium, magnesium, potassium, sodium, sodium adsorption ratio, sulphate, and total dissolved solids (TDS). To further characterize the groundwater composition and mineral saturation, the hydrogeochemical model PHREEQC (Parkhurst and Appelo 2013) uses the Pitzer aqueous model (Plummer et al. 1988) was used. The analysis was conducted on all SP's on July 17, 2017 (time of reduced salinity) and on August 10, 2018 (time of increased salinity).

4.6.4 Precipitation and evapotranspiration

Various weather data, including air temperature, humidity, solar radiation, and wind speed, were collected from both the Provincial Government weather station "Portage" (T. Ojo, Personal Communication, April 11, 2018; April 14, 2019; July 11, 2019; April 13, 2020), and a Federal Government weather station "Portage Romance" (Environment Canada 2019b) located in Portage la Prairie, MB approximately 20 kilometres from the study area. Potential evapotranspiration (PET) was calculated using the Penman-Monteith equation (Allen et al. 2005). During the data collection period, the field was not irrigated or regularly wetted. Therefore, it was determined that the Glugla method (Bonta and Müller 1999; Glugla et al. 2003) of estimating actual evapotranspiration (AET) for the area was deemed preferable to the crop coefficient method described by Allen et al. (1998).

Due to SP #4 being located at the edge of a wooded area that contains a dense stand of various shrubs, immature and mature deciduous trees which include maples, elms, and ashes. It was assumed that there would be a greater AET due to the effect of the trees than within the field. Specific sap flow and transpiration measurements of the wooded area were not measured to determine the exact effect. For modelling purposes, AET was estimated during model calibration to be 3 mm/d in peak summer months, 1.5 mm/d in early fall, and 0.5 mm/d in late fall. These values agree with findings by Brümmer et al. (2012), where summer ET values were determined to be between 2-4 mm/d and fall ET values between 0-1 mm/d in both Manitoba boreal, Saskatchewan deciduous boreal, and Ontario mixed wood forests.

4.6.5 Determination of flood levels

A 1-D steady-state HEC-RAS model was used to evaluate the canal's performance during the 2011 flood event and to determine water elevations throughout the canal at several flow rates (566 m^3/s, 708 m^3/s, 850 m^3/s, and 963 m^3/s) for future design purposes. Details on the model setup can be found in Hatch Ltd. (2015). The model was modified in this research to incorporate flows from 5 m^3/s up to 963 m^3/s and generated a rating curve to interpolate water elevations at the study site using hydrometric data at the canal inlet during the flood of 2017. Two different flood events were modelled using this approach. The 2017 flood event was used for calibration, and the 2011 flood was used to determine the effect on groundwater elevations during the largest recorded flood event.

The flood of 2017 was a spring flood event for which the drainage canal operated for a total of 68.5 days, achieving a maximum flow rate of 699 m^3/s. This event was recorded concurrently with piezometric levels within the adjacent land and was used for model calibration. The flood of 2011 was unprecedented in both flow rate and duration of the drainage canals operation. The canal conveyed a maximum flow rate of 963 m^3/s and operated for 123 consecutive days. The 2011 flood was modelled using the model calibration derived from the 2017 flood to determine the maximum distance at which the canal affects groundwater elevations.

4.6.6 Snowpack measurements

Snowpack heights were visually estimated to be approximately 3 m within and on the edges of the wooded area and <20 cm within the field. Snow density measurements were not analyzed in this study. However, it was assumed that the snow density within this area was approximately

0.260 g/cm^3 (Sturm et al. 2010) and utilizing the standard snow water equivalent (SWE) equation given by Sturm et al. (2010):

$$SWE = h_s \frac{p_b}{p_w} \quad \text{Eq. 4.1}$$

where h_s is equal to the height of snowpack, ρ_b is the density of the snow (in g/cm^3), and ρ_w is the standard density of water (0.997 g/cm^3). An SWE of 200 mm was used in this simulation.

4.7 Numerical modelling

4.7.1 Model design

The model domain developed for this study is approximately 1250 m x 1250 m and is 3-dimensional, with seven layers spanning a total depth of 11.3 m. The western edge of the model was considered to be beyond the region of the hydrologic influence of the canal. The model contains approximately 36,550 triangular elements and around 3750 nodes per slice. Mesh generation was completed using the mesh generator interface "Triangle" (Shewchuk 2014) within FEFLOW. Mesh refinement was further conducted in 3 areas within the model, around the drainage canal's dike, the surficial sand structure, and around the SPs (Figure 4.4).

Both recharge and AET were analyzed over the season and were incorporated into a fully saturated model that utilized a phreatic surface. A phreatic surface was simulated using a simplified linear approach that estimated the unsaturated zone by multiplying saturated hydraulic conductivity by saturation, assuming a minimum residual water depth. In this case, the model assumed a minimum residual water depth of 1.01 mm. To further account for the unsaturated zone, it was assumed that the maximum effect of evapotranspiration would be limited to 1.5 m below ground surface based on the maximum root zone of the crops within the study area (soybeans – *Glycine max*, and oats – *Avena sativa*) (Canadell et al. 1996).

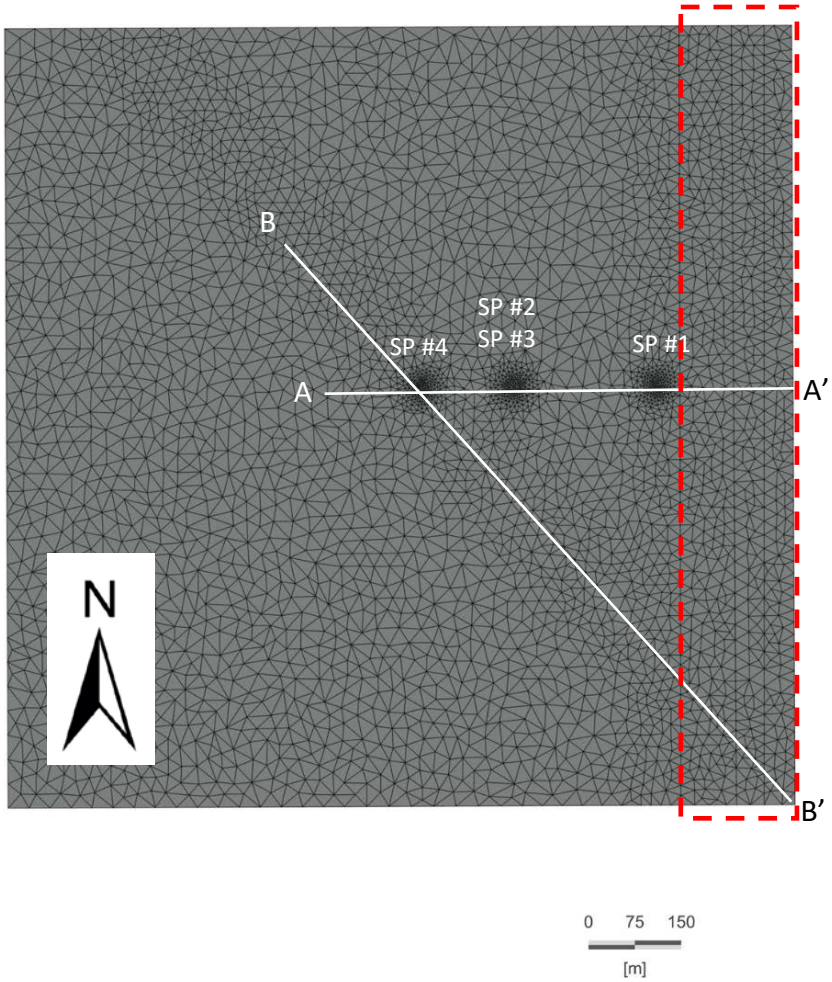

Figure 4.4 Plan view of the model area showing model discretization. Standpipes are located at varying depths at the defined circles and the canal is within the dashed area.

The model was divided into seven horizontal slices based on stratigraphy and the need for further vertical discretization. The top six slices (five layers) represented the alluvial sediments and offshore silt unit which were modelled as one unit, the seventh slice (sixth layer) at the base of the model represented the glaciolacustrine clay unit (Figure 4.5A) which in reality likely acts as an aquitard. Based on field and laboratory measurements each layer was divided into different soil types/textures. The top layer consisted of four soil textures/soil types, including: silty clay loam,

silty clay, fine sandy loam, and relatively impervious dike material. Layers two to five consisted of silty clay loam, silty clay, fine sandy loam Figure 4.5B.

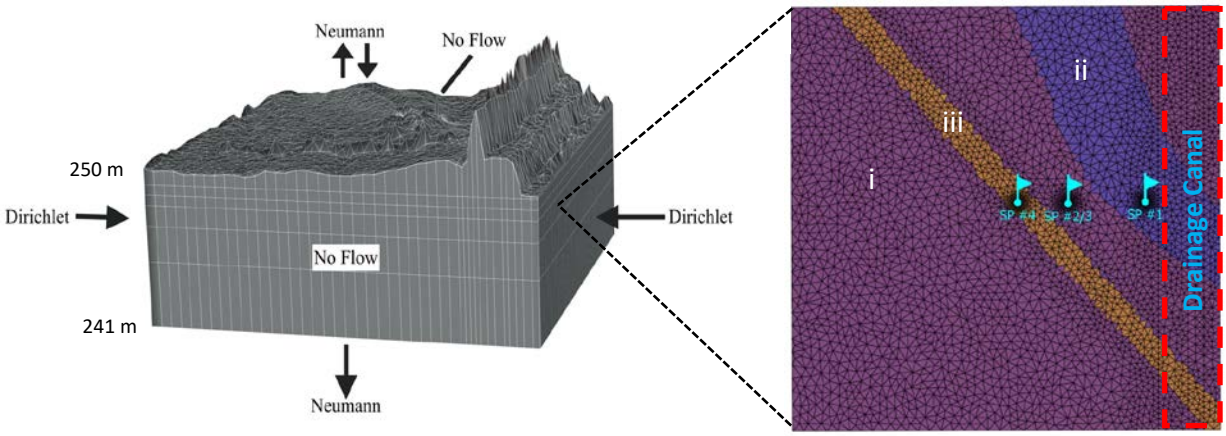

Figure 4.5 A) 3-Dimensional view of the model area, illustrating the model slices and boundary conditions. B) Plan view of the slice at elevation 248.4 m illustrating the distribution of the i) silty clay loam, ii) silty clay, iii) fine sandy loam.

4.7.2 Initial model parameterization

Initial model parameters were derived from a combination of sources. These included using in-situ hydraulic conductivity measurements, which were compared to the values given in Michalyna and Smith (1972) for the corresponding regional soil types of similar textured soils (US Department of Agriculture 2019). The initial hydraulic conductivity values used were $2x10^{-7}$ m/s in the silty clay loam, $6.6x10^{-5}$ m/s in the fine sandy loam, and $5.7x10^{-9}$ m/s within the glaciolacustrine clay.

Initial specific yield values were estimated based on particle size and texture. The silt clay loam and silty clay contained, on average, approximately 50% silt and were classified as intermediate plasticity clays. The soils monitored consisted of the Neuhorst silty clay loam (SP #1) and the Deadhorse Clay (SP #3); the Neuhorst silty clay loam is homogenous, whereas the Deadhorse clay is heterogeneous and comprised interbedded silts and sands. The glaciolacustrine clay contained 66% clay and was classified as a high plasticity clay, and the fine sandy loam contained 91% sand and was classified as silty sand. Based on the particle size analysis and soil classification, the following specific yield values were assigned based on Fetter (2001), silty clay loam and silty clay: 10%, glaciolacustrine clay: 1%, and the fine sand 20%, respectively.

Model boundaries were implemented on the east/west, and base of the model with the north/south boundaries being considered to be no-flow boundaries (Figure 4.5A). The two boundary types used in this area were specified head (Dirichlet condition) and flux (Neumann condition). Specified head boundaries were implemented on both the east/west model edges to simulate subsurface water elevations to the west and water elevations within the drainage canal to the east. The eastern specified head boundary was well defined and is shown in Figure 4.6, in contrast to the eastern boundary the western boundary was not well defined as there were no piezometric data in the immediate area. Therefore, initial piezometric levels of the western boundary were assumed to be a similar depth below grade to those of SPs #2 and 3. Throughout the season a linear 1.5 m decrease in head was applied to the boundary based on the average regional decrease in piezometric head it was also assumed that any inaccuracies with the boundary would have little to no effect on the model performance due to its distance from the canal. A linear decrease in groundwater level was also assumed on the eastern boundary for the period following the operation of the canal (Figure 4.6B) with the final elevation being based on the local piezometric head.

Flux boundaries were implemented on both the base and top of the model to simulate recharge/evapotranspiration and a downward gradient. A downward flux of 1E-5 m/d was implemented on the base of the model to simulate downward flow from the alluvial sediments into the glaciolacustrine clay and further into the underlying till a process described by Cherry et al. (1971). The initial head within the study area was determined based on the observed heads on March 29, 2017 (which corresponds to day 0 within the model domain) and was interpolated over the entire model domain.

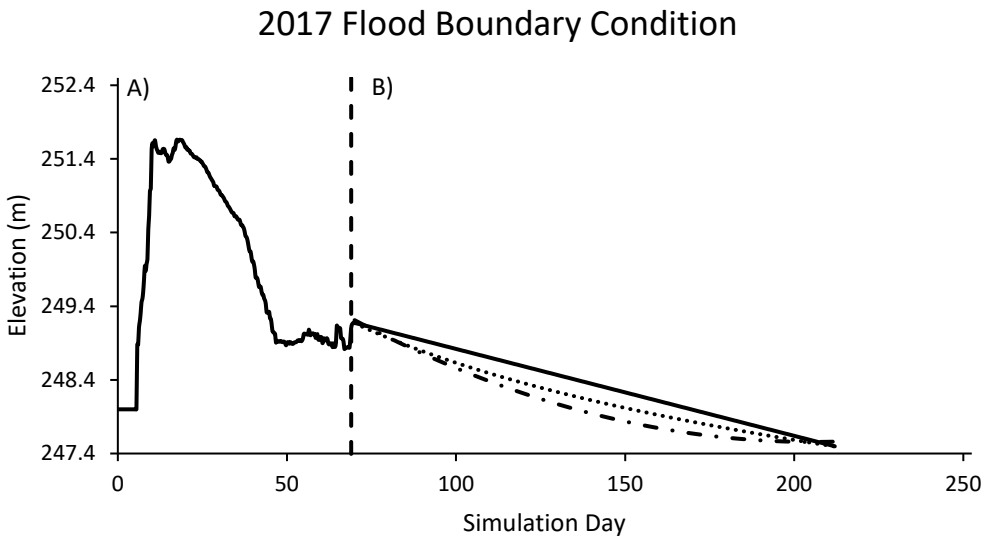

Figure 4.6 Eastern boundary condition where A) is the HEC-RAS simulated piezometric elevations, and B) is the assumed decrease in the piezometric head after the operation of the canal showing both linear and non-linear scenarios.

4.7.3 Model calibration

Model calibrations can be evaluated qualitatively to assess trends, and quantitatively through statistical analysis to determine how well the model predicts (Jackson et al. 2019; Meyer et al. 2014; Moriasi et al. 2007). Standard statistical analyses as used in this study comprise of Root Mean Squared Error (RMSE), Mean Error (ME), Mean Absolute Error (MAE) (Moriasi et al. 2007; Jackson et al. 2019), all of which are defined in meters, and the Nash-Sutcliffe Model Efficiency (NSE) (Nash and Sutcliffe 1970).

Moreover, Singh et al. (2004) and Moriasi et al. (2007) further defined MAE and RMSE as low and acceptable when the MAE and RMSE values are less than half the standard deviation of measured values. Thresholds for NSE values were defined by Skaggs et al. (2012) as acceptable, good, and excellent where NSE of >0.40 is acceptable, >0.60 is good, and >0.75 is excellent. The statistical equations are given below:

RMSE:

$$\sqrt{\sum_{i=1}^{n} \frac{(|y_i^{obs} - y_i^{sim}|)^2}{n}} \qquad \text{Eq. 4.2}$$

ME:

$$\frac{\sum_{i=1}^{n}(y_i^{obs}-y_i^{sim})}{n}$$ Eq. 4.3

MAE:

$$\frac{\sum_{i=1}^{n}|y_i^{obs}-y_i^{sim}|}{n}$$ Eq. 4.4

and, NSE:

$$1-\frac{\sum_{i=1}^{n}(y_i^{obs}-y_i^{sim})^2}{\sum_{i--1}^{n}(y_i^{obs}-y^{mean})^2}$$ Eq. 4.5

where y_i^{obs} is the initial observed value, y_i^{sim} is the corresponding initial simulated value, y^{mean} is the average of the observed values, and *n* is the total number of samples.

In this study, a transient calibration of the 2017 spring-fall season (April 2017 to November 2017) was conducted using the assumed western boundary condition and the real-time HEC-RAS modelled eastern boundary, described above. Calibration was completed over a simulation time of 200 days (April – October) to match observed piezometric heads to the model output. Both hydraulic conductivity and specific yield were manually calibrated using transient simulations comparing the observed piezometric head elevations to the water elevations within the drainage canal.

The simulation began during the spring runoff of 2017; additional recharge was added into the model to account for snowmelt and infiltration during this period (Table 4.2). Specifically, at SP #4, a significant infiltration was added due to its location being at the edge of a wooded area. However, less recharge was added at SPs #2 and #3 because they were located in the open compared to SP #4.

Table 4.2 Daily amounts of recharge added to simulate snowmelt in cm.

	SP #1	SPs #2 & #3	SP #4
Day 0	1.30	2.5	4
Day 1	-0.03	3.5	5
Day 2	-0.12	3	3.5
Day 3	-0.03	2	2.5
Day 4	-0.10	1	1
Day 5	-0.15	1	1
Day 6	-0.18	1	1
Day 7	-0.14	1	1
Day 8	-0.16	1	1
Day 9	-0.19	0.1	0.1

4.7.4 Sensitivity analysis

A sensitivity analysis was conducted to determine the extent of the input parameters' effect on the model output. Such analyses can be conducted manually or automatically using automated programs such as SENSAN (Reilly and Harbaugh 2004). Sensitivity analyses can be used in a global methodology in which multiple parameters are adjusted simultaneously using various methods such as the Screening Method, Regression Analysis, Variance Based Method, and the Meta Modelling Method (Song et al. 2015).

One alternative to undertaking a global sensitivity analysis is to carry out a local sensitivity analysis. This is where individual parameters are individually adjusted to determine the effect on the model output (Czitrom 2015; Reilly and Harbaugh 2004; Song et al. 2015). In cases where there are many parameters to consider, which is often the case in hydrological modelling, the global method is preferred (Song et al. 2015). However, local sensitivity analysis is considered accurate and acceptable (Czitrom 2015; Reilly and Harbaugh 2004). In the current study, both K and S_y were the primary variables within the model. Therefore, they were evaluated individually using the local analysis technique. Hydraulic conductivity values were individually adjusted by one order of magnitude, and S_y was incrementally adjusted by 5%.

4.8 Results

4.8.1 Calibration results

In general, the model was able to replicate observations from the 2017 year (Figure 4.7), except for SP #1, which yielded the least desirable statistical results due to the under prediction of the observed values after day 40. Statistically, the remaining SPs (2, 3, and 4) produced good to excellent NSE results, acceptable MAE results, and RMSE results. With the exception of the RMSE result of SP #3 that was 0.38 m, which was slightly above half the measured standard deviation (0.34 m) of the measured values (Table 4.3).

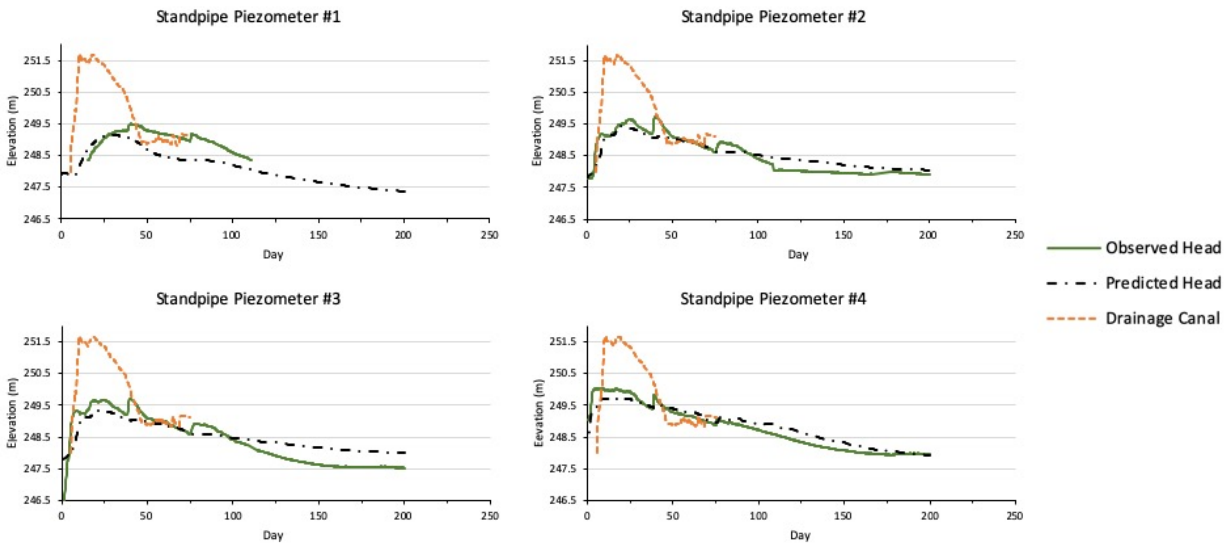

Figure 4.7 Model calibration results of the SPs showing observed head vs. predicted head along with water level in the canal.

Table 4.3 Calibrated material parameters within the monitored layer and statistical analysis of the model fit as a whole. Statistical fitting is defined as: Acceptable (A) and Not Acceptable (NA) for RMSE and MAE, and Good (G) and Excellent (E) for NSE.

Piezometer	Screened Soil Texture	K (m/s)	S_y (%)	RMSE (m)	ME (m)	MAE (m)	NSE	Literature Accepted K Values (m/s);
SP #1	Interbedded Silt, Sand, and Silty Clay Loam	6.0E-07	12	0.5 (NA)	-0.37	0.44 (NA)	-2.27 (NA)	1.4E-5 - 3.5E-7 (1, 2)
SP #2	Silty Clay Loam	3.0E-07	6	0.25 (A)	-0.06	0.19 (A)	0.81 (E)	4.2E-6 - 3.5E-7 (1, 2)
SP #3	Clay	9.0E-09	1	0.38 (NA)	-0.10	0.30 (A)	0.70 (G)	4.2E-7 – 1.0E-11 (2, 3)
SP #4	Fine Sandy Loam	6.0E-05	15	0.21 (A)	<0.01	0.17 (A)	0.9 (E)	1.1E-4 - 4.2E-6 (1, 2)

Notes:

1. Michalyna and Smith (1972) analyzed soil within the study region and USDA (2019) analyzed various soil samples based on texture

2. [1)]USDA (2019); [2)] Michalyna and Smith (1972); [3)] Fetter (2001)

4.8.2 Sensitivity analysis

The sensitivity analysis of the model area indicated the both changes in K and S_y can have an effect of the piezometric levels within the SPs, indicating that the model is sensitive to these parameters. However, certain monitored materials were not affected as much as others. All SPs were sensitive to changes in K and only two were sensitive to changes in S_y, for the range of sensitivities given in Table 4.4. A further examination of SP #4 indicates that the piezometric head within the fine sandy loam unit is sensitive to both K and S_y with K values ranging from $1.0x10^{-3}$ m/s to $1x10^{-9}$ m/s, and S_y values ranging from 3% to 25% (Figure 4.8), values exceeding these ranges caused model instability and/or improper piezometric level reactions based on the monitored material type (i.e. $1x10^{-9}$ m/s in Figure 4.8).

Table 4.4. Range of model sensitivities from SPs #1-4 where "N/A" indicates insensitive..

Parameter	SP #1 Range		SP #2 Range		SP #3 Range		SP #4 Range	
K (m/s)	$1.0x10^{-3}$	$1.0x10^{-7}$	$1.0x10^{-3}$	5.0E-08	$1.0x10^{-5}$	$1.0x10^{-10}$	$1.0x10^{-3}$	$1.0x10^{-9}$
S_y (%)	N/A		2	9	N/A		3	25

Statistical analysis of SP #4 was performed using the same analyses as within the model calibration including: RMSE, ME, MAE, and NSE (Table 4.5), where elevated NSE and lower RMSE, ME, and MAE values indicate the model fit. As expected similar results were observed when compared to the model calibration analyses (Table 4.3) when values were near the calibrated data.

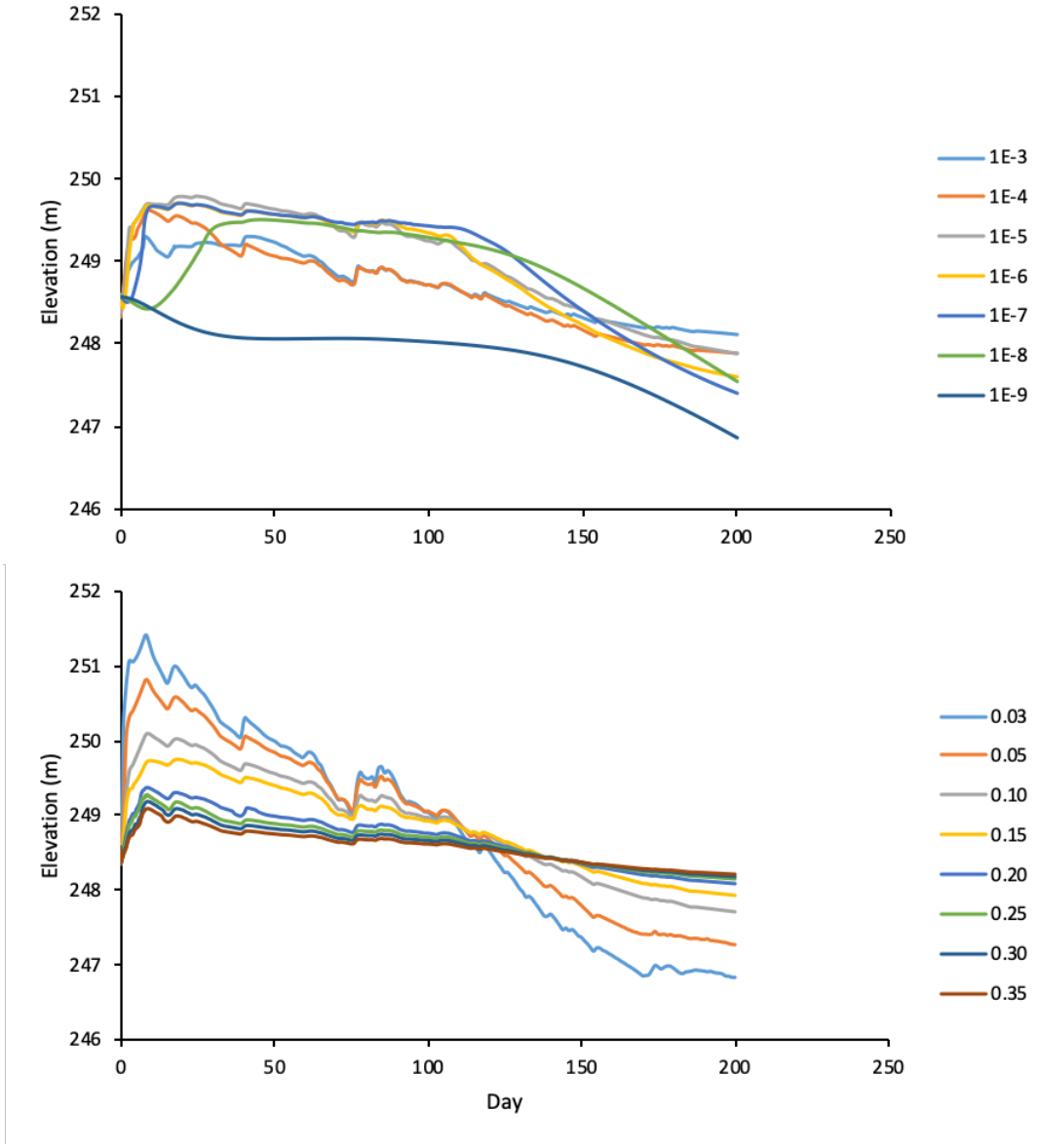

Figure 4.8 Summary of the sensitivity analysis of SP #4 where A) is hydraulic conductivity (m/s) and B) is specific yield (S_y).

Table 4.5 Statistical analysis of SP #4 sensitivities.

K (m/s)	RMSE (m)	ME (m)	MAE (m)	NSE
1E-03	0.45	0.23	0.33	0.57
1E-04	0.3	0.21	0.25	0.8
1E-05	0.34	-0.16	0.3	0.75
1E-06	0.34	-0.08	0.3	0.75
1E-07	0.45	-0.1	0.37	0.56
1E-08	0.73	0.11	0.56	-0.15
1E-09	1.22	1.12	1.12	-2.21
S_y (%)				
3	0.78	-0.42	0.73	-0.31
5	0.49	-0.31	0.47	0.48
10	0.2	-0.13	0.17	0.91
15	0.21	-0.004	0.17	0.9
20	0.43	-0.26	0.37	0.59
25	0.53	0.35	0.46	0.38
30	0.6	0.41	0.52	0.21
35	0.65	0.45	0.57	0.09

4.8.3 Effect of the 2017 and 2011 flood events

To evaluate the maximum extent of influence, two cross-sections were generated (Figure 4.4): one to determine the influence within the alluvial sediments along a transect perpendicular to the canal (A-A'); and one to assess the effects within a fine sandy loam unit, which is the historical remnants of a tributary that obliquely intersects the canal (B-B'). The maximum influence of the 2017 flood on the adjacent sediments was determined by measuring equipotential lines from the base of the dike. It was measured to be approximately 80 m (Figure 4.9) perpendicular to the dike within the alluvial deposits, whereas the influence within the fine sandy loam was measured along the sand channel (which is oblique to the dike) and was determine to be approximately 190 m (Figure 4.10) .

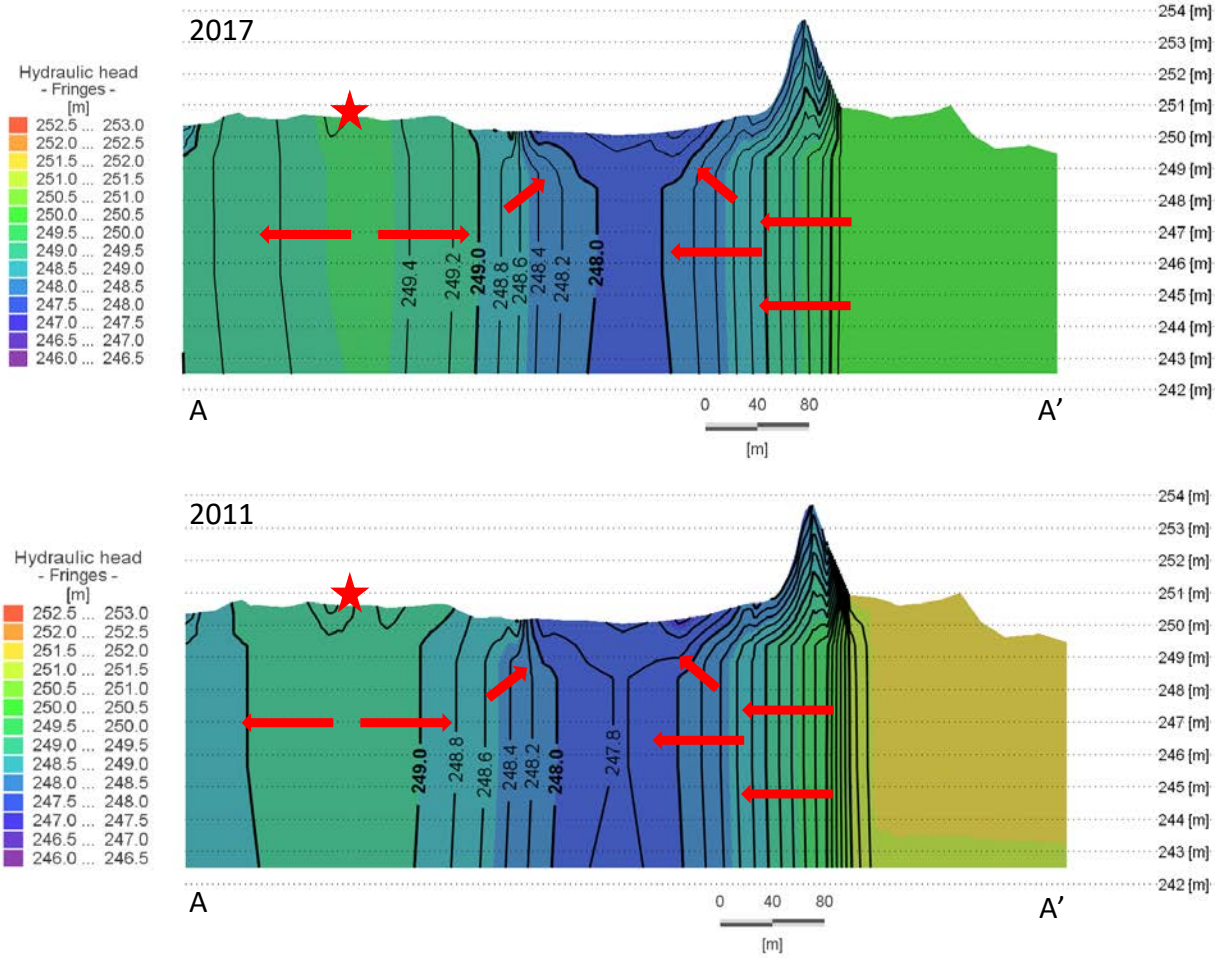

Figure 4.9 Cross-Section A-A' showing the lateral movement of groundwater from the canal dike through the alluvial soils during both the 2017 and 2011 flood events, where the red star denotes the approximate location of the treed/homestead area.

Using the same model and methodology as the 2017 flood event, the maximum influence determined by the 2011 flood was approximately 112 m within the alluvial sediments (Figure 4.9), and about 240 m within the fine sandy loam (Figure 4.10). Additionally, the maximum head elevation difference between the 2017 and 2011 flood events was only 0.4 m. The increased piezometric influence could be attributed to the length of the high-water level event in the canal rather than the height of the water level in the canal.

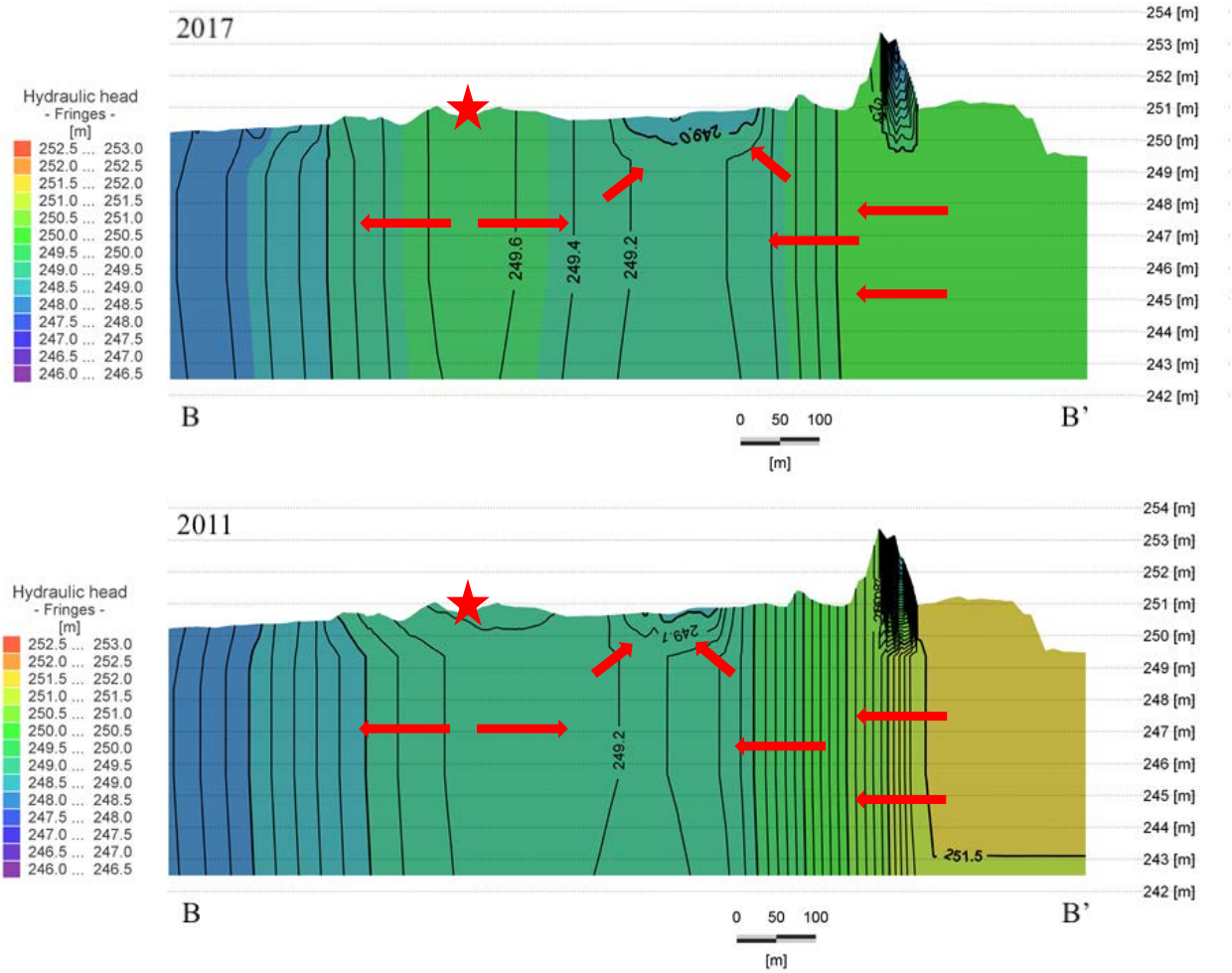

Figure 4.10 Cross-Section B-B' showing the lateral movement of groundwater from the canal dike through the fine sandy loam during both the 2017 and 2011 flood events, where the red star denotes the approximate location of the treed/homestead area.

4.8.4 Groundwater chemistry

Groundwater samples salinity levels were classified by TDS content using the schemes given in both Grasby and Betcher (2002) and Hem (1985). Salinity classifications of the samples varied from freshwater to brackish, with maximum TDS values of 9940 ppm, which were recorded in both the alluvial sediments (SPs #1 and 2) and glaciolacustrine clay (SP #3). Within the fine sandy loam (SP #4), the groundwater is fresh and contained a maximum TDS value of 757 ppm. Chemical analysis of the groundwater samples corresponded well with those of the EM surveys where elevated soil salinity areas correspond to elevated groundwater salinity values (Figures 4.2 and 4.11). Groundwater samples with elevated salinity values within the alluvial sediments, namely SP #2 and glaciolacustrine clay were sulphate rich with maximum sulphate values of

12,100 ppm and 12,800, respectively. Chloride values remained low relative to the sulphate values, with maximum values of 333 ppm within the alluvial sediments and 376 ppm within the glaciolacustrine clay. Where in contrast to the alluvial sediments in SP #2, the sole sample collected from SP #1 was classified as freshwater with a sulphate value of 631 ppm, and chloride value of 12.5 ppm.

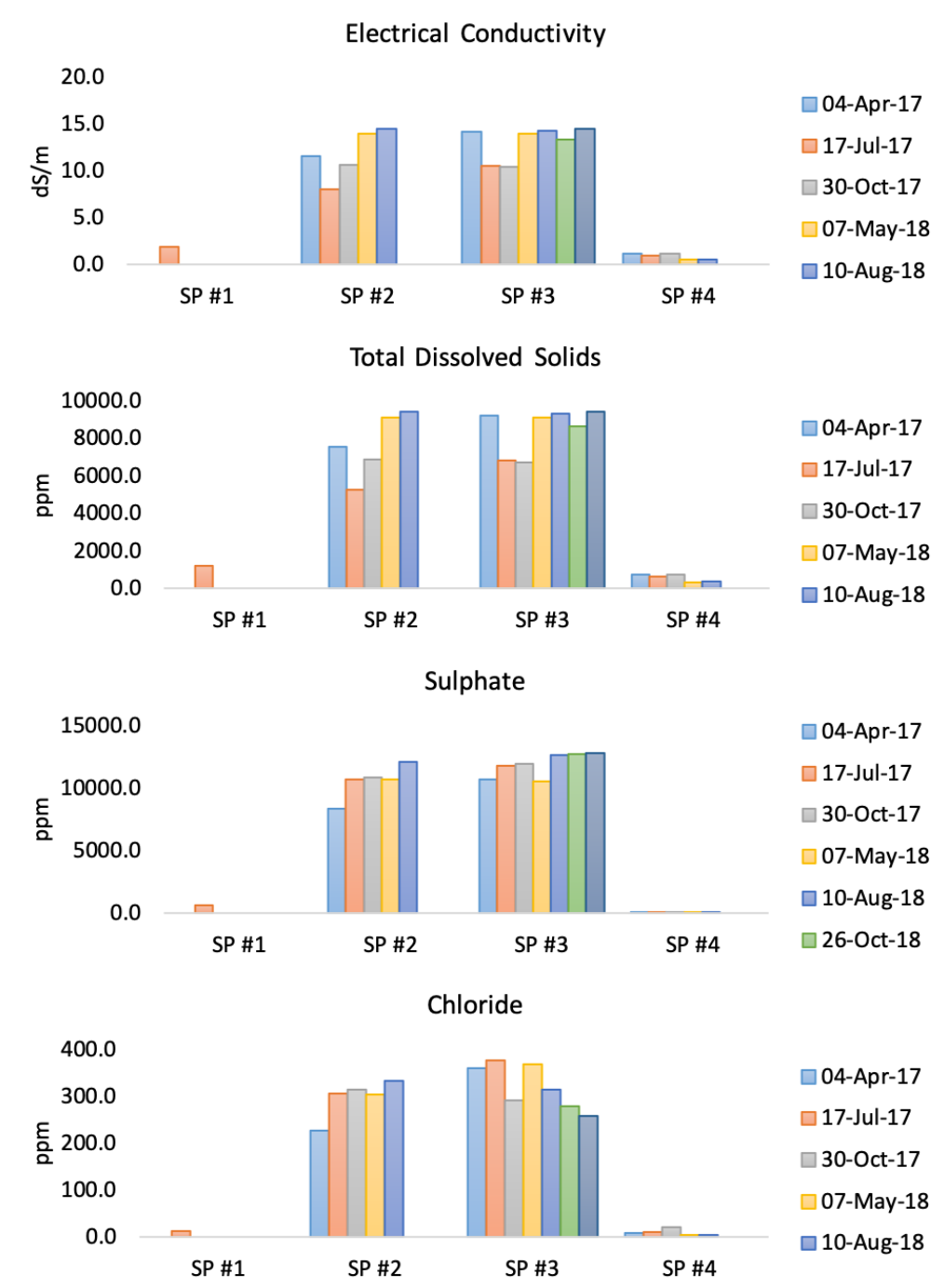

Figure 4.11 Groundwater sampling results for the standpipes within the study area.

Saturation indices were calculated for various minerals using PHREEQC to determine the dominant salt mineral within the study area. In all analyzed samples, the saturation indices of both gypsum and anhydrite were elevated. Gypsum was saturated to supersaturated in both SP #2 and SP #3 (Table 4.6 and Figure 4.12). In addition to the gypsum saturation in both SP #2 and SP #3 at low temperatures, goergeyite was near to saturation but decreased in saturation with increasing temperature (Table 4.6 and Figure 4.12).

Table 4.6 Saturation indices of analyzed groundwater samples at 25°C.

	Saturation Index						
Phase	SP #1	SP #2		SP #3		SP #4	
(Formula)	17-Jul-17	17-Jul-17	08-Aug-18	17-Jul-17	08-Aug-18	17-Jul-17	08-Aug-18
Gypsum ($CaSO_4$•$2H_2O$)	-1.01	0.01	-0.01	0.02	-0.02	-1.79	-2.78
Anhydrite ($CaSO_4$)	-1.36	-0.33	-0.35	-0.32	-0.36	-2.14	-
Hexahydrite ($MgSO_4$•$6H_2O$)	-	-2.03	-1.97	-1.96	-1.95	-	-
Leonhardrite ($CaAl_2Si_4O_{12}$•$3H_2O$)	-	-2.71	-2.64	-2.64	-2.62	-	-
Pentahydrite ($MgSO_4$•$5H_2O$)	-	-2.31	-2.25	-2.24	-2.23	-	-
Epsomite ($MgSO_4$•$7H_2O$)	-	-1.75	-1.69	-1.69	-1.67	-	-
Goergeyite ($K_2Ca_5(SO_4)_6$•H_2O)	-	-2.42	-2.77	-2.33	-2.75	-	-

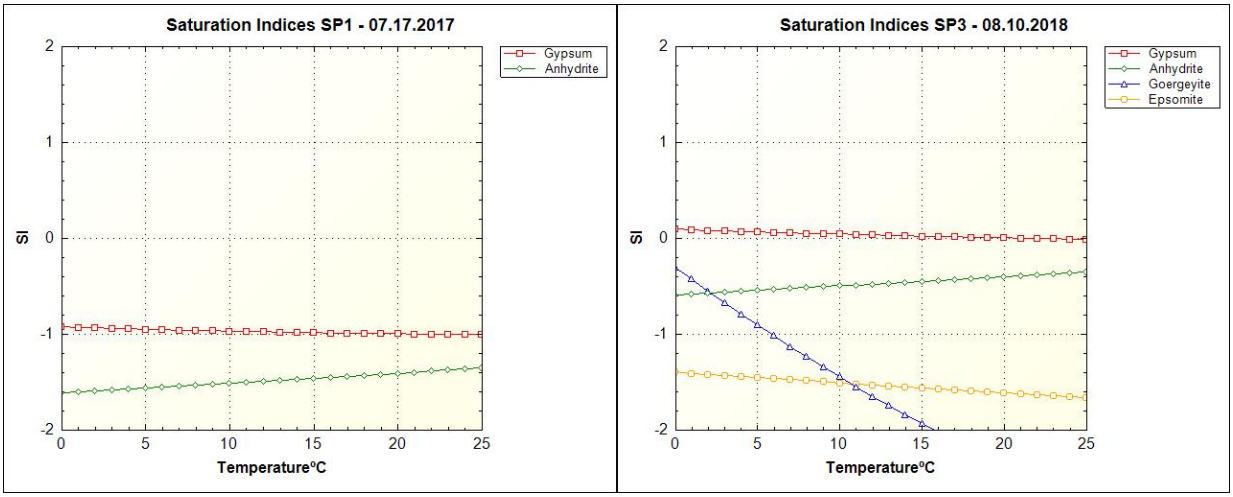

Figure 4.12 Saturation Indices of SP #1 and SP #3.

4.9 Discussion

4.9.1 Uncertainties in the model performance

Piezometric head decreases on both the western and eastern model (after the operation of the canal) boundaries were linear due to insufficient data. The western boundary condition decrease was determined by calculating the average decline in various regional standpipe piezometers. In contrast, the eastern boundary assumed a linear decrease following the operation of canal (Figure 4.6) to be near equal to the local piezometric head. Recognizing that groundwater storage is non-linear, simulations conducted assuming a non-linear decrease on both the east (Figure 4.6B) and west boundaries were attempted. The results of this change had a negligible effect on the model results.

Generally, all SPs except SP #1 behaved well with good to excellent NSE values, whereas SP #1 performed poorly statistically. SP #1 is located approximately 10 m from the base of the canal dike and remained dry throughout the study period, except during the 2017 flood event and into early the following summer. The single water sample collected was classified as freshwater, which is unique relative to SP #2 since it is also located within alluvial sediments, and classified as brackish (Grasby and Betcher 2002; Hem 1985). Given the chemical differences and location, it can only be assumed that SP #1 was influenced by seepage from the canal.

Statistical and observational analysis of the calibration of SP #1 is poor, with an NSE value of -3.8 and an RMSE of 0.6 (Table 4.3). The poor performance of SP #1 has been attributed to a combination of issues, namely: inconsistent heterogeneous soil conditions due to the deposition style of alluvial fans (i.e. a change in soil texture or conditions between SP #1 and the dike); inconsistencies with the modelled canal boundary condition; and the possible subsurface influence of the dike. The load applied to the subsurface soils by the dike may have caused additional compaction of the surrounding soils and sediments. Vertical stresses can produce a bulbing effect below the structure that dissipates but expand laterally with depth (Budhu 2011). Attempts made to incorporate this effect into calibrations were unsuccessful, likely due to sparse soil information.

4.9.2 Source of sulphate

The sulphate concentration source is likely derived from upward flow from either the till or bedrock aquifers. A previous groundwater study west of the study area examined groundwater

salinity and flow within the bedrock, till, and upper lacustrine clay aquifers (Cherry et al. 1971). That study determined that the source of various ions contributing to the salinity, particularly sulphate, is derived from the till. In pinch outs of the coarser grained till material, it was determined that an upwards gradient would occur between the upper clays and till. Additionally, the study area is located near Lake Manitoba, where both Gilliand (1965) and Grasby and Betcher (2002) determined that upwards flow from the sulphate rich bedrock may also occur.

4.9.3 Soil salinization influences and the effect of the Portage Diversion

Previous investigations by Rentz et al. (Accepted(b)) determined that the sediments within 400 m of the canal dike were weakly to strongly saline with gypsum crystals at or near surface. In the current study it was also noted that the glaciolacustrine clay unit contained gypsum crystals. Gypsum, compared to other common salts in saline soils, is less soluble and almost always occurs with the mineral calcite which is less soluble than gypsum. When comparing mineral solubility's of various salts, gypsum is the benchmark (Seelig 2000; Visconti et al. 2010). It is the lower solubility of gypsum that is important, especially in a gypsum-dominant system. The solubility causes it to precipitate out of solution preferentially, leaving crystals within the soils that do not readily re-dissolve due to the soil water being saturated with gypsum. However, cation exchange can occur between gypsum and other sodium-rich salts to produce sodium sulphate, a much more soluble salt (Tanji and Kielen 2002).

If the soils are not adequately drained, whether naturally or through processes such as tile drainage, there will be limited leaching of the soils. This causes gypsum and other salts to accumulate within the soil profile (Kim et al. 2018; Tanji and Kielen 2002). The soils' ability to drain and leach becomes increasingly important when gypsum is used as an amendment for sodium salinized soils (Tanji and Kielen 2002).

Due to the high gypsum concentration within the groundwater, the imperfect drainage of the soils and sediments within the study area (Michalyna and Smith 1972), and gypsum's insolubility, the risk of gypsum salinization is elevated. Recently-formed gypsum-saturated groundwater may then approach or enter the root zone during each rise in the piezometric head and will saturate the sediments. Once this occurs, processes such as evapotranspiration (Rhoades et al. 1999; Seelig 2000) will cause salt precipitation (Rhoades et al. 1999; Seelig 2000), further increasing the salt content of the sediments.

Snowmelt within the study area caused a near-surface piezometric head around the treed/homestead area which extended laterally into the field which is indicated by high piezometric head levels which dissipate with distance from the area (Figures 4.9 and 4.10). Similarly, seepage from the canal extended towards the west during the flood events as seen in Figures 4.9 and 4.10. For the rise in the piezometric head to affect crop productivity, the salt-laden groundwater must infiltrate or near the root zone which is typically considered to be 150 cm from ground surface (Dobos et al. 2012). In imperfect to poorly drained soils this process is increasingly important as the excess moisture will not adequately drain away from the root zone. This can lead to two adverse results, firstly if water enters the root zone the excess dissolved salts within the water will decrease the water availability for the crops. Secondly, if the water is either in or near the root zone capillary rise will bring the dissolved salts upwards (Manitoba Agriculture Food and Rural Initiatives 2008). These processes become increasingly important in finer grained soils (such as within the alluvial sediments in the study area) due increased soil capillarity.

Both the snowmelt and precipitation can also raise the elevation of the water table in the study area near or into the root zone (leading to the effects described above). However, the effect of the canal is less clear for two reasons. Firstly, the underprediction of SP #1 during model calibration caused the underprediction in water table elevations in the vicinity of the canal dikes. Secondly, we assumed that the material properties of the fine sandy loam are constant throughout the sand vein. Model simulations for both the 2017 and 2011 floods indicate that the water table in the area of the dikes does not reach 1.5 m below the surface, which is contradictory to the data observed in SP #1, which shows the water table approximately 1 m from the surface in 2017 (Figure 4.3). In the fine sandy loam, the maximum distance affecting the root zone is about 184 m from the canal dike. Quantitatively, it is not possible to determine the individual impact of each of these processes, although it appears that extensive snowmelt, infiltration, and evapotranspiration are all major contributing factors.

In a further attempt to estimate the maximum effect of the canal on the root zone, a simulation of the 2011 flood event was run, where the snowmelt infiltration that took place near the homestead area was removed from the model simulation. The snowmelt infiltration effect is observed in Figure 4.10, where elevated groundwater levels from the treed/homestead area prevented groundwater movement from the canal by providing a counter hydraulic gradient that the seepage was unable to overcome. Within the fine sandy loam, the maximum distance from the

canal dike in which the water table entered the root zone decreased to approximately 110 m. This did not significantly change the results in the alluvial sediments as the piezometric head did not reach the root zone. The absence of a pressure head imposed by the snowmelt allowed the water to flow unimpeded through the sand, which prevented the water table from rising into the root zone. Within the alluvial sediments, it was further determined that without snowmelt infiltration, the maximum distance groundwater was influenced by the canal was approximately 120 m.

4.9.4 Model applications within the region

When comparing the sediments that regionally underlie the study area to those immediately adjacent to the canal, the sediment types are similar in composition, have similar hydraulic conductivities, and are often classified as the same material (Michalyna and Smith 1972). Since wooded homestead areas are typically not located close to the canal in this region, the snowmelt infiltration from the homestead area can be neglected. In this case, it is believed that the maximum distance travelled within the alluvial sediments (~120 m) may be used as a rough estimate throughout the area, assuming that the initial head near the canal is at a similar depth from the surface as this study area. However, it is unclear at what distance the water rises to the root zone. If connected to the canal, the root zone within the sandy loam was determined to be affected up to a distance of approximately 110 m.

4.10 Conclusions

Groundwater monitoring and modelling programs were implemented to determine if a drainage canal's operation has contributed to the increasing soil salinity in agricultural fields adjacent to a drainage canal. A series of four standpipe piezometers were installed in a transect perpendicular to the drainage canal to monitor groundwater elevations to collect data on groundwater chemistry, and to create a hydrogeological model of the area to determine the extent of groundwater influence from the canal.

The extent of groundwater influence from the canal within the model area was evaluated for the 2017 flood year. It was determined to be approximately 80 m within the alluvial sediments and 190 m within the fine sandy loam. The model was further expanded to simulate the 2011 year to incorporate the canal's most prolonged operational period. The seepage extent from the 2011 year was approximately 112 m within the alluvial sediments, and 240 m within the fine sandy

loam. The maximum extent of the groundwater influence within the root zone was about 184 m within the fine sandy loam, or approximately 110 m assuming a scenario with no contribution from snowmelt infiltration.

Aside from the canal's influence, two other processes were also identified as contributing to increased soil salinization within the study area. These include evapotranspiration and excessive recharge. Increased evapotranspiration corresponded with increased salinity measurements, and excessive recharge caused piezometric levels to rise to near-surface elevations bringing salt-laden groundwater near the surface.

Chemical analysis of the groundwater samples indicated that the study area's primary salinity ion is a sulphate. Geochemical modelling determined that gypsum is near-saturated to supersaturated within the groundwater over temperatures ranging from 0ºC to 25ºC. The sulphate and gypsum source have been identified in previous studies as a combination of upwards flow from the till and dissolution of the sulphate rich bedrock with upwards flow into the overburden sediments.

5 Overall conclusions

An investigation into the effects of the Portage Diversion was undertaken between the fall 2016 and summer 2020 and was divided into two parts. The first part of the investigation included conducting electromagnetic induction surveys over a series of 14 sites that included: a soil sampling program consisting of 542 samples that covered 8 depths from 0-120 cm at 65 sites, analysis of apparent conductivity as it relates to saturated-paste conductivity, pore-water conductivity, moisture content, and other parameters. The second part of the investigation included groundwater modelling to ascertain the distance at which the Portage Diversion may affect the groundwater and hydrogeochemical modelling. The overall findings of the investigation are:

- Of the 14 sites surveyed using electromagnetic induction, five contained areas that exceeded EC_e values of 4 dS m^{-1} to a maximum of 16 dS m^{-1}. Within these areas, it would be expected that decreased crop yields would be observed. There is a distinct correlation between microtopography and soil electrical conductivity within two of these fields where topographic lows correlate with elevated levels of soil electrical conductivity.

- One of the 14 sites that exceeded EC_e values of 4 dS m^{-1} is located next to a large borrow pit created for the Portage Diversion. The borrow pit may act as a source of soil salinity over the area due to increases in evapotranspiration and influence from surface recharge, causing an increase in the head within the borrow pit.
- Regression analysis of apparent conductivity with saturated-paste conductivity and pore water conductivity yielded strong Pearson coefficients that exceeded 0.75 (V-H mode) and 0.86 (V-V mode) and were significant at a 99% confidence level. In contrast, analyses including volumetric water content yielded low Pearson coefficients of 0.21 (V-H mode) and 0.145 (V-V mode).
- Analysis of moisture content alone yielded poor statistical results when predicting apparent conductivity. However, the moisture content does have an effect, which is evident when including it in the regression parameter $EC_w \cdot \theta^2$ and comparing it with EC_w. Its inclusion yielded stronger statistical results.
- When evaluating EC_a with volumetric water content threshold effects were observed in the regressions. It was determined that a threshold value of approximate 10% existed below which EC_a would not be affected by volumetric water content.
- The strong correlations between apparent conductivity and saturated-paste or pore water conductivity and weak correlation with moisture content are likely explained by the field moisture conditions being near capacity at the time of the survey.
- Groundwater model calibration of observed values yielded good to excellent NSE results for all but one standpipe. The results indicated that the maximum distance at which the Portage Diversion may influence the local groundwater was approximately 112 m within the upper alluvial soils and 240 m within the sand unit. Aside from the Portage Diversion's influence, the modelling results indicated that two other processes might also affect soil salinity. These are evapotranspiration and excessive snowmelt/recharge along a treed area.
- Hydrogeochemical modelling within the model area indicated that the primary salinity ion is sulphate in which the groundwater is near to supersaturated within the temperature range of 0ºC to 25ºC.

6 Practical extension of this work

Based on the findings of the works presented in Sections 3 and 4, it is recommended that additional data collection and analysis be undertaken in future work. The recommendations include:

- Additional soil sample parameters are analyzed after collecting surficial soil samples (<1.2 m). The samples were not analyzed for porosity, volumetric water content, pore water conductivity, and degree of saturation within the current study. As such, these parameters had to be calculated using known relationships with other parameters, which likely introduced some amount of compounding error into the analysis (though error propagation calculations indicated that this was minimal).
- Additional drilling, sampling, and soil characterization be undertaken along the Portage Diversion dikes should additional monitoring and modelling be undertaken. Within the current study, SP 1 under-predicted the observed values and the record of this SP could not be replicated to an acceptable level based on NSE. Due to the under-prediction of the piezometric head, the results within the alluvial soils are likely to be larger than predicted.
- The installation of additional SPs should be considered to further characterize the interactions between the upper soils, till units, and bedrock units.
- The installation of an additional SP should be considered within the treed/homestead area to evaluate the effect of snowmelt.
- The development of a solute transport model should be considered to evaluate the source and transport of gypsum.
- Lastly, it is recommended that any future studies include monitoring the lake effect from Lake Manitoba to determine the maximum extent that the groundwater was influenced during a high-water year, such as in 2011.

7 References

Abdu, H., D.A. Robinson and S.B. Jones. 2007. Comparing bulk soil electrical conductivity determination using the DUALEM-1S and EM38-DD electromagnetic induction instruments. *Soil Science Society of America Journal* 71(1): 189. https://doi.org/10.2136/sssaj2005.0394.

Akram, A.A. and R. Mendelsohn. 2017. Agricultural water allocation efficiency in a developing country canal irrigation system. *Environment and Development Economics* 22(5): 571–593. https://doi.org/10.1017/S1355770X17000171.

Alexander, M.D. and K.T.B. MacQuarrie. 2005. The measurement of groundwater temperature in shallow piezometers and standpipes. *Canadian Geotechnical Journal* 42(5): 1377–1390. https://doi.org/10.1139/t05-061.

Allen, R.G., L.S. Pereira, D. Raes and M. Smith. 1998. FAO Irrigation and Drainage Paper No. 56 - Crop Evapotranspiration (March).

Allen, R.G., I.A. Walter, R. Elliott, T.A. Howell, D. Itenfisu and M.E. Jensen. 2005. The ASCE standardized reference evapotranspiration equation. Task Committee on Standardization of Reference Evapotranspiration Environment and Water Resources Institute of the ASCE. American Society of Civil Engineers, Reston, VA, 2005.

Allred, B., R. Freeland, K. Grote, E. McCoy, L. Martinez, D. Gamble, Z. Lu, G. Wilson, et al. 2008. *Handbook of Agricultural Geophysics*. Boca Raton: CRC Press - Taylor & Francis Group. https://doi.org/10.4133/sageep.29-001.

Amezketa, E. 2007. Soil salinity assessment using directed soil sampling from a geophysical survey with electromagnetic technology : a case study. *Spanish Journal of Agricultural Research* 5(1): 91–101. https://doi.org/10.5424/sjar/2007051-225.

Anderson, D.W. 1988. Soil degradation in saskatchewan, a pedological perspective. Proc. Soils and Crops Workshop. Saskatoon, SK. 11–26.

Anderson, M.P., W.W. Woessner and R.J. Hunt. 2015. *Applied Groundwater Modeling*. 2nd edition. Academic Press, Inc. http://pubs.er.usgs.gov/publication/70160331.

Araki, T., D. Yasutake, W. Wang, Y. Wu and M. Mori. 2011. Saline water seepage from drainage canals induces soil salinization and growth depression in the adjacent cornfields in the Upper Yellow River Basin. *Environmental Control in Biology* 49(3): 127–132.

Ashraf, A. and Z. Ahmad. 2008. Regional groundwater flow modelling of Upper Chaj Doab of Indus Basin, Pakistan using finite element model (Feflow) and geoinformatics. *Geophysical Journal International* 173: 17–24. https://doi.org/10.1111/j.1365-246X.2007.03708.x.

ASTM Method D4448-01 (Reapproved 2013). n.d. Standard guide for sampling ground-water monitoring wells. West Conshohocken, Pennsylvania. https://doi.org/10.1520/D4448-01R13.2.

Bachu, S. and B. Hitchon. 1996. Regional-scale flow of formation waters in the Williston basin:American Association of Petroleum Geologists Bulletin 80: 248–264.

Bannatyne, B.B. 1959. Gypsum-anhydrite deposits in Manitoba, Manitoba Mines and Natural Resources, Mines Branch, Publication 58-2.

Bates, P.D., M.D. Stewart, A. Desitter, M.G. Anderson, J.P. Renaud and J.A. Smith. 2000. Numerical simulation of floodplain hydrology. *Water Resources Research* 36(9): 2517–2529. https://doi.org/10.1029/2000WR900102.

Bernstein, L. 1975. Effects of salinity and sodicity on plant growth. *Annual Review of Phytopathology* 13(1): 295–312. https://doi.org/10.1146/annurev.py.13.090175.001455.

Betcher, R.N. 1988. Groundwater availability map series, Neepawa map area. Manitoba Natural Resources, Water Resources.

Betcher, R.N., G. Grove and C. Pupp. 1995. Groundwater in Manitoba, hydrogeology, quality concerns, management. Environment Canada, Saskatoon.

Bonta, J. V. and M. Müller. 1999. Evaluation de la méthode Glugla pour estimer l'évapotranspiration et la recharge de la nappe phréatique. *Hydrological Sciences Journal* 44(5): 743–761. https://doi.org/10.1080/02626669909492271.

Bormann, H., H.M. Holländer, T. Blume, W. Buytaert, G.B. Chirico, J.-F. Exbrayat, D. Gustafsson, H. Hölzel, et al. 2011. Comparative discharge prediction from a small artificial catchment without model calibration: Representation of initial hydrological catchment development. *Bodenkultur* 62(1–4): 23–29.

Bouksila, F., M. Persson and R. Berndtsson. 2008. Soil water content and salinity determination using different dielectric methods in saline gypsiferous soil. *Hydrological Sciences Journal* 53(1): 253–265. https://doi.org/10.1623/hysj.53.1.253.

Bouksila, F., M. Persson, A. Bahri and R. Berndtsson. 2012. Electromagnetic induction prediction of soil salinity and groundwater properties in a Tunisian Saharan oasis electromagnetic induction prediction of soil salinity and groundwater properties in a Tunisian Saharan oasis. *Hydrological Sciences Journal* 6667(57): 7. https://doi.org/10.1080/02626667.2012.717701.

Bouwer, H. and R.C. Rice. 1976. A slug test for determining hydraulic conductivity of unconfined aquifers with completely or partially penetrating wells. *Water Resources Research* 12(3): 6115–6119. https://doi.org/10.1002/anie.201800887.

Brillante, L., O. Mathieu, B. Bois, C. van Leeuwen and J. Lévêque. 2014. The use of soil electrical resistivity to monitor plant and soil water relationships in vineyards. *Soil Discussions* 1(1): 677–707. https://doi.org/10.5194/soild-1-677-2014.

Brooks, R.H. and A.T. Corey. 1964. Hydraulic Properties of Porous Media and Their Relation to Drainage Design. *Hydrol. Paper No. 3* 3. https://doi.org/10.13031/2013.40684.

Brümmer, C., T.A. Black, R.S. Jassal, N.J. Grant, D.L. Spittlehouse, B. Chen, Z. Nesic, B.D. Amiro, et al. 2012. How climate and vegetation type influence evapotranspiration and water use efficiency in Canadian forest, peatland and grassland ecosystems. *Agricultural and Forest Meteorology* 153: 14–30. https://doi.org/10.1016/j.agrformet.2011.04.008.

Budhu, M. 2011. *Soil Mechanics and Foundations*. 3rd edition. Hoboken, New Jersey: John Wiley & Sons, Inc..

Calamita, G., L. Brocca, A. Perrone, S. Piscitelli, V. Lapenna, F. Melone and T. Moramarco. 2012. Electrical resistivity and TDR methods for soil moisture estimation in central Italy test-sites. *Journal of Hydrology* 454–455: 101–112. https://doi.org/10.1016/j.jhydrol.2012.06.001.

Calamita, G., A. Perrone, L. Brocca, B. Onorati and S. Manfreda. 2015. Field test of a multi-frequency electromagnetic induction sensor for soil moisture monitoring in southern Italy test sites. *Journal of Hydrology* 529: 316–329. https://doi.org/10.1016/j.jhydrol.2015.07.023.

Callaghan, M. V., E.E. Cey and L.R. Bentley. 2016. Adjustment of soil saturated paste extract electrical conductivity and sodium adsorption ratio for excess gypsum dissolution using equilibrium geochemical modeling. *Soil Science Society of America Journal* 80(4): 878–887. https://doi.org/10.2136/sssaj2016.01.0012.

Canadell, J., R.B. Jackson, J.R. Ehleringer, H.A. Mooney, O.E. Sala and E.-D. Schulze. 1996. Maximum rooting depth of vegetation types at the global scale. *Oceologia* 108: 583–595.
Cannon, M.E., R.C. Mckenzie and G. Lachapelle. 1994. Soil salinity mapping with electromagnetic induction and satellite-based navigation methods. *Canadian Journal of Soil Science* 74: 335–343. https://doi.org/10.4141/cjss94-046.
Carter, D.L. 1982. Salinity and plant productivity. In: Rechcigl Jr, M., (ed) CRC Handbook of Agricultural Productivity. CRC Series in Nutrition and Food, Volume 1. CRC Press, Boca Raton, Florida, pp 117-133. CRC Handbook Of Agricultural ProductivityI.
Carter, M.R. and E.. Gregorich. 2008. *Soil Sampling and Methods of Analysis*. 2nd edition. Boca Raton. https://doi.org/10.1017/S0014479708006546.
Cattaneo, L., A. Comunian, G. de Filippis, M. Giudici and C. Vassena. 2016. Modeling groundwater flow in heterogeneous porous media with YAGMod. *Computation* 4(1): 1–19. https://doi.org/10.3390/computation4010002.
Chang, C., G.C. Kozub and D.C. Mackay. 1985. Soil salinity status and its relation to some of the soil and land properties of three irrigation districts in southern Alberta. *Canadian Journal of Soil Science* 65: 187–193.
Cherry, J.A., B.T. Beswick, W.E. Clister and M. Lutchman. 1971. Flow patterns and hydrochemistry of two shallow groundwater regimes in the Lake Agassiz Basin, Southern Manitoba. In *Geoscience Studies in Manitoba, Geological Association of Canada, Special Paper 9*, 321–332.
Clarke, C.J., R.J. George, R.W. Bell and T.J. Hatton. 2002. Dryland salinity in south-western Australia: Its origins, remedies, and future research directions. *Australian Journal of Soil Research* 40(1): 93–113. https://doi.org/10.1071/SR01028.
Cordeiro, M.R.C., R.S. Ranjan and N. Cicek. 2011a. Assessment of potential nutrient build-up around beef cattle production areas using electromagnetic induction. *Environmental Technology* 33(15–16): 1825–33. https://doi.org/10.1080/09593330.2011.559275.
Cordeiro, M.R.C., R. Sri Ranjan and I.J. Ferguson. 2011b. Calibration models for electromagnetic induction methods to assess nutrient accumulation beneath confined livestock areas. *Environmental Technology* 32(1): 103–117. https://doi.org/10.1080/09593330.2010.487921.
Corwin, D.L., S.R. Kaffka, J.W. Hopmans, Y. Mori, J.W. Van Groenigen, C. Van Kessel, S.M. Lesch and J.D. Oster. 2003. Assessment and field-scale mapping of soil quality properties of a saline-sodic soil. *Geoderma* 114: 231–259. https://doi.org/10.1016/S0016-7061(03)00043-0.
Corwin, D.L. and S.M. Lesch. 2005a. Apparent soil electrical conductivity measurements in agriculture. *Computers and Electronics in Agriculture* 46: 11–43. https://doi.org/10.1016/j.compag.2004.10.005.
Corwin, D.L. and S.M. Lesch. 2005b. Characterizing soil spatial variability with apparent soil electrical conductivity: Part II. Case study. *Computers and Electronics in Agriculture* 46(1-3 SPEC. ISS.): 135–152. https://doi.org/10.1016/j.compag.2004.11.003.
Corwin, D.L. and S.M. Lesch. 2013. Protocols and guidelines for field-scale measurement of soil salinity distribution with ECa-directed soil sampling. *Journal of Environmental & Engineering Geophysics* 18(1): 1–25. https://doi.org/10.2113/jeeg18.1.1.
Corwin, D.L. and E. Scudiero. 2019. Review of soil salinity assessment for agriculture across multiple scales using proximal and/or remote sensors. *Advances in Agronomy* 158: 1–130. https://doi.org/10.1016/bs.agron.2019.07.001.

Czitrom, V. 2015. One-factor-at-a-time versus designed experiments. *The American Statistician* 53(2): 126–131.
Dalton, F.N. and M.T. Van Genuchten. 1986. The time-domain reflectometry method for measuring soil water content and salinity. *Geoderma* 38: 237–250. https://doi.org/10.1016/0016-7061(86)90018-2.
Davis, J.C. 1986. *Statistics and Data Analysis in Geology*. 2nd edition. John Wiley & Sons, Inc..
Dobos, R.R., H.R.J. Sinclair and M.P. Robotham. 2012. National commodity crop productivity index (NCCPI) user guide, Version 2. Lincoln Nebraska.
Doolittle, J., M. Petersen and T. Wheeler. 2001. Comparison of two electromagnetic induction tools in salinity appraisals. *Journal of Soil and Water Conservation* 56(3): 257–262.
Doolittle, J. and E. Brevik. 2014. The use of electromagnetic induction techniques in soils studies. *Geoderma* 223–225: 33–45. https://doi.org/10.1016/j.geoderma.2014.01.027.
Doolittle, J. and M. Collins. 1995. Use of soil information to determine application of ground penetrating radar. *Journal of Applied Geophysics* 33: 101–108. https://doi.org/10.1016/0926-9851(95)90033-0.
Environment Canada. 2019a. Daily data report 2009-2019. https://climate.weather.gc.ca/climate_data/daily_data_e.html?hlyRange=%7C&dlyRange=2007-01-01%7C2020-04-17&mlyRange=2007-01-01%7C2007-11-01&StationID=45987&Prov=MB&urlExtension=_e.html&searchType=stnName&optLimit=yearRange&StartYear=1840&EndYear=2020&selR (2019 /11/23)
Environment Canada. 2019b. Historical data. https://climate.weather.gc.ca/climate_data/daily_data_e.html?hlyRange=%7C&dlyRange=2007-01-01%7C2020-04-13&mlyRange=2007-01-01%7C2007-11-01&StationID=45987&Prov=MB&urlExtension=_e.html&searchType=stnName&optLimit=yearRange&StartYear=1840&EndYear=2020&selR (2019 /9/20)
Fang, X., A. Minke, J.W. Pomeroy, T. Brown, C. Westbrook, X. Guo and S. Guangul. 2007. A review of Canadian prairie hydrology: principles, modelling and response to land use and drainage change; Center for Hydrology Report No. 2. Technical Report October, University of Saskatchewan - Center for Hydrology, Saskatoon.
Fenton, M.M. 1970. The Pleistocene stratigraphy and surficial geology of the Assiniboine River to Lake Manitoba area, Manitoba. Masters Thesis. University of Manitoba, Winnipeg, Manitoba, Canada. University of Manitoba.
Fenton, M.M. and D.T. Anderson. 1971. Pleistocene stratigraphy of the Portage la Prairie Area, Manitoba. The Geological Association of Canada Special Paper Number 9, 1971.
Ferguson, I.J. and G.A.J. Desrosiers. 1998. Monitoring winter freezing in a silt soil in southern Manitoba, Canada using surface DC resistivity soundings. *Journal of Environmental and Engineering Geophysics* 3: 49–61.
Fernald, A.G. and S.J. Guldan. 2006. Surface water-groundwater interactions between irrigation ditches, alluvial aquifers, and streams. *Reviews in Fisheries Science* 14(1–2): 79–89. https://doi.org/10.1080/10641260500341320.
Fetter, C.W. 2001. *Applied Hydrogeology*. 4th edition. Upper Saddle River, New Jersey: Prentice Hall.
Fitterman, D. V and V.F. Labson. 2005. Electromagnetic induction methods for environmental problems, 301–356.

Fortes, R., S. Millán, M.H. Prieto and C. Campillo. 2015. A methodology based on apparent electrical conductivity and guided soil samples to improve irrigation zoning. *Precision Agriculture* 16: 441–454. https://doi.org/10.1007/s11119-015-9388-7.

Friedman, S.P. 2005. Soil properties influencing apparent electrical conductivity: A review. *Computers and Electronics in Agriculture* 46: 45–70. https://doi.org/10.1016/j.compag.2004.11.001.

Gartley, K. 2011. Recommended methods for measuring soluble salts in soils. In *Recommended Soil Procedures for the Northeastern United States. Cooperative Bulletin 493. University of Delaware Cooperative Extension.*, 87–94. Newark. http://extension.udel.edu/lawngarden/files/2012/10/CHAP10.pdf.

Gershenzon, N.I., R.W. Ritzi, D.F. Dominic, E. Mehnert and R.T. Okwen. 2016. Comparison of CO2 trapping in highly heterogeneous reservoirs with Brooks-Corey and van Genuchten type capillary pressure curves. *Advances in Water Resources* 96: 225–236. https://doi.org/10.1016/j.advwatres.2016.07.022.

Gilliland, J. 1965. Geological and groundwater investigation for the portage diversion. Department of Water Control and Conservation, Province of Manitoba.

Glugla, G., P. Jankiewicz, C. Rachimow, K. Lojek, K. Richter, G. Fürtig and P. Krahe. 2003. BAGLUVA - Wasserhaushaltsverfahren zur Berechnung vieljähriger Mittelwerte der tatsächlichen Verdunstung und des Gesamtabflusses. Koblenz, Germany.

Grasby, S., K. Osadetz, R. Betcher and F. Render. 2000. Reversal of the regional-scale flow system of the Williston basin in response to Pleistocene glaciation. *Geology* 28(7): 635–638. https://doi.org/10.1130/0091-7613(2000)28<635:ROTRFS>2.0.CO;2.

Grasby, S.E. 2000. Saline spring geochemistry, west-central Manitoba; in Report of Activities, Manitoba Industry, Trade and Mines, Manitoba Geological Survey.

Grasby, S.E. and R.N. Betcher. 2002. Regional hydrogeochemistry of the carbonate rock aquifer, southern Manitoba. *Canadian Journal of Earth Sciences* 39(7): 1053–1063. https://doi.org/10.1139/e02-021.

Greenway, H. and R. Munns. 1980. Mechanisms of salt tolerance in nonhalophytes. *Annual Review of Plant Physiology* 31(1): 149–190. https://doi.org/10.1146/annurev.pp.31.060180.001053.

Grote, K., S. Hubbard and Y. Rubin. 2003. Field-scale estimation of volumetric water content using ground-penetrating radar ground wave techniques. *Water Resources Research* 39(11): 1–14. https://doi.org/10.1029/2003WR002045.

Hatch Ltd. 2015. *If and as required hydrotechnical services - 2011 flood*. Winnipeg, Manitoba.

Heil, K. and U. Schmidhalter. 2015. Comparison of the EM38 and EM38-MK2 electromagnetic induction-based sensors for spatial soil analysis at field scale. *Computers and Electronics in Agriculture* 110(1): 267–280. https://doi.org/10.1016/j.compag.2014.11.014.

Hem, J.D. 1985. *Study and Interpretation of the Chemical Characteristics of Natural Water*. 3rd edition. U.S. Geological Survey, Water-Supply Paper 2254.

Hendrickx, J.M.H., B. Baerends, Z.I. Raza, M. Sadig and M.A. Chaudhry. 1992. Soil salinity assessment by electromagnetic induction of irrigated land. *Soil Science Society of America Journal* 56(6): 1933–1941. https://doi.org/10.2136/sssaj1992.03615995005600060047x.

Henry, J.L., B. Harron and D. Flaten. 1987. The nature and management of salt-affected land in saskatchewan. Saskatchewan Agriculture, Soils and Crops Branch, Regina, Saskatchewan.

Hogeboom, R.H.J., P.R. Van Oel, M.S. Krol and M.J. Booij. 2015. Modelling the influence of groundwater abstractions on the water level of Lake Naivasha, Kenya under data-scarce conditions 4447–4463. https://doi.org/10.1007/s11269-015-1069-9.

Holländer, H., Z. Wang, K.A. Assefa and A.D. Woodbury. 2016. Improved recharge estimation from portable, low-cost weather stations. *Groundwater* 54(2). https://doi.org/10.1111/gwat.12346.

Holländer, H.M., T. Blume, H. Bormann, W. Buytaert, G.B. Chirico, J.F. Exbrayat, D. Gustafsson7, H. Hölzel, et al. 2009. Comparative predictions of discharge from an artificial catchment (Chicken Creek) using sparse data. *Hydrology and Earth System Sciences* 13: 2069–2094.

Holländer, H.M., H. Bormann, T. Blume, W. Buytaert, G.B. Chirico, J.-F. Exbrayat, D. Gustafsson, H. Hölzel, et al. 2014. Impact of modellers' decisions on hydrological a priori predictions. *Hydrology and Earth System Sciences* 18(6): 2065–2085. https://doi.org/10.5194/hess-18-2065-2014.

Hollanders, P., B. Schultz, W. Shaoli and C. Lingen. 2005. Drainage and salinity assessment in the Huinong Canal Irrigation District, Ningxia, China. *Irrigation and Drainage* 54(2): 155–173. https://doi.org/10.1002/ird.159.

Huang, J., T. Kilminster, E.G. Barrett-Lennard and J. Triantafilis. 2017. Characterization of field-scale dryland salinity with depth by quasi-3d inversion of DUALEM-1 data. *Soil Use and Management* 33: 205–215. https://doi.org/10.1111/sum.12345.

Hydata. 2020. Hydata, Province of Manitoba, Groundwater Management, Winnipeg, ManitobaWinnipeg, Manitoba: Province of Manitoba, Groundwater Management, 2020.

Inman, D.J., R.S. Freeland, J.T. Ammons and R.E. Yoder. 2002. Soil investigation using electromagnetic induction and ground-penetrating radar in southwest Tennessee. *Soil Science Society of America Journal* 66: 206–211.

Iqbal, Z., R.T. MacLean, B.D. Taylor, F.J. Hecker and D.R. Bennett. 2002. Seepage losses from irrigation canals in southern Alberta. *Canadian Biosystems Engineering* 44: 21–27.

Ireson, A., C. Makropoulos and C. Maksimovic. 2006. Water resources modelling under data scarcity: coupling MIKE BASIN and ASM groundwater model. *Water Resources Management* 20: 567–590. https://doi.org/10.1007/s11269-006-3085-2.

Jackson, E.K., W. Roberts, B. Nelsen, G.P. Williams, E.J. Nelson and D.P. Ames. 2019. Introductory overview: Error metrics for hydrologic modelling – A review of common practices and an open source library to facilitate use and adoption. *Environmental Modelling and Software* 119(May): 32–48. https://doi.org/10.1016/j.envsoft.2019.05.001.

Jain, M.K., U.C. Kothyari and K.G. Ranga Raju. 2004. A GIS based distributed rainfall-runoff model. *Journal of Hydrology* 299(1–2): 107–135. https://doi.org/10.1016/j.jhydrol.2004.04.024.

Job, J.O., J.L. Gonzalez Barrios and M. Rivera Gonzalez. 1999. Effect of soil moisture on the determination of soil salinity using electromagnetic induction. *European Journal of Environmental and Engineering Geophysics* 3(3): 187–199.

Johnson, C.K., J.W. Doran, H.R. Duke, B.J. Wienhold, K.M. Eskridge and J.F. Shanahan. 2001. Field-scale electrical conductivity mapping for delineating soil condition. *Soil Science Society of America Journal* 65(6): 1829–1837. https://doi.org/10.2136/sssaj2001.1829.

Jolly, I.D., K.L. Mcewan and K.L. Holland. 2008. A review of groundwater – surface water interactions in arid / semi-arid wetlands and the consequences of salinity for wetland ecology. *Ecohydrology* 58: 43–58. https://doi.org/10.1002/eco.

de Jong, E., A.K. Ballantyne, D.R. Cameron and D.W.L. Read. 1979. Measurement of apparent electrical conductivity of soils by an electromagnetic induction probe to aid salinity surveys. *Soil Science Society of America Journal* 43(4): 810–812.

Joshi, P.K. and A.K. Agnihotri. 1984. An assessment of the adverse effects of canal irrigation in India. *Indian Journal of Agricultural Economics* 39(3): 528–536.

Kachanoski, R.G., E.G. Gregorich and I.J. Van Wesenbeeck. 1988. Estimating spatial variations of soil water content using noncontacting electromagnetic inductive methods. *Canadian Journal of Soil Science* 68(4): 715–722. https://doi.org/10.4141/cjss88-069.

Kachanoski, R.G., E. De Jong and I.J. Van Wesenbeeck. 1990. Field scale patterns of soil water storage from non-contacting measurements of bulk electrical conductivity. *Canadian Journal of Soil Science* 70(3): 537–542. https://doi.org/10.4141/cjss90-056.

Keller, C.K. and G. Van der Kamp. 1988. Hydrogeology of two Saskatchewan tills, II. Occurrence of sulfate and implications for soil salinity. *Journal of Hydrology* 101(1–4): 123–144. https://doi.org/10.1016/0022-1694(88)90031-5.

Khakural, B.R., P.C. Robert and D.R. Hugins. 1998. Use of non-contacting electromagnetic inductive method for estimating soil moisture across a landscape. *Communications in Soil Science and Plant Analysis* 29(11–14): 2055–2065. https://doi.org/10.1080/00103629809370093.

Khorsandi, F. and F.A. Yazdi. 2011. Estimation of saturated paste extracts' electrical conductivity from 1:5 soil/water suspension and gypsum. *Communications in Soil Science and Plant Analysis* 42: 315–321. https://doi.org/10.1080/00103624.2011.538885.

Kibria, G. and M.S. Hossain. 2012. Investigation of geotechnical parameters affecting electrical resistivity of compacted clays. *Journal of Geotechnical and Geoenvironmental Engineering* 138(12): 1520–1529. https://doi.org/10.1061/(ASCE)GT.1943-5606.0000722.

Kim, H.S., K.R. Kim, S.H. Lee, A. Kunhikrishnan, W. Il Kim and K.H. Kim. 2018. Effect of gypsum on exchangeable sodium percentage and electrical conductivity in the Daeho reclaimed tidal land soil in Korea—a field scale study. *Journal of Soils and Sediments* 18(2): 336–341. https://doi.org/10.1007/s11368-016-1446-x.

Knight, R.J. and A.L. Endres. 2005. An introduction to rock physics principles for near-surface geophysics. In *Near-Surface Geophysics Society of Exploration Geophysicists*, 31–70. Tulsa, Oklahoma.

Kottek, M., J. Grieser, C. Beck, B. Rudolf and F. Rubel. 2006. World Map of the Köppen-Geiger climate classification updated. *Meteorologische Zeitschrift* 15(3): 259–263.

Lambot, S., L. Weihermüller, J.A. Huisman, H. Vereecken, M. Vanclooster and E.C. Slob. 2006. Analysis of air-launched ground-penetrating radar techniques to measure the soil surface water content. *Water Resources Research* 42(11): 1–12. https://doi.org/10.1029/2006WR005097.

Lapenskie, K. and J.D. Bamburak. 2016. Gypsum investigations in the Harcus area, southwestern Manitoba (NTS 62J10): 2016 update; in Report of Activities 2016, Manitoba Growth, Enterprise and Trade, Manitoba Geological Surveypp. 181–186, 2016.

Latif, M. and M.A. Ahmad. 2009. Groundwater and soil salinity variations in a canal command area in Pakistan. *Irrigation and Drainage* 58: 456–468. https://doi.org/10.1002/ird.

Lekakis, E.H. and V.Z. Antonopoulos. 2015. Modeling the effects of different irrigation water salinity on soil water movement, uptake and multicomponent solute transport. *JOURNAL OF HYDROLOGY* 530: 431–446. https://doi.org/10.1016/j.jhydrol.2015.09.070.

Lesch, S.M., J.D. Rhoades, L.J. Lund and D.L. Corwin. 1992. Mapping soil salinity using calibrated electromagnetic measurements. *Soil Science Society of America Journal* 56(2): 540–548. https://doi.org/10.2136/sssaj1992.03615995005600020031x.

Lesch, S.M., J. Herrero and J.D. Rhoades. 1998. Monitoring for temporal changes in soil salinity using electromagnetic induction techniques. *Soil Science Society of America Journal* 62: 232–242. https://doi.org/10.2136/sssaj1998.03615995006200010030x.

Lesch, S.M. and D.L. Corwin. 2003. Using the dual-pathway parallel conductance model to determine how different soil properties influence conductivity survey data. *Agronomy Journal* 95(2): 365–379. https://doi.org/10.2134/agronj2003.0365.

Liu, X., X. Dong, Q. Xue, D.I. Leskovar, J. Jifon, J.R. Butnor and T. Marek. 2018. Ground penetrating radar (GPR) detects fine roots of agricultural crops in the field. *Plant and Soil* 423: 517–531. https://doi.org/10.1007/s11104-017-3531-3.

Manitoba Agriculture Food and Rural Initiatives. 2008. Soil Management Guide. https://www.gov.mb.ca/agriculture/environment/soil-management/soil-management-guide/.

Manitoba Infrastructure and Transportation. 2013. 2011 Flood : Technical Review of Lake Manitoba , Lake St . Martin and Assiniboine River Water Levels. Winnipeg, Manitoba.

Manitoba Land Resource Unit. 1997. Soils and terrain. An introduction to the land resource. Rural municipality of Portage la Prairie. Information Bulletin 97-22, Brandon Research Center, Research Branch, Agriculture and Agri-Food Canada 28.

McFarlane, D.J., R.J. George, E.G. Barrett-Lennard and M. Gilfedder. 2016. Innovations in dryland agriculture. In *Innovations in Dryland Agriculture*, 521–547. Springer, Cham. https://doi.org/10.1007/978-3-319-47928-6.

Mckenzie, R.C. 1988. Tolerance of plants to soil salinity; Soil and Water Program, 1987, Alberta Special Crops and Research Center, Brooks Alberta.

Mckenzie, R.C., R.J. George, S.A. Woods, M.E. Cannon and D.L. Bennett. 1997. Use of the electromagnetic-induction meter (EM38) as a tool in managing salinization. *Hydrogeology Journal* 5(1): 37–50.

McNeill, J.D. 1980. *Electromagnetic terrain conductivity measurement at low induction numbers*. *Technical note TN* TN--6, p. 13, 1980. http://www.geonics.com/pdfs/technicalnotes/tn6.pdf.

McNeill, J.D. 1990. Use of electromagnetic methods for groundwater studies. In *Geotechnical and Environmental Geophysics, Volume I Review and Tutuorial, Society of Geophysicists*, 191–218. Tulsa, Oklahoma.

Meyer, P.A., M. Brouwers and P.J. Martin. 2014. A three-dimensional groundwater flow model of the Waterloo Moraine for water resource management. *Canadian Water Resources Journal* 39(2): 167–180. https://doi.org/10.1080/07011784.2014.914800.

Michalyna, W. and R.E. Smith. 1972. *Soils of the Portage la Prairie area. Manitoba Department of Agriculture, Winnipeg*. Soils of the Portage la Prairie Area. https://doi.org/10.1017/CBO9781107415324.004.

Miller, J.J. and D. Curtin. 2008. Electrical conductivity and soluble ions. In *Soil Sampling and Methods of Analysis*, 161–171.

Misra, R.K. and J. Padhi. 2014. Assessing field-scale soil water distribution with electromagnetic induction method. *Journal of Hydrology* 516: 200–209. https://doi.org/10.1016/j.jhydrol.2014.02.049.

Moore, K.R., H.M. Holländer, M. Basri and M. Roemer. 2019. Application of geochemical and groundwater data to predict sinkhole formation in a gypsum formation in Manitoba, Canada. *Environmental Earth Sciences* 78(6): 1–12. https://doi.org/10.1007/s12665-019-8188-1.

Moriasi, D.N., J.G. Arnold, M.W. Van Liew, R.L. Bingner, R.D. Harmel and T.L. Veith. 2007. Model evaluation guidelines for systematic quantification of accuracy in watershed simulations. *Transactions of the American Society of Agricultural and Biological Engineers* 50(3): 885–900.

Morris, E.R. 2009. Height-above-ground effects on penetration depth and response of electromagnetic induction soil conductivity meters. *Computers and Electronics in Agriculture* 68(2): 150–156. https://doi.org/10.1016/j.compag.2009.05.009.

Morway, E.D., T.K. Gates and R.G. Niswonger. 2013. Appraising options to reduce shallow groundwater tables and enhance flow conditions over regional scales in an irrigated alluvial aquifer system. *Journal of Hydrology* 495: 216–237. https://doi.org/10.1016/j.jhydrol.2013.04.047.

Mualem, Y. 1976. A New Model for Predicting the Hydrualic Conductivity of Unsaturated Porous Media. *Water Resources Research* 12(3): 564–566. https://doi.org/10.1029/WR012i003p00564.

Nagy, V., G. Milics, N. Smuk, A.J. Kovács, I. Balla, M. Jolánkai, J. Deákvári, K.D. Szalay, et al. 2013. Continuous field soil moisture content mapping by means of apparent electrical conductivity (ECa) measurement. *Journal of Hydrology and Hydromechanics* 61(4): 305–312. https://doi.org/10.2478/johh-2013-0039.

Nash, J.E. and J.V. Sutcliffe. 1970. River flow forecasting through conceptual models part I - a discussion of principles. *Journal of Hydrology* 10: 282–290.

Ndomba, P., F. Mtalo and A. Killingtveit. 2008. SWAT model application in a data scarce tropical complex catchment in Tanzania. *Physics and Chemistry of the Earth* 33: 626–632. https://doi.org/10.1016/j.pce.2008.06.013.

Nicolas, M.P.B., G.L.D. Matile, G.R. Keller and J.D. Bamburak. 2010. Phanerozoic geology of southern Manitoba; Manitoba Innovation, Energy and Mines, Manitoba Geological Survey, Stratigraphic Map SM2010-1, 2 sheets, scale 1:600 000.

Parkhurst, D.L. and C.A.J. Appelo. 2013. *Description of Input and Examples for PHREEQC Version 3 — a Computer Program for Speciation, Batch-Reaction, One-Dimensional Transport, and Inverse Geochemical Calculations. U.S. Geological Survey Techniques and Methods, Book 6, Chapter A43, 497 P.* U.S. Geological Survey Techniques and Methods, book 6, chapter A43. https://pubs.usgs.gov/tm/06/a43/.

Peel, M.C., B.L. Finlayson and T.A. McMahon. 2007. Updated world map of the Köppen-Geiger climate classification. *Hydrology and Earth System Sciences* 11: 1633–1644. https://doi.org/10.1002/ppp.421.

Plummer, L.N., D.L. Parkhurst, G.W. Fleming and S.A. Dunkle. 1988. A computer program incorporating Pitzer's equations for calculation of geochemical reactions in brines. US Geological Survey Water-Resources Investigation Report 88-4153. US Geological Survey9.

Rannie, W.F., L.H. Thorleifson and J.T. Teller. 1989. Holocene evolution of the Assiniboine River paleochannels and Portage la Prairie alluvial fan. *Canadian Journal of Earth Sciences* 26: 1834–1841. https://doi.org/10.1139/e89-156.

Read, D.W.L. and D.R. Cameron. 1979. Relationship between salinity and Wenner resistivity for some dryland soils. *Canadian Journal of Soil Science* 59(4): 381–385. https://doi.org/10.4141/cjss79-043.

Reilly, B.T.E. and A.W. Harbaugh. 2004. Guidelines for evaluating ground-water flow models, United States Geological Survey, Scientific Investigation 2004-5038. Reston, VA.

Rentz, J.W., R. Sri Ranjan and H.M. Holländer. n.d. Hydrogeological investigation of soil salinity adjacent to a flood protection infrastructure. *Environmental Earth Sciences*.

Rentz, J.W., R. Sri Ranjan, I.J. Ferguson and H.M. Holländer. n.d. Effects of salinity and water content on apparent conductivity in an alluvial setting in the Canadian prairies. *Environmental Earth Sciences*.

Revil, A. and P.W.J. Glover. 1998. Nature of surface electrical conductivity in natural sands, sandstones, and clays. *Geophysical Research Letters* 25(5): 691–694.

Rhoades, J. 1982. Soluble salts. In *Methods of Soil Analysis. Part 2. Chemical and Microbial Methods.*, Madison, WI: Agron Monogr. 9. ASA and SSSA. https://dl.sciencesocieties.org/publications/books/abstracts/agronomymonogra/methodsofsoilan2/167.

Rhoades, J. 1993. Electrical conductivity methods for measuring and mapping soil salinity. *Advances in Agronomy* 49: 201–251.

Rhoades, J.D., P.A.C. Raats and R.J. Prather. 1976. Effects of liquid-phase electrical conductivity, water content, and surface conductivity on bulk soil electrical conductivity. *Soil Science Society of America Journal* 40(5): 651. https://doi.org/10.2136/sssaj1976.03615995004000050017x.

Rhoades, J.D., N.A. Manteghi, P.J. Shouse and W.J. Alves. 1989a. Soil electrical conductivity and soil salinity: New formulations and calibrations. *Soil Science Society of America Journal* 53(2): 433–439.

Rhoades, J.D., N.A. Manteghi, P.J. Shouse and W.J. Alves. 1989b. Estimating soil salinity from saturated soil-paste electrical conductivity. *Soil Science Society of America Journal* 53(2): 428–433. https://doi.org/10.2136/sssaj1989.03615995005300020067x.

Rhoades, J.D. 1996. Salinity: Electrical Conductivity and Total Dissolved Solids. In *Methods of Soil Analysis Part 3—Chemical Methods* 5, 417–435. https://doi.org/10.2136/sssabookser5.3.c14.

Rhoades, J.D., S.M. Lesch, R.D. LeMert and W.J. Alves. 1997. Assessing irrigation/drainage/salinity management using spatially referenced salinity measurements. *Agricultural Water Management* 35: 147–165.

Rhoades, J.D., F. Chanduvi and S. Lesch. 1999. Soil salinity assessment: methods and interpretation of electrical conductivity measurements. *FAO Irrigation and Drainage Paper*.

Rhoades, J.D. and D.L. Corwin. 1981. Determining soil electrical conductivity-depth relations using an inductive electromagnetic soil conductivity meter. *Soil Science Society of America Journal* 45: 255–260. https://doi.org/10.2136/sssaj1981.03615995004500020006x.

Rosenthal, E., G. Weinberger, B. Berkowitz, A. Flexer and J. Kronfeld. 1992. The Nubian Sandstone aquifer in the central and northern Negev, Israel: delineation of the hydrogeological model under conditions of scarce data. *Journal of Hydrology* 132: 107–135. https://doi.org/10.1016/0022-1694(92)90175-U.

Saleh, A.M., A.B. Belal and E.S. Mohamed. 2017. Mapping of Soil Salinity Using Electromagnetic Induction: A Case Study of East Nile Delta, Egypt. *Egyptian Journal of Soil Science* 57(2): 167–174. https://doi.org/10.21608/ejss.2017.3705.

Samouëlian, A., I. Cousin, A. Tabbagh, A. Bruand and G. Richard. 2005. Electrical resistivity survey in soil science: A review. *Soil and Tillage Research* 83: 173–193. https://doi.org/10.1016/j.still.2004.10.004.

Schwartz, F.W., J.A. Cherry and J.R. Roberts. 1982. A case study of a chemical spill: polychlorinated biphenyls (PCBs) revisited. *Water Resources Research* 18(3): 535–545. https://doi.org/10.1029/WR020i002p00317.

Schwartz, F.W., A.S. Crowe, M.J. Hendry and D.W. Chorley. 1987. A Case Study to Assess the Potential for Saline Soil Development due to Irrigation. *Journal of Hydrology* 91: 1–27.

Scianna, J. 2002. Salt-affected soils: their causes, measure, and classification, HortNote No. 5.

Seelig, B.D. 2000. Salinity and sodicity in North Dakota soils. In *North Dakota State University Extension* May, 1–16.

Sheets, R. and J.M.H. Hendrickx. 1995. Noninvasive soil water content measurement using electromagnetic induction. *Water Resources Research* 31(10): 2401–2409.

Shewchuk, J. 2014. Reprint of: Delaunay refinement algorithms for triangular mesh generation. *Computational Geometry: Theory and Applications* 47(7): 741–778. https://doi.org/10.1016/j.comgeo.2014.02.005.

Simunek, J., M. van Genuchten and M. Sejna. 2012. The HYDRUS Software Package for Simulating the Two- and Three-Dimensional Movement in Variably-Saturated Porous Media, Technical Manual. *Technical Manual 2.0* (January): 2:258.

Singh, J., H.V. Knapp and M. Demissie. 2004. Hydrological modeling of the Iroquois River watershed using HSPF and SWAT. *Illinois State Water Survey Contract Report 2004-08*. https://doi.org/10.1111/j.1752-1688.2005.tb03740.x.

Skaggs, R.W., M.A. Youssef and G.M. Chescheir. 2012. Drainmod: model use, calibration, and validation. *Transactions of the American Society of Agricultural and Biological Engineers* 55(4): 1509–1522.

Skarie, R.L., J.L. Richardson, A. Maianu and G.K. Clambey. 1986. Soil and groundwater salinity along drainage ditches in eastern North Dakota. *Journal of Environment Quality* 15(4): 335–340. https://doi.org/10.2134/jeq1986.00472425001500040004x.

Song, X., J. Zhang, C. Zhan, Y. Xuan, M. Ye and C. Xu. 2015. Global sensitivity analysis in hydrological modeling : Review of concepts , methods , theoretical framework , and applications. *JOURNAL OF HYDROLOGY* 523(225): 739–757. https://doi.org/10.1016/j.jhydrol.2015.02.013.

Sonmez, S., D. Buyuktas, F. Okturen and S. Citak. 2008. Assessment of different soil to water ratios (1:1, 1:2.5, 1:5) in soil salinity studies. *Geoderma* 144: 361–369. https://doi.org/10.1016/j.geoderma.2007.12.005.

Sperling, T., W.K. Munro and R.A. Freeze. 1989. Groundwater control at Highland Valley Copper. *International Journal of Surface Mining, Reclamation and Environment* 3(3): 167–174. https://doi.org/10.1080/09208118908944271.

Stein, R. and F.W. Schwartz. 1990. On the origin of saline soils at Blackspring Ridge, Alberta, Canada. *Journal of Hydrology* 117(1–4): 99–131. https://doi.org/10.1016/0022-1694(90)90088-F.

Steppuhn, H. 2013. Principles and crop yield response to root-zone salinity. *Prairie Soils and Crops Journal* 6: 40–51.

Sturm, M., B. Taras, G.E. Liston, C. Derksen, T. Jonas and J. Lea. 2010. Estimating snow water equivalent using snow depth data and climate classes. *Journal of Hydrometerology* 11: 1380–1394. https://doi.org/10.1175/2010JHM1202.1.

Sudduth, K.A.A., N.R. Kitchen, G.A. Bollero, D.G. Bullock and W.J. Wiebold. 2003. Comparison of electromagnetic induction and direct sensing of soil electrical conductivity. *Agronomy Journal* 95: 472–482.

Sueltenfuss, J.P., D.J. Cooper, R.L. Knight and R.M. Waskom. 2013. The creation and maintenance of wetland ecosystems from irrigation canal and reservoir seepage in a semi-arid landscape. *Wetlands* 33(5): 799–810. https://doi.org/10.1007/s13157-013-0437-6.

Switzman, H., P. Coulibaly and Z. Adeel. 2015. Modeling the impacts of dryland agricultural reclamation on groundwater resources in Northern Egypt using sparse data. *Journal of Hydrology* 520: 420–438. https://doi.org/10.1016/j.jhydrol.2014.10.064.

Taghizadeh-Mehrjardi, R., B. Minasny, F. Sarmadian and B.P. Malone. 2014. Digital mapping of soil salinity in ardakan region, central iran. *Geoderma* 213: 15–28. https://doi.org/10.1016/j.geoderma.2013.07.020.

Tanji, K.K. and N.C. Kielen. 2002. Agricultural drainage water management in arid and semi-arid areas. In *Irrigation and Drainage Paper No. 61. Food and Agriculture Organization of the United Nations, Rome, Italy.*.

Topp, G.C., G.W. Parkin and T.P.A. Ferré. 2008. Soil water content. In *Soil Sampling and Methods of Analysis*, ed. E.G. Carter, M. R., Gregorich, 939–961. Boca Raton, Fla.

Triantafilis, J., G.M. Laslett and A.B. McBratney. 2000. Calibrating an electromagnetic induction instrument to measure salinity in soil under irrigated cotton. *Soil Science Society of America Journal* 64(3): 1009–1017. https://doi.org/10.2136/sssaj2000.6431009x.

Triantafilis, J., I.O.A. Odeh and A.B. McBratney. 2001. Five geostatistical models to predict soil salinity from electromagnetic induction data across irrigated cotton. *Soil Science Society of America Journal* 65(3): 869–878. https://doi.org/10.2136/sssaj2001.653869x.

Triantafilis, J. and F.A. Monteiro Santos. 2013. Electromagnetic conductivity imaging (EMCI) of soil using a DUALEM-421 and inversion modelling software (EM4Soil). *Geoderma* 211–212(1): 28–38. https://doi.org/10.1016/j.geoderma.2013.06.001.

Truman, C.C., H.F. Perkins, L.E. Asmussen and H.D. Allison. 1988. Using ground-penetrating radar to investigate variability in selected soil properties. *Journal of Soil & Water Conservation* 43(4): 341–345.

Tycholiz, C., I.J. Ferguson, B.L. Sherriff, M. Cordeiro, R. Sri Ranjan and M.A. Pérez-Flores. 2016. Geophysical delineation of acidity and salinity in the Central Manitoba gold mine tailings pile, Manitoba, Canada. *Journal of Applied Geophysics* 131: 29–40. https://doi.org/10.1016/j.jappgeo.2016.05.006.

U.S. Department of Agriculture, N.R.C.S. 2019. National soil survey handbook, title 430-VI. https://www.nrcs.usda.gov/wps/portal/nrcs/detail/soils/ref/?cid=nrcs142p2_054240.

U.S. Salinity Laboratory Staff. 1954. USDA Handbook No. In: 60 - Diagnosis and improvement of saline and alkali soils. USDA, Washington, D.C..

Urdanoz, V. and R. Aragüés. 2011. Pre- and Post-Irrigation Mapping of Soil Salinity with Electromagnetic Induction Techniques and Relationships with Drainage Water Salinity. *Soil Science Society of America Journal* 75(1): 207. https://doi.org/10.2136/sssaj2010.0041.

Uribeetxebarria, A., J. Arnó, A. Escolà and J.A. Martínez-Casasnovas. 2018. Apparent electrical conductivity and multivariate analysis of soil properties to assess soil constraints in orchards affected by previous parcelling. *Geoderma* 319(November 2017): 185–193. https://doi.org/10.1016/j.geoderma.2018.01.008.

USDA, 2019. n.d. Saturated Hydraulic Conductivity in Relation to Soil Texture. https://www.nrcs.usda.gov/wps/portal/nrcs/detail/soils/survey/office/ssr10/tr/?cid=nrcs144p2_074846.

van Genuchten, M.T. 1980. Closed-form equation for predicting the hydraulic conductivity of unsaturated soils. *Soil Science Society of America Journal* 44: 892–898. https://doi.org/10.2136/sssaj1980.03615995004400050002x.

Visconti, F., J.M. de Paz and J.L. Rubio. 2010. Calcite and gypsum solubility products in water-saturated salt-affected soil samples at 25 ◦ C and at least up to 14 dS m − 1. *European Journal of Soil Science* 61: 255–270. https://doi.org/10.1111/j.1365-2389.2009.01214.x.

Visconti, F. and J.. de Paz. 2016. Electrical conductivity measurements in agriculture: the assessment of soil salinity. In *New Trends and Developments in Metrology*, 99–126. InTech Open. https://doi.org/10.5772/52807.

Vogel, T. and M. Cislerova. 1988. On the reliability of unsaturated hydraulic conductivity calculated from the moisture retention curve. *Transport in Porous Media* 3: 1–15. https://doi.org/10.1007/BF00222683.

Wang, H.F. and M.P. Anderson. 1995. *Introduction to Groundwater Modeling: Finite Difference and Finite Element Methods*. Elsevier Science. https://books.google.ca/books?id=uJT-jwTZQW8C.

Watson, H.D., H.L. Neely, C.L.S. Morgan, K.J. McInnes and C.C. Molling. 2017. Identifying subsoil variation associated with gilgai using electromagnetic induction. *Geoderma* 295: 34–40. https://doi.org/10.1016/j.geoderma.2017.01.029.

Westdal, H., R. Bowering and B. Macbride. 2015. Provincial flood control infrastructure review of operating guidelines. August. Winnipeg, Manitoba.

Wollenhaupt, N.C., J.L. Richardson, J.E. Foss and E.C. Doll. 1986. A rapid method for estimating weighted soil salinity from apparent soil electrical conductivity measured with an aboveground electromagnetic induction eter. *Canadian Journal of Soil Science* 66(2): 315–321. https://doi.org/10.4141/cjss86-032.

Zhang, H., J.L. Schroder, J.J. Pittman, J.J. Wang and M.E. Payton. 2005. Soil salinity using saturated paste and 1:1 soil to water extracts. *Soil Science Society of America Journal* 69(4): 1146. https://doi.org/10.2136/sssaj2004.0267.

Appendix A – Apparent conductivity overview maps

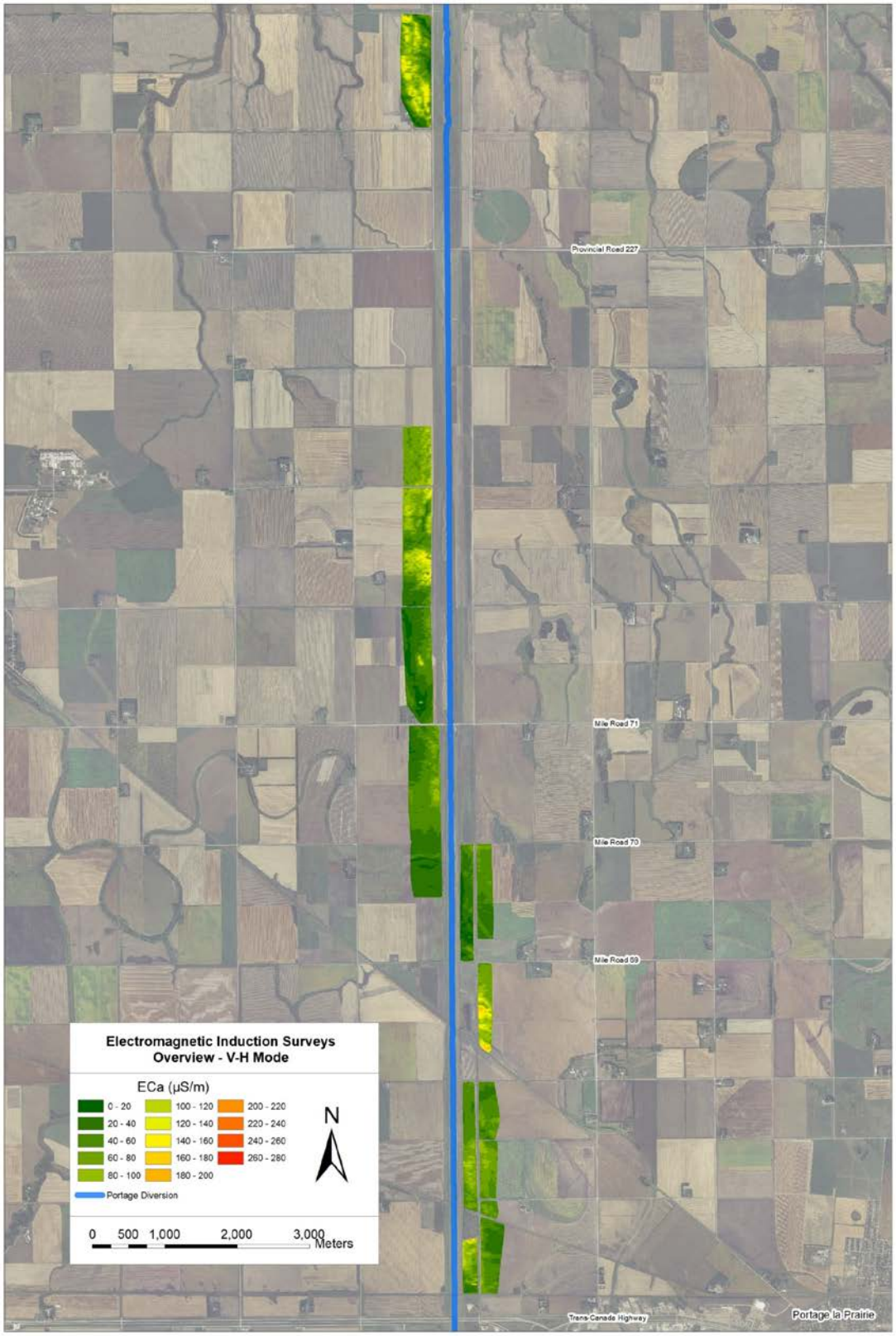

Figure A.1 Overview of the apparent conductivity results within the study region (exploration depth 0.5 m).

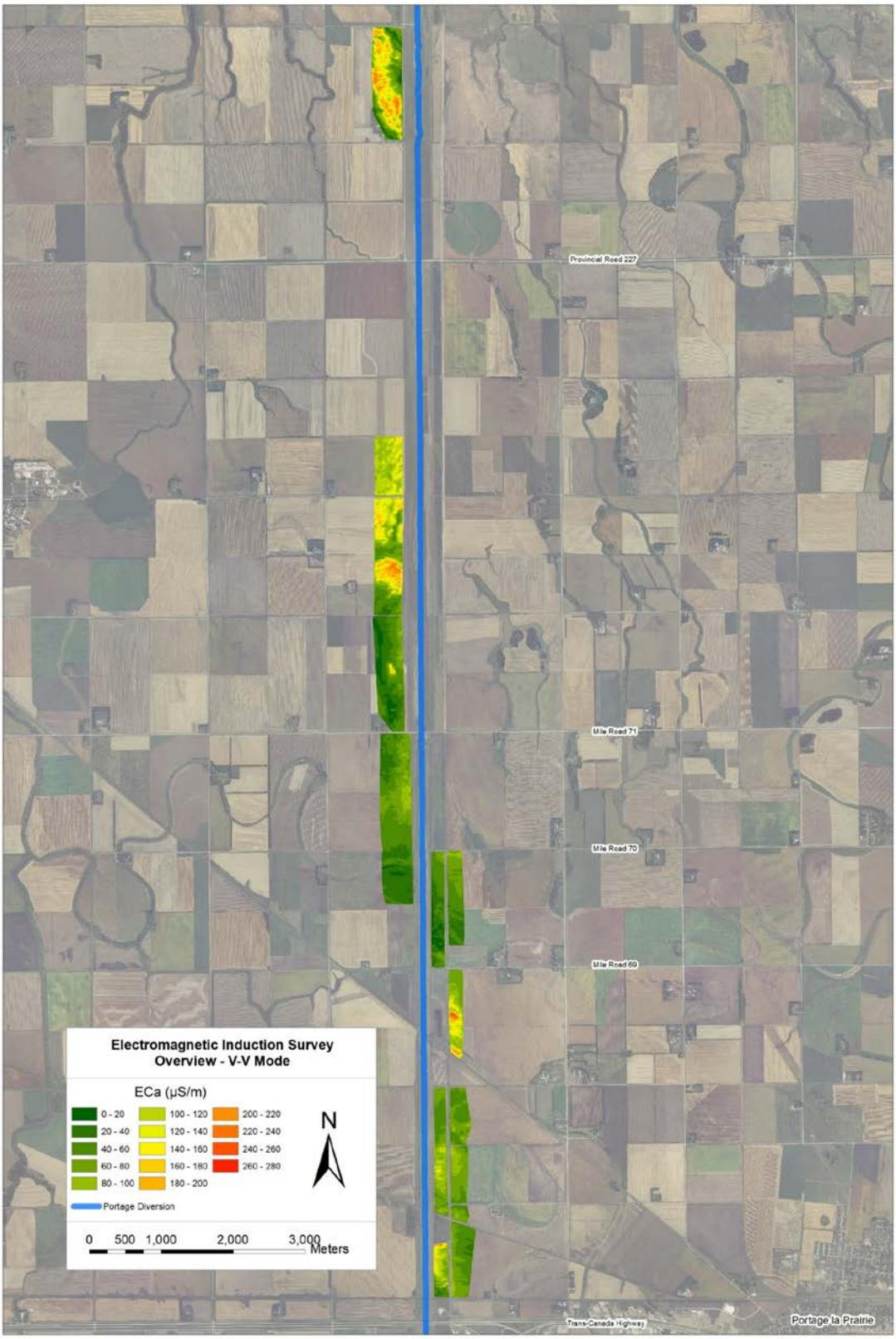

Figure A.2 Overview of the apparent conductivity results within the study region (exploration depth 1.5 m).

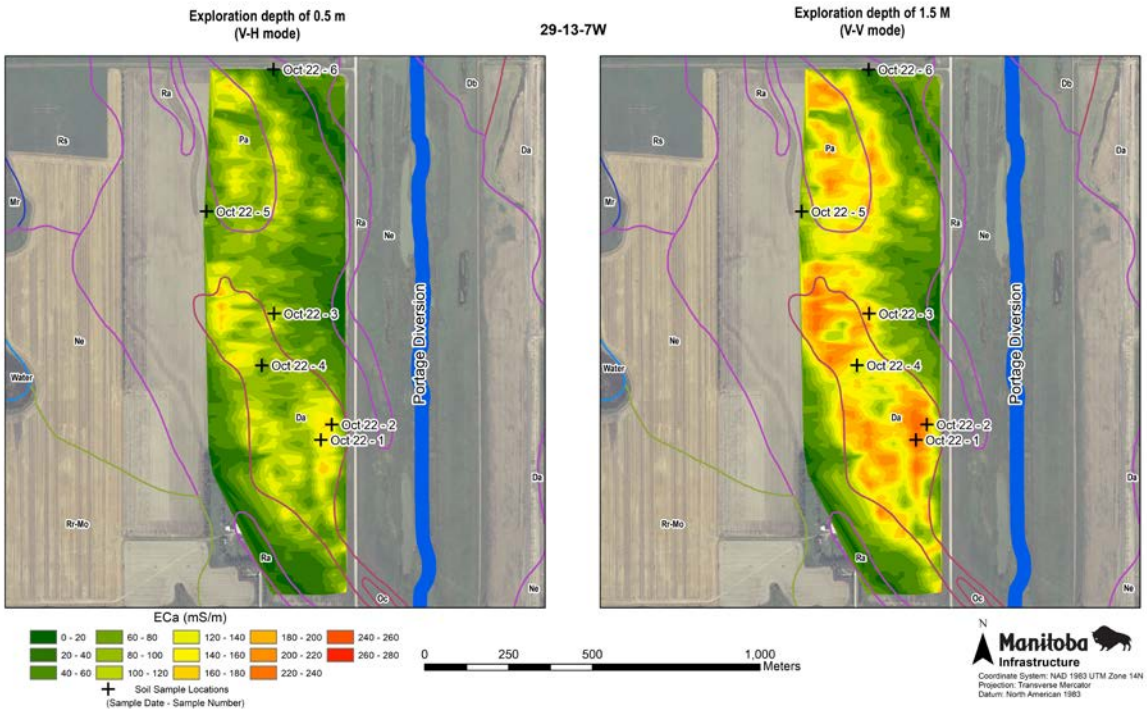

Figure A.3 Apparent conductivity map of Section 29-13-7W.

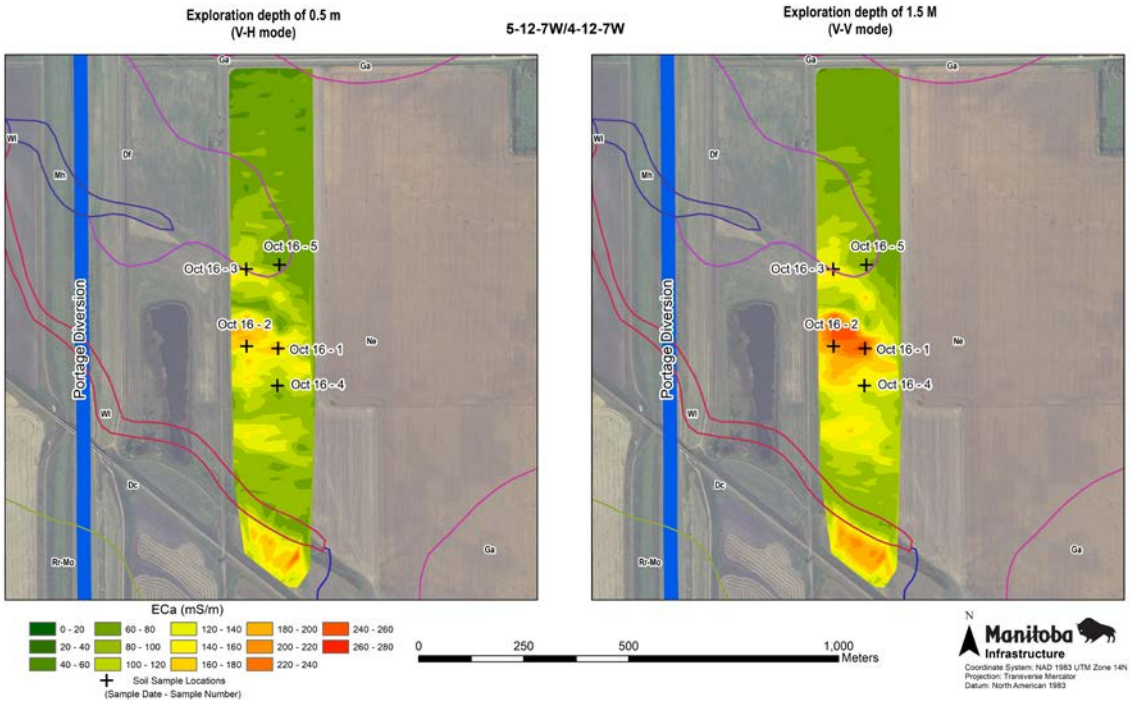

Figure A.4 Apparent conductivity map of Section 16-12-7W.

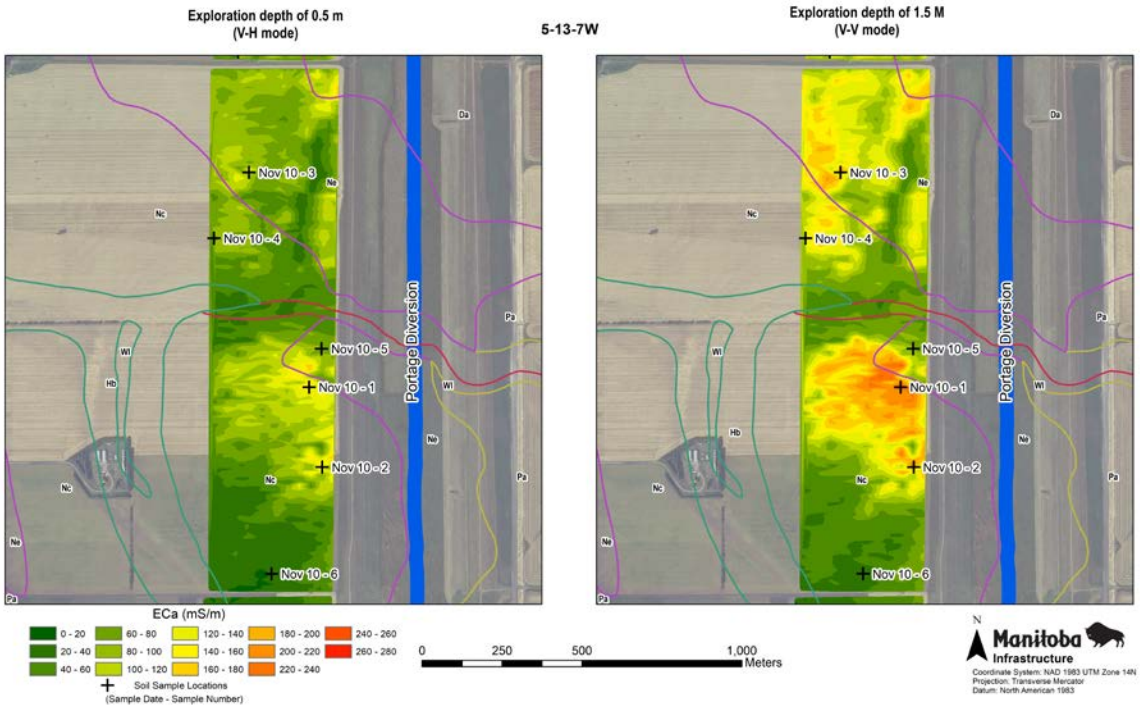

Figure A.5 Apparent conductivity map of Section 5-13-7W.

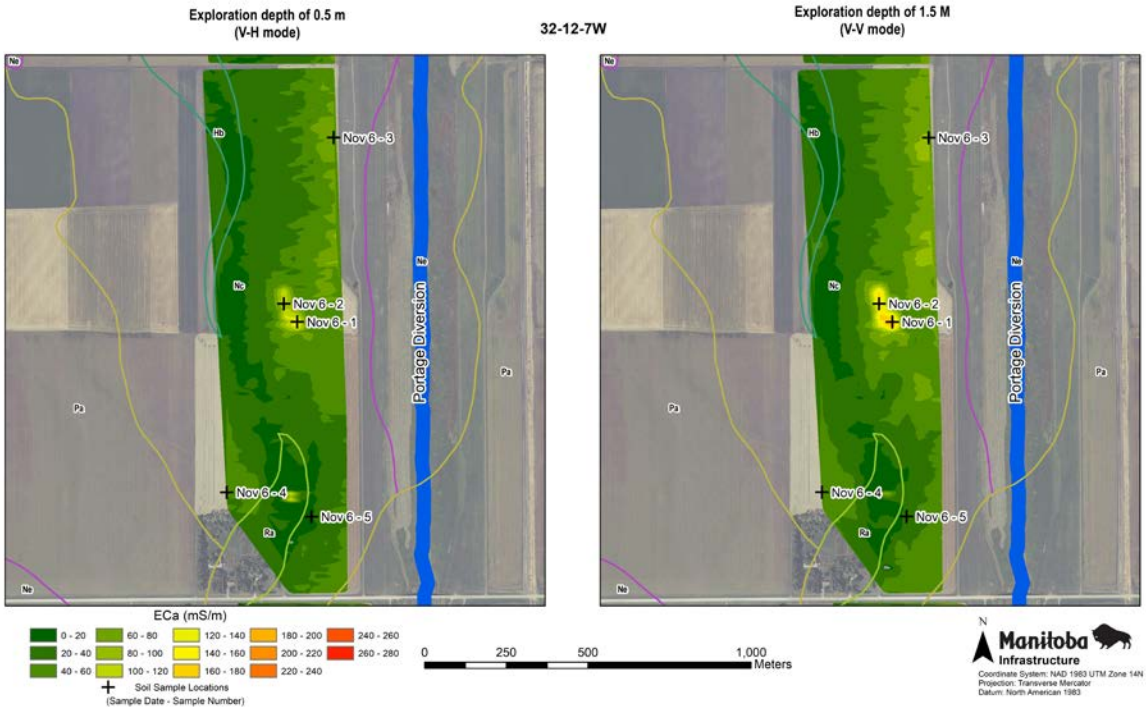

Figure A.6 Apparent conductivity map of Section 32-12-7W.

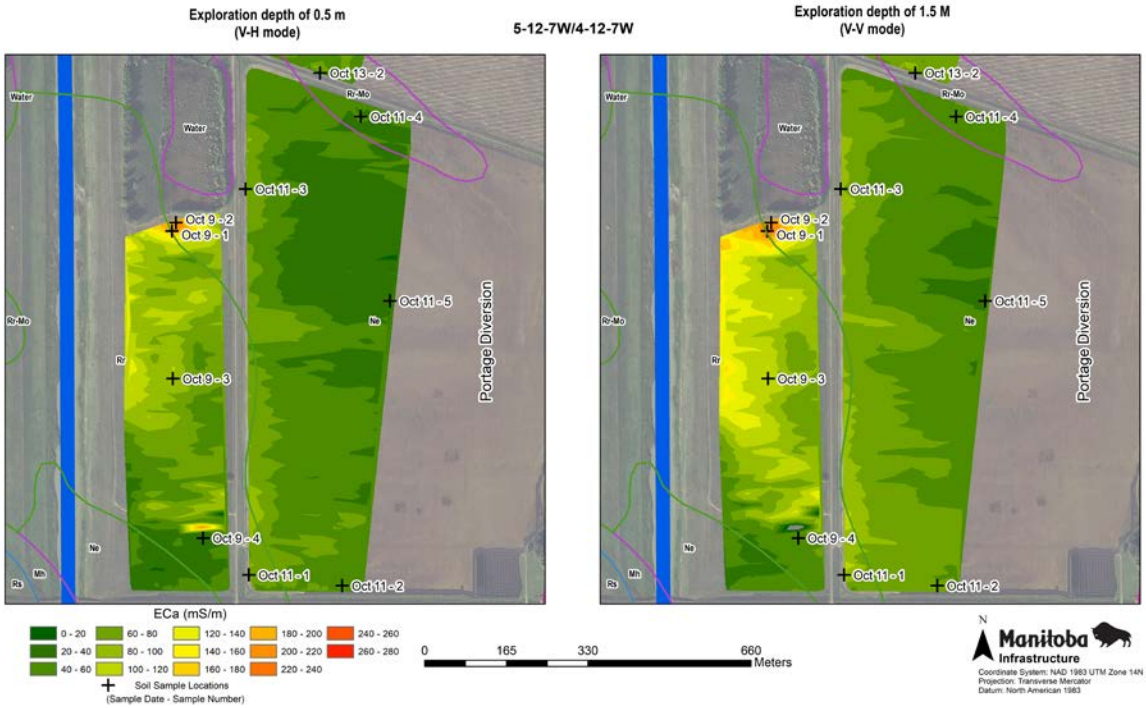

Figure A.7 Apparent conductivity map of Sections 5-12-7W and 4-12-7W.

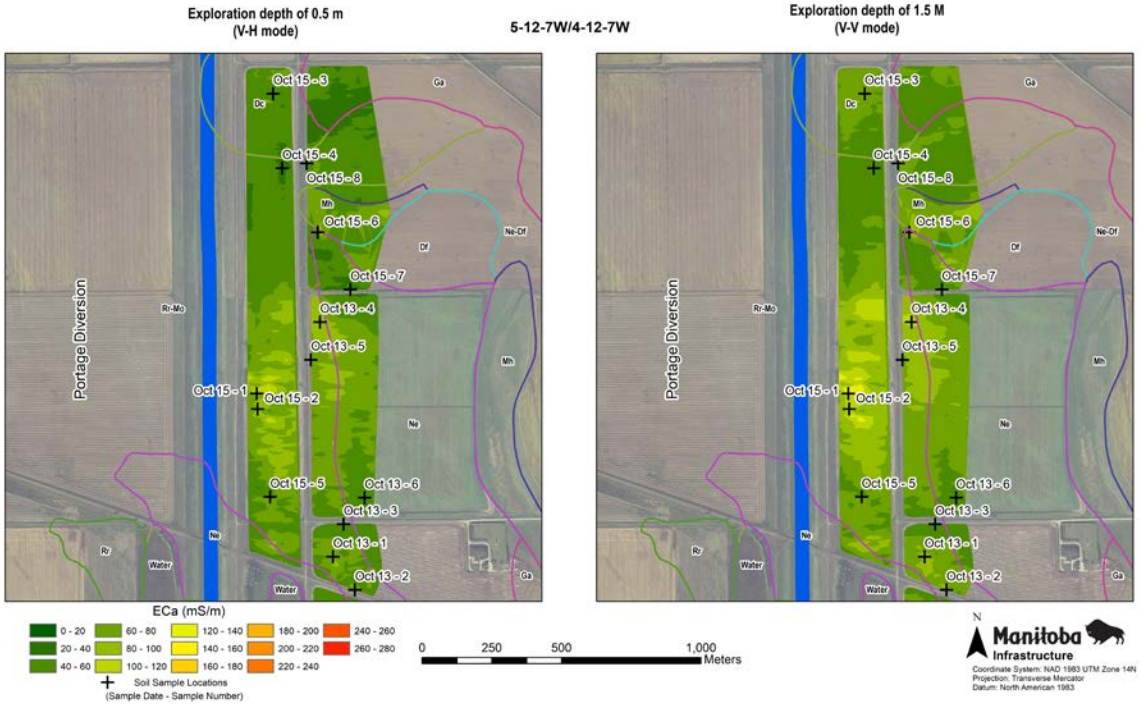

Figure A.8 Apparent conductivity map of Sections 8-12-7W, 9-12-7W, and N4-12-7W.

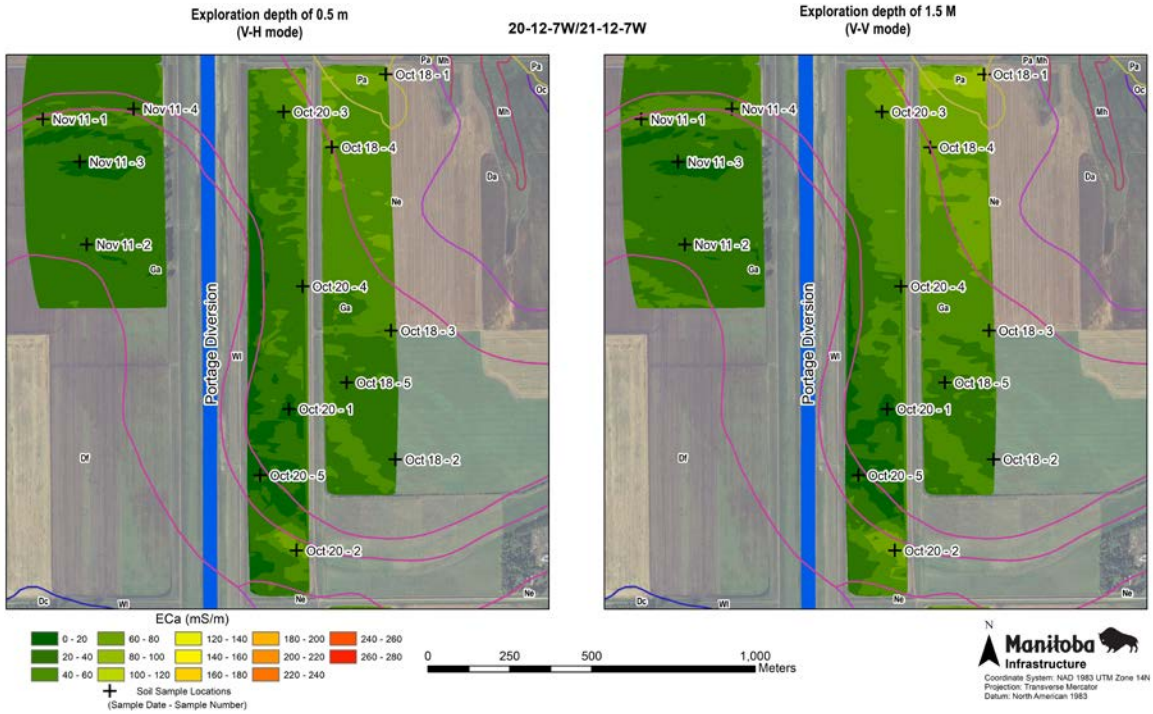

Figure A.9 Apparent conductivity map of Sections 20-12-7W and 21-12-7W.

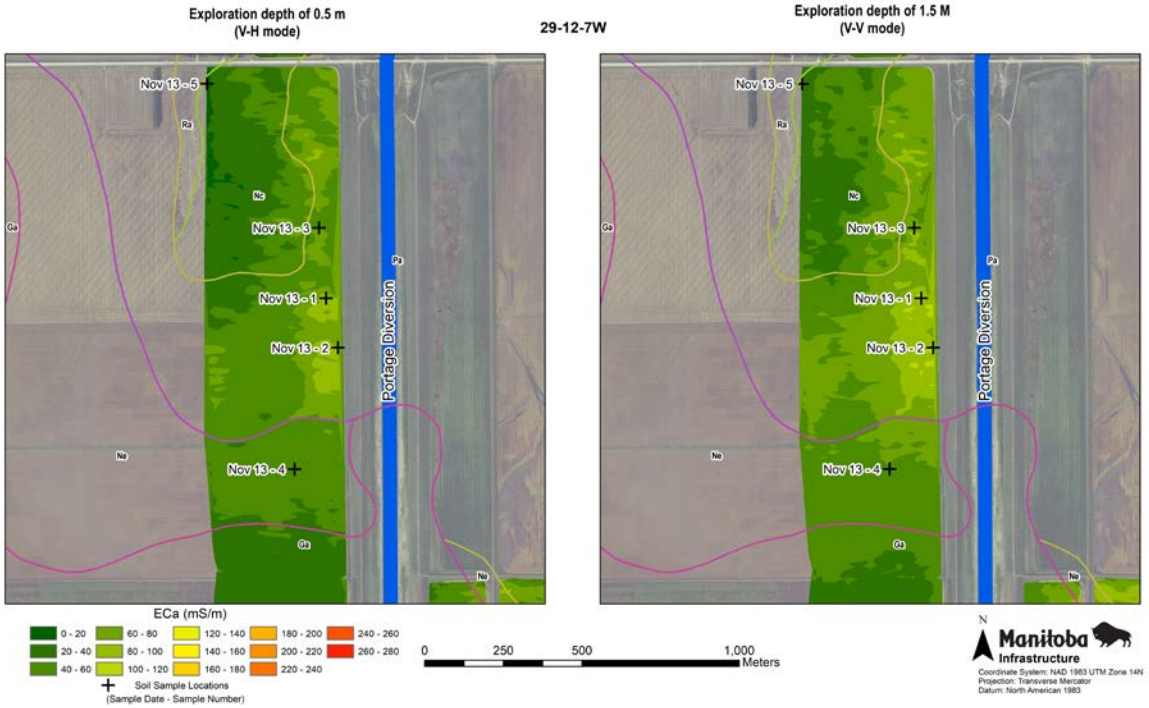

Figure A.10 Apparent conductivity map of Section 29-12-7W.

Appendix B – Additional soil salinity maps

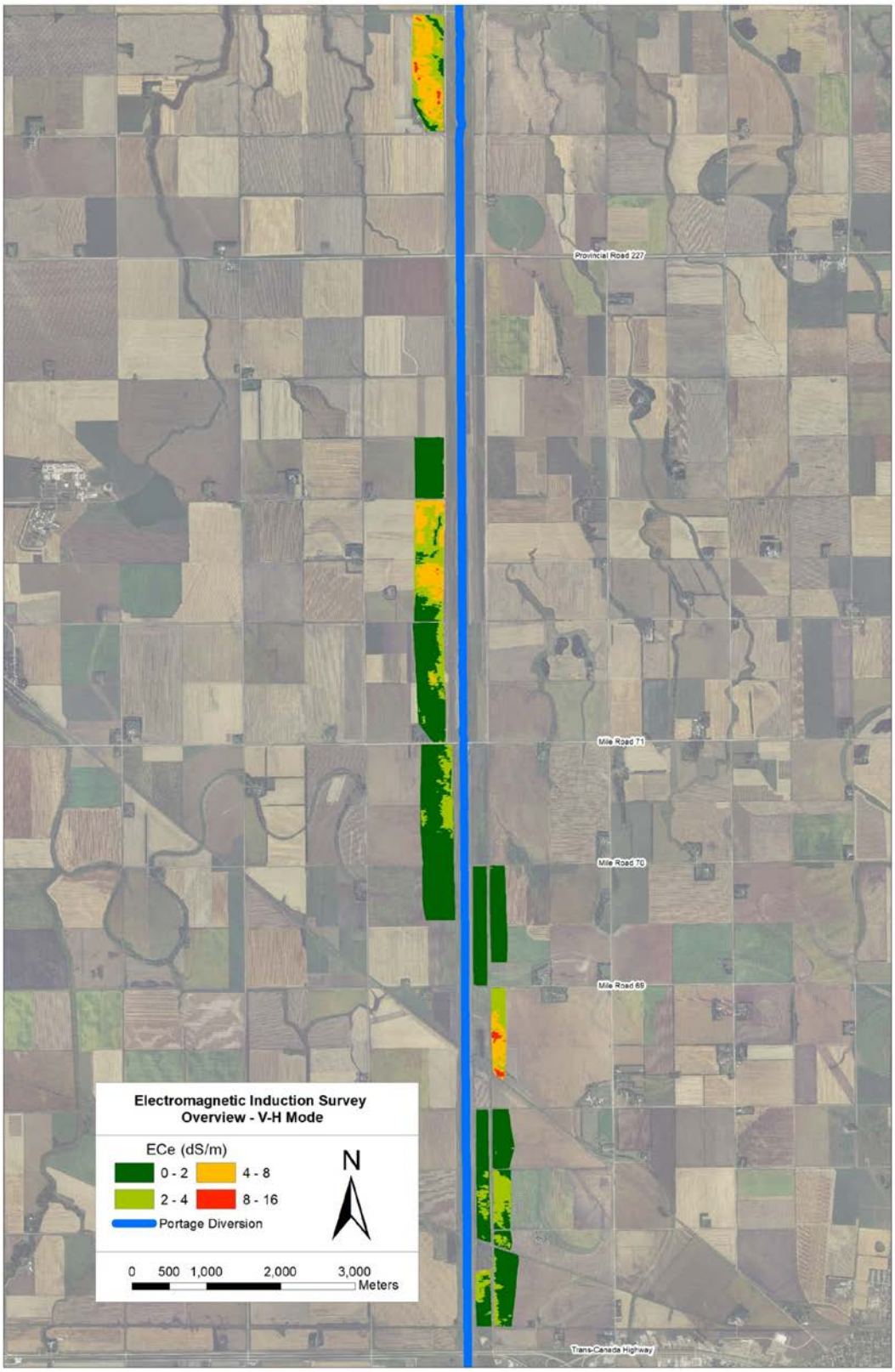

Figure B.11 Overview of the equivalent ECe results within the study region (exploration depth 0.5 m).

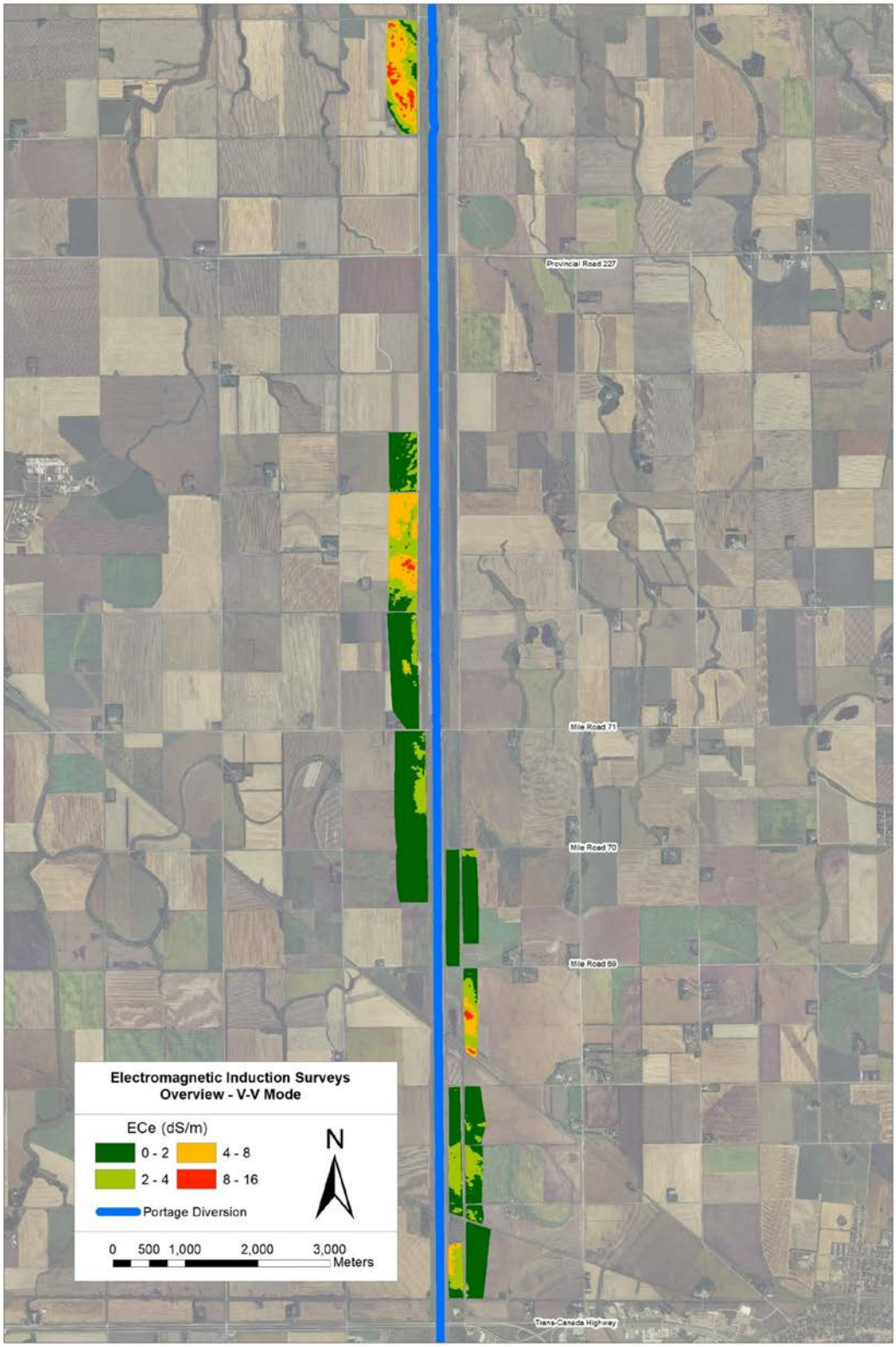

Figure B.12 Overview of the equivalent ECe results within the study region (exploration depth 1.5 m).

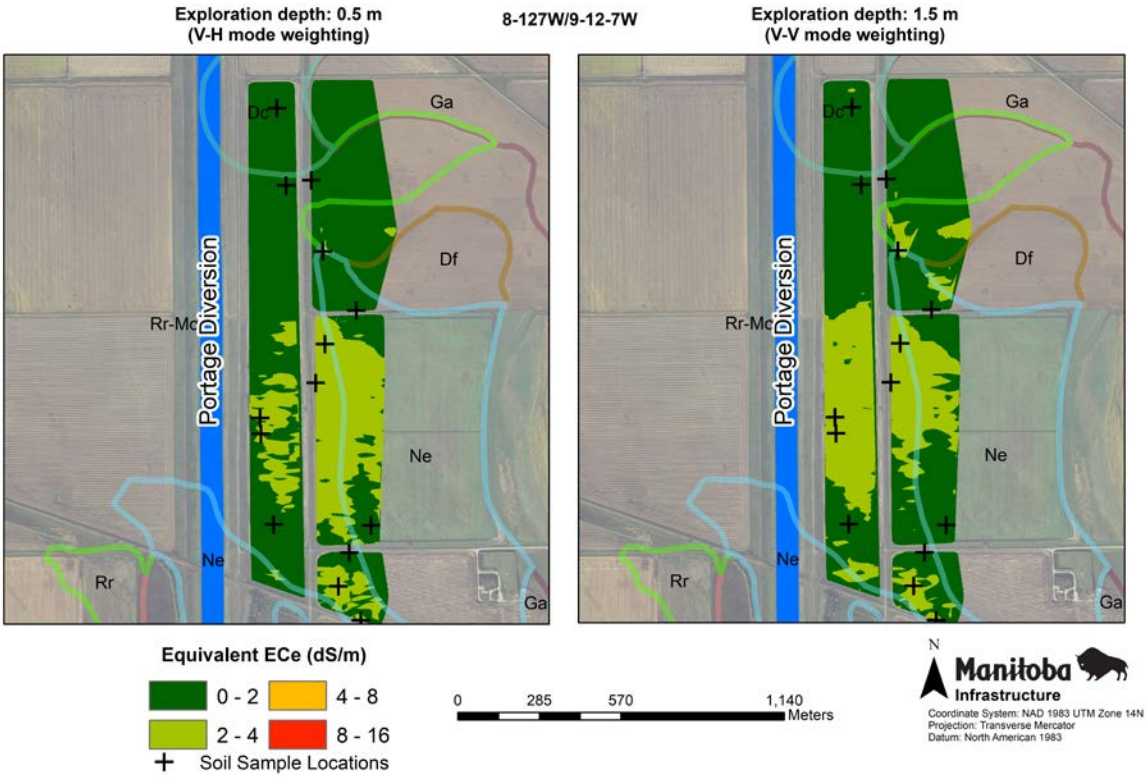

Figure B.13 Soil salinity survey of Sections 8-12-7W and 9-12-7W showing both V-H and V-V mode.

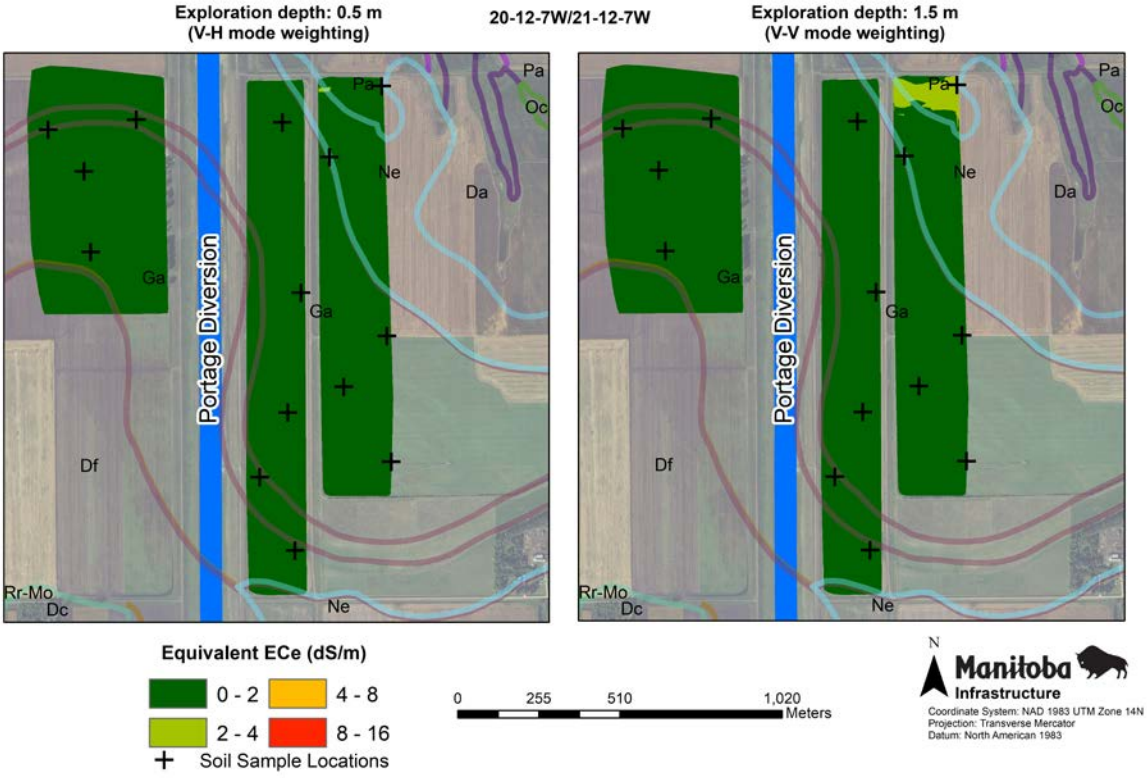

Figure B.14 Soil salinity survey of Sections 20-12-7W and 21-12-7W showing both V-H and V-V mode.

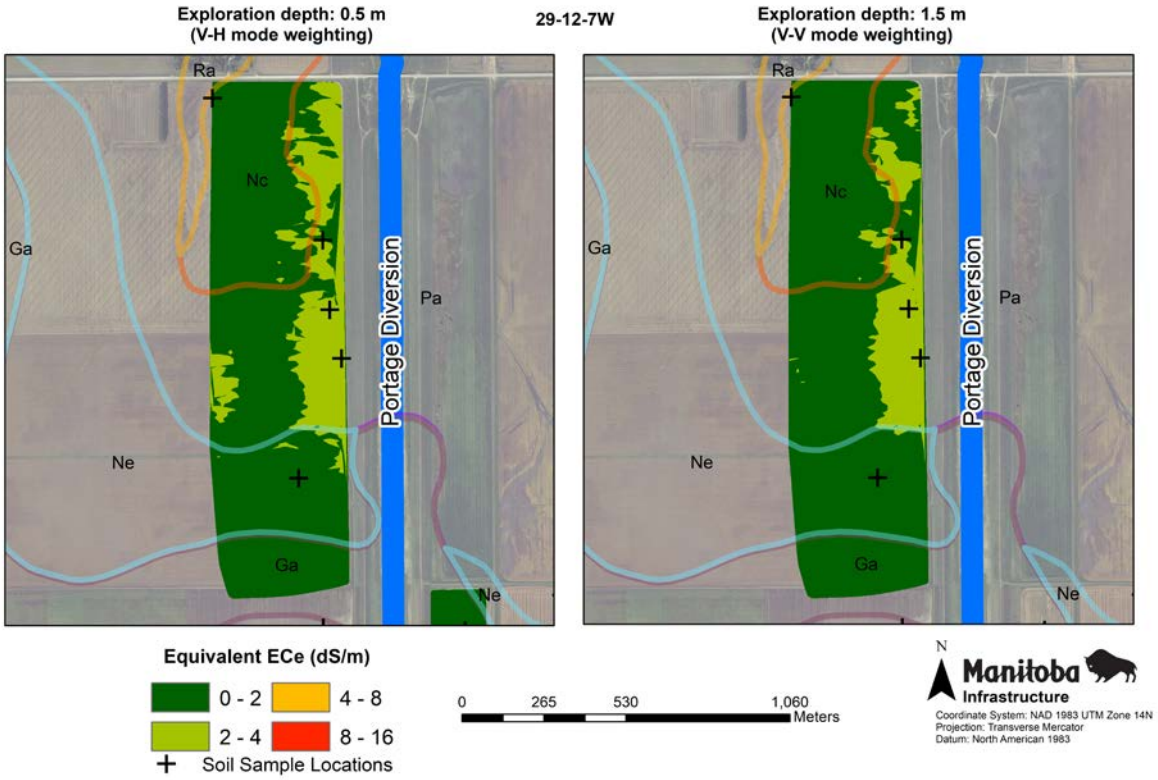

Figure B.15 Soil salinity survey of Section 29-12-7W showing both V-H and V-V mode.

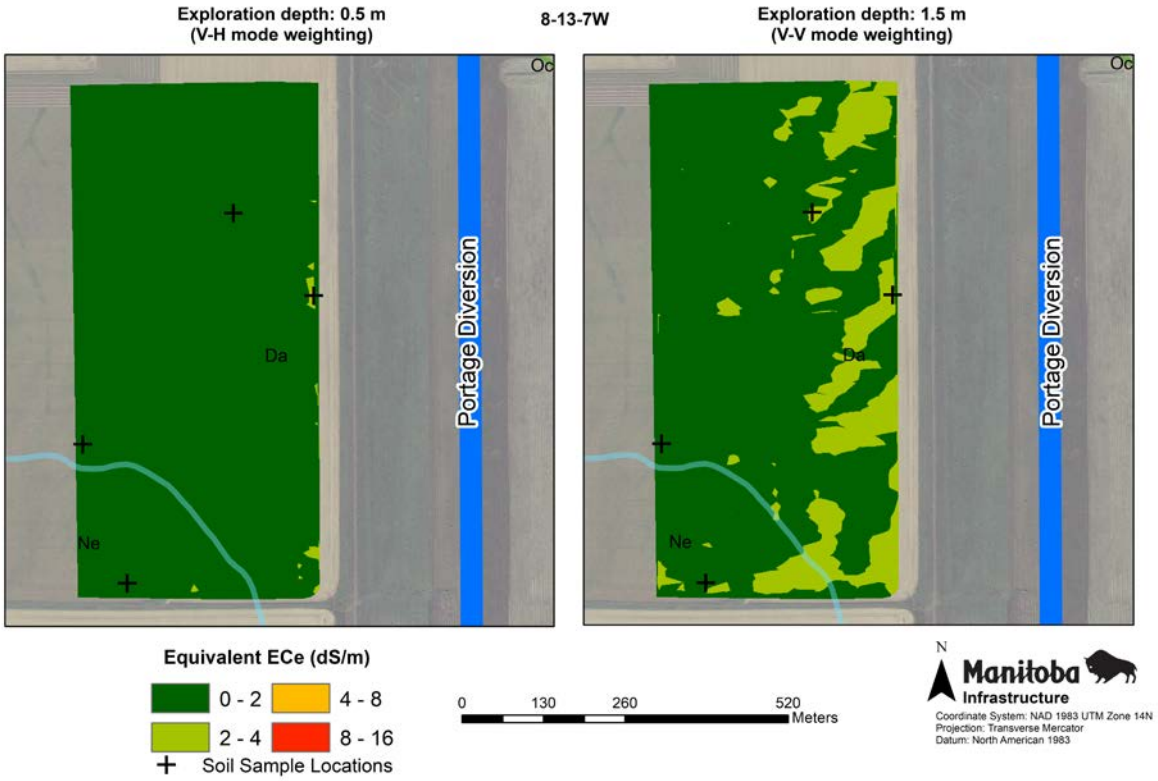

Figure B.16 Soil salinity survey of Section 8-13-7W showing both V-H and V-V mode